THE UNIVERSITY OF MICHIGAN
INDUSTRY PROGRAM OF THE COLLEGE OF ENGINEERING

HEAT TRANSFER TO LIQUID DROPS

Eugene Robert Elzinga, Jr.

This dissertation was submitted in partial fulfillment of the requirements for the degree of Doctor of Philosophy in the University of Michigan, 1956.

January, 1957

IP-198

Doctoral Committee:

Associate Professor Julius T. Banchero, Chairman
Associate Professor Stuart W. Churchill
Professor Joseph J. Martin
Professor G. Brymer Williams
Associate Professor C. S. Yih

ACKNOWLEDGMENTS

The author wishes to express his appreciation to all those persons who have contributed, in various ways, to this study:

Especially to Professor J. T. Banchero, chairman of the doctoral committee, for his sincere interest, encouragement and advice.

The other members of the doctoral committee, Professors S. W. Churchill, J. J. Martin, G. B. Williams and C. S. Yih.

Professor K. F. Gordon was most helpful, whenever his aid was sought.

The shop and office personnel of the Department of Chemical and Metallurgical Engineering, for their services.

The Allied Chemical and Dye Corporation and the Hercules Powder Company, for their generous financial support, and to the Industry Program of the University of Michigan, College of Engineering for the preparation and reproduction of this dissertation.

The patience and devotion of the author's wife during this period is appreciated most of all.

TABLE OF CONTENTS

TABLE OF CONTENTS (CONT'D)

LIST OF TABLES

LIST OF FIGURES

LIST OF FIGURES (CONT'D)

I. INTRODUCTION

The transfer of heat, mass and momentum, between a continuous phase and a dispersed phase is important in a number of industrial operations. In distillation, for example, the transfer takes place between a liquid phase and a gas phase, and the efficiency of the operation depends upon the rate at which this transfer proceeds. Other examples are liquid-liquid extractors and reactors in which a reaction occurs between two phases. Many investigators have studied various aspects of the transfer mechanisms in these processes, both theoretically and experimentally. The present work is a study of the heat transfer mechanism between a continuous liquid phase and a single stream of immiscible liquid drops flowing through the continuous phase. Also included are some relevant observations on the dynamic behavior of these drops. It is intended that this work should be of a more fundamental nature, and that it should bring out some of the aspects not so obvious in most of the previous work in this field.

Of all the research done on interphase transfer, those dealing with mass transfer are most numerous. This includes a great deal of work on the efficiency of distillation columns and liquid-liquid extractors. These studies can be divided roughly into the following categories, those dealing with mass transfer between swarms of drops or bubbles and a continuous phase, and those dealing with the transfer from a single bubble or drop. The latter is the one more related to the present work and includes several recent articles,[8,36,37,54] all of which deal with various aspects of mass transfer to drops in liquid-liquid systems. Probably the most extensive research in this line has been carried out by Garner and

co-workers, whose most recent contribution[13] deals with the role of surface active agents in liquid-liquid extraction.

While all of this work has been going on in the field of mass transfer, relatively little has been done with heat transfer, probably because the mass transfer results are more directly applicable to existing industrial operations. However, there have been a number of papers published which deal directly with heat transfer to drops in various liquid-liquid systems. Treybal[52] mentions that extraction columns have been evaluated at various operating conditions by measuring the heat transferred between phases. Garwin and Smith[15] measured the overall heat transfer rates in an extraction column where water was the continuous phase and benzene the dispersed phase. More recently, Pierce[47] studied heat transfer rates between swarms of mercury drops in water flowing countercurrent to the mercury. He found that circulation and vertical mixing of the continuous phase took place due to the presence of the falling drops of mercury. These last two studies have direct application in the field of nuclear engineering where direct-contact type reactors have been contemplated.

McDowell and Myers[42] recently studied heat transfer rates between drops of various organics in water and drops of water in an organic phase. Their work is similar to what has been done in the present study, except that their experimental technique does not lend itself to very accurate determinations of heat transfer rates. However, their work is sufficiently accurate to show that the transfer rate is greatly dependent upon the internal motion of the drop. The present work, and that of McDowell and Myers, differs from previous studies on heat transfer to liquid drops in that a single stream of drops was used, and the temperature of the continuous phase was maintained essentially constant along the path of the drops.

Although there has not been a great amount of work done which has any direct application to the present research, several investigators have presented results on related topics. Ingebo[26] studied heat and mass transfer rates between an air stream and liquid films on cork spheres. He found that the heat transfer coefficient could be correlated in terms of dimensionless groups, but since the heat transfer rates were dependent upon the mass transfer this correlation contains a group which takes this into account. Kinzer and Gunn[31] used a different experimental technique, which simulated more exactly the evaporation of falling drops, to determine heat and mass transfer rates. They use a less empirical approach than Ingebo in their analysis of the results, but again, as would be expected, the heat transfer rates were intimately related to the mass transfer rates. While direct application of these results to the present research is not possible, some similarity in the form of the results can be expected.

The results for heat transfer rates to spheres are also applicable in some respects to this investigation. Most of the literature in this field is summarized in McAdams[40]. The more recent work of Kramers[32] is useful in that it covers a wide range of most of the variables involved. Cary[5] experimentally determined local heat transfer rates around the circumference of a sphere in an air stream. Although his results are for much higher Reynolds numbers than those obtained in the present work, they do show how the heat transfer coefficient might vary over the surface of the the drop.

The present work is a systematic study of some of the important variables for the transfer of heat to drops in a liquid-liquid system. This investigation covers a range of liquid properties, drop sizes, and drop frequencies subject to the restrictions imposed by the requirement

of relatively immiscible liquids and a relatively noncorrosive continuous phase. Interpretation of the results was aided by photographs and shadowgraphs taken during each run.

APPARATUS

The primary purpose of the experimental apparatus was to measure the change in temperature of a stream of drops as they rose or fell through a continuous phase. Provisions were also made so that the size and velocity of the drops could be measured. To accomplish this, the apparatus was designed to facilitate the procurement of the necessary experimental data in as simple a manner as possible. Since at the time of construction, no corrosion problem was forseen, the materials of construction were, for the most part, plain carbon steel and galvanized iron pipe.

Figure 1 is a flow sheet showing the general layout of the equipment. The temperature of the continuous phase was kept uniform by circulating this phase through an external electric heater. This circulation was accomplished by a centrifugal pump which draws the liquid from the test section. The flow of the continuous phase was controlled by a bypass valve on the pump, and its rate could be observed by means of a rotameter. In all cases, this flow rate was set to give a temperature drop for the continuous phase of less than one degree Fahrenheit over the length of the test section. The continuous phase was brought to the desired operating temperature by means of a steam heater, and maintained at this temperature by means of a 1500-watt electric heater. A silica gel drier was also provided, so that the concentration of water in the continuous phase could be controlled. This drier also served as a filter to remove small amounts of suspended material. The dispersed phase liquid was forced from its storage tank by means of nitrogen pressure. The nitrogen pressure used was always less than 20 psig and the flow rate was controlled by means of a needle-type control valve. The flow

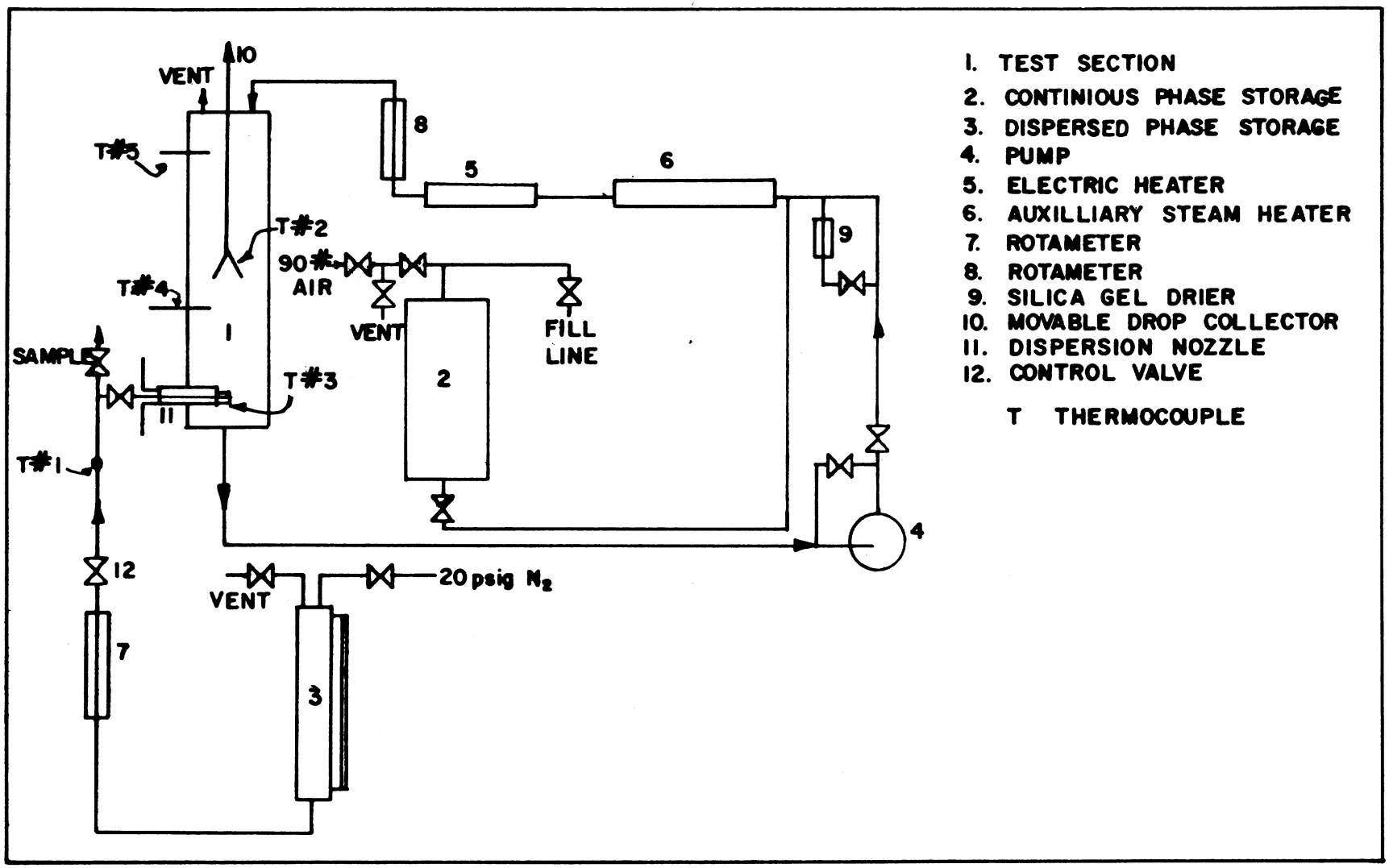

Figure 1. Flow Diagram of Liquid-Liquid Heat Transfer Apparatus

rate could be observed by either of two small rotameters, depending upon the flow rate and the drop material. After leaving the control valve, the liquid to be dispersed entered the test section through a water-jacketed nozzle which was inserted through the side of the test section. Drops were collected in the test section by means of a glass collector which could be raised or lowered to capture drops at any desired position. The level of the coalesced drops in the collector was kept constant by adjusting a clamp on the rubber tubing which carried off the liquid. The temperature of the dispersed liquid was measured at the point of drop formation and at the point of drop coalescence. The test section was rectangular in shape, and its front and back sides were fitted with glass windows. The glass sides permitted photographic and visual observations of the drops to be made. In the following paragraphs, the details of some of the features mentioned above will be described.

Dispersion Nozzles: A typical example of the type of nozzle used to form a single stream of drops is shown in Figure 2. These nozzles were fabricated from copper pipe and tubing and entered horizontally through a one-inch O-ring seal in the side of the test section. This type of seal allowed the nozzle to be leveled and centered prior to making a run. Cooling water was circulated through the jacket of each nozzle to control the temperature of the drop fluid. The drop fluid enters through the tee at one end of the nozzle, and leaves through the conical tip at the other end. A copper-constantan thermocouple was used to measure the temperature of the fluid just prior to its leaving the nozzle. The tip at which the drops were formed was machined from 3/8-inch round copper stock. After drilling, one end of the tip was carefully beveled at 45° so that the edge was sharp and even. The drop size was determined by the

size of the hole in the tip. Table I gives the letter used to designate each nozzle and the size of the drill used to drill the tips.

TABLE I

LIST OF NOZZLES USED

Letter Designation	Drill Diameter (inches)
a	0.022
b	0.0313
c	0.0625
d	0.0938
e	0.125
f	0.250

The nozzle is shown in place in Figure 3, and a cross sectional drawing, Figure 4, gives the important dimensions.

Drop Collector: The drops, after rising or falling through the test section, were captured by a glass funnel at one end of the drop collector. This collector is shown in place in Figure 3, for the case of downward flow of the dispersed phase, and the details of the end where the drops are allowed to coalesce is shown in detail in Figure 5. The outside jacket of the collector was one-inch Pyrex tubing and the inner passage was two-millimeter capillary tubing. The jacket was silvered and evacuated to minimize heat transfer to the material inside the collector. The collector entered through an O-ring seal at either end of the test section and could, therefore, be positioned to pick up drops at any height.

The design of the bell-shaped chamber at the end of the collector was based on some experimental observations in which it was noted that drops tended to break up more readily when forced out over a flat

glass surface at the liquid-liquid interface. This flat glass surface is shown by (A) in Figure 5, at one end of the bell-shaped chamber. The chamber above this glass surface allows entrained continuous phase matetial to fall back to the interface. The temperature of the collected drop material was measured by a small thermocouple just inside the entrance to the capillary tubing at the top of the chamber.

Even though heat transfer in the collector had been minimized, some transfer still took place by conduction along the glass walls and through the liquid-liquid interface. To determine the extent of this conduction, the collector was calibrated and a correction factor determined which would correct for the temperature change occurring during collection. In some cases, this correction amounted to as much as 25% of the temperature difference between the continuous phase and the drop temperature; however, in most cases it ranged between 0 and 10%. The method of calibration and the results are given in Appendix B.

Test Section: Figure 3, is a photograph of the test section showing the nozzle and collector in place. The section was fabricated of two pieces of six-inch channel iron, twenty five inches long, placed parallel to each other with the flat side of the web facing in and welded at both ends to rectangular flanges. The front and back of the section were formed of 3/16-inch plate glass, made leakproof by inserting a Neoprene gasket between the glass and a smooth surface machined on the lips of the channels. The windows were backed up with a strip of 1/2-inch sponge rubber and a rectangular steel flange. This flange was one-inch wide and 1/8 inch thick, and it served with the help of the sponge rubber to distribute the bolt load evenly around the glass. Quarter-inch studs were placed at two-inch intervals around the periphery of the window, and the nuts on these drawn up finger tight. With this arrangement,

there was never any trouble with leakage around the window. The entrance and exit were each six inches long and were bolted to the flanges at either end of the test section. The entrance section was provided with a weir, which distributed the incoming continuous phase more uniformly. Figure 6, shows the important dimensions of the test section, and the relative location of the various components.

The flow pattern of the continuous phase in the proximity of the drops is fairly uniform. This flow was investigated by injecting methyl violet dye at one end of the test section and observing the flow throughout the section. This observation was made at a superficial velocity of about one centimeter per second, which represents the highest continuous phase flow rate used. The following points were noted regarding the flow pattern: The liquid flowed fairly uniformly along the test section until it came to the funnel at the end of the collector. At this point, the liquid was diverted outward towards the walls of the test section. The motion of the liquid along the drop path between the collector and the nozzle was unusually quiet, and moved at a rate which was much less than the rate near the walls of the test section. Motion pictures of drops rising in the test section with and without circulation of the continuous phase confirmed the visual observation that most of the fluid flows along the walls of the test section.

The flow of the continuous phase in the test section was in all cases countercurrent to the drops. Therefore, for systems where the dispersed phase was lighter than the continuous phase, the drops entered at the bottom of the test section while the continuous phase entered through the top. For the opposite case, the drop nozzles were placed at the top of the test section and the continuous-phase entrance was moved to the bottom of the test section.

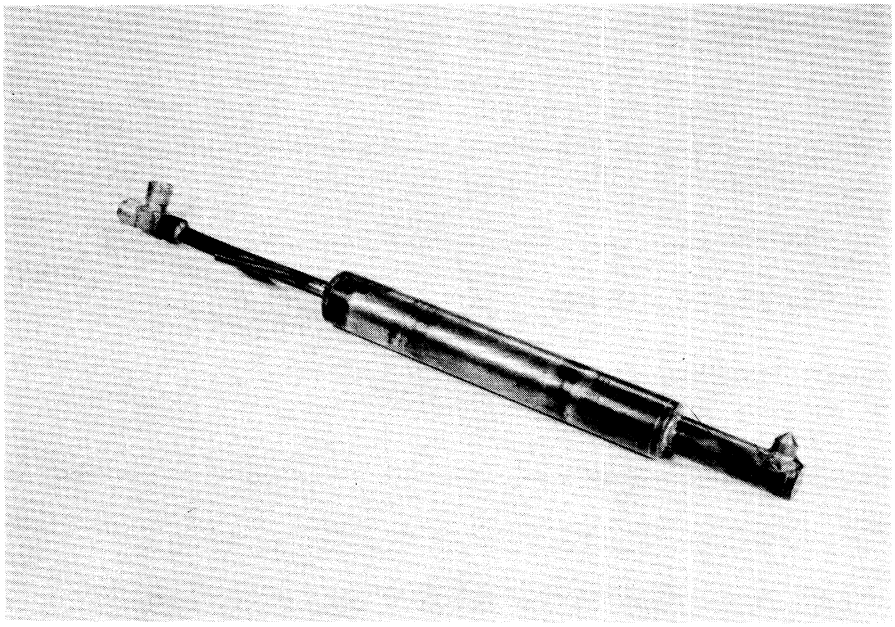

Figure 2. **Dispersion** Nozzle

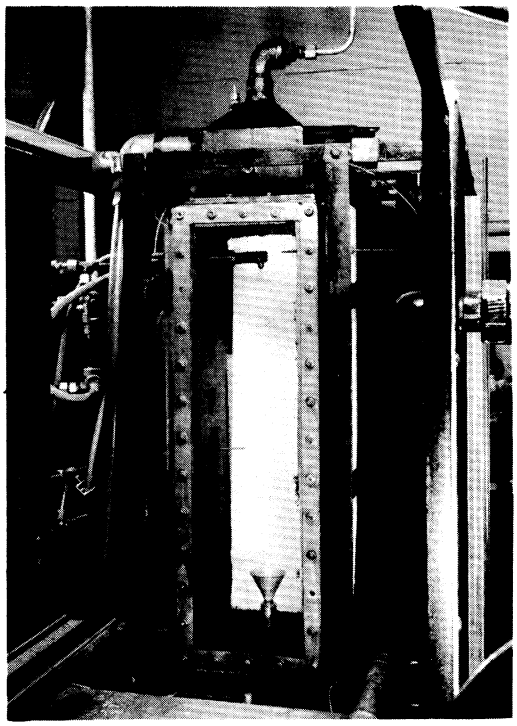

Figure 3. Test Section

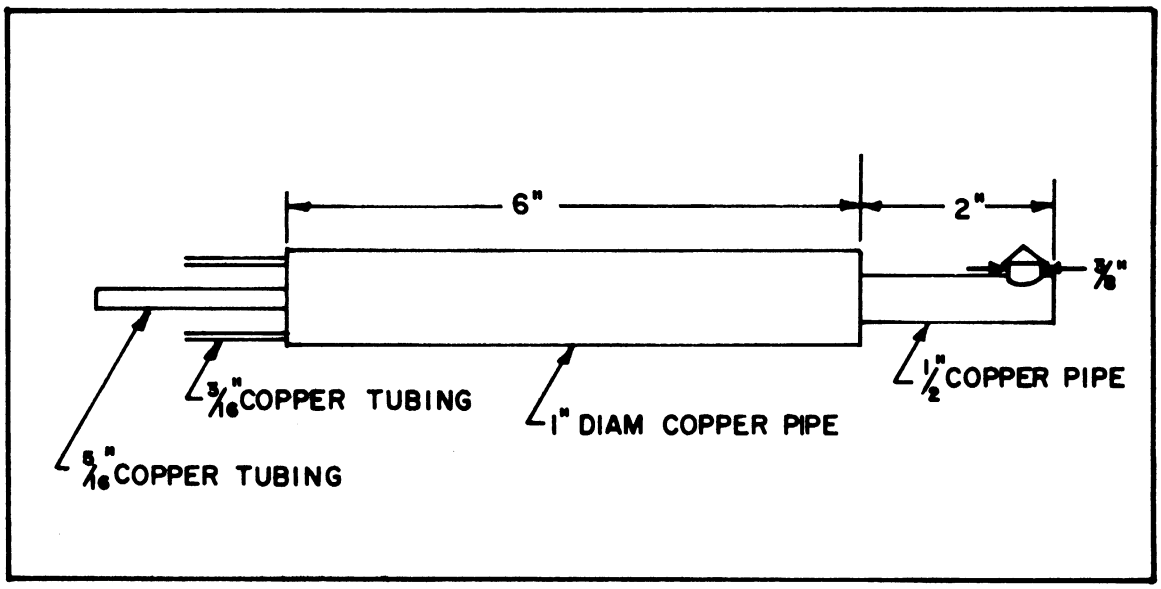

Figure 4. Details of Dispersion Nozzle

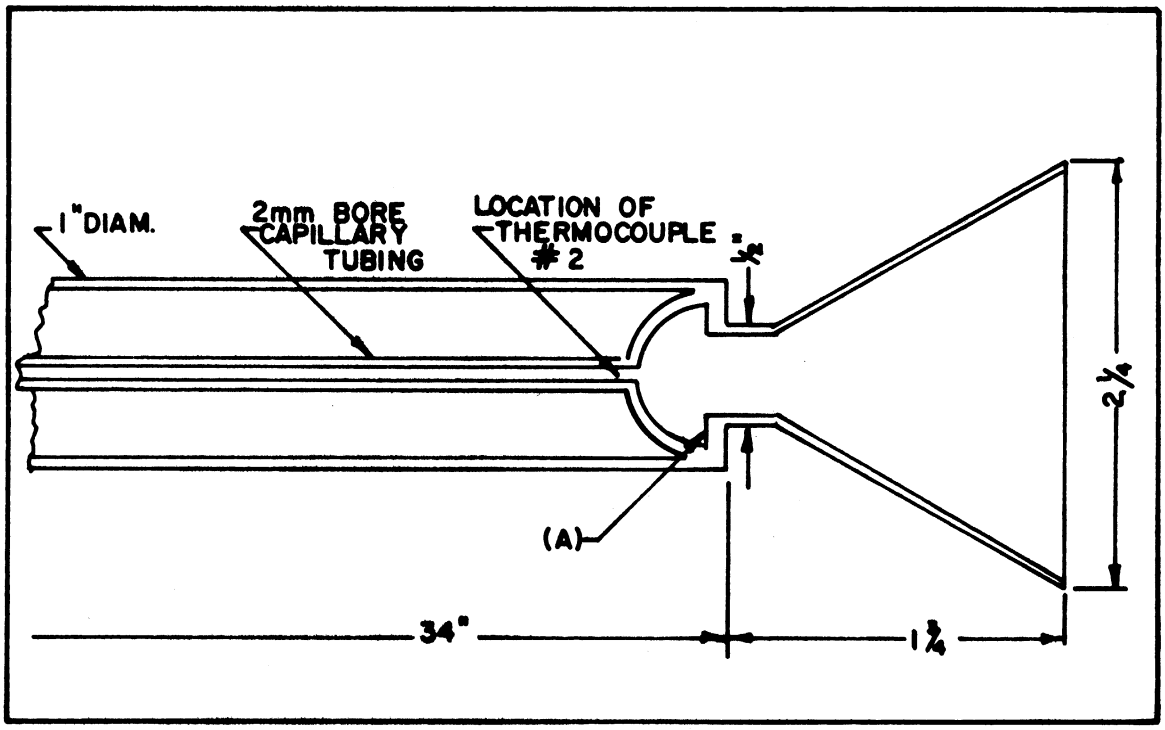

Figure 5. Details of Drop Collector

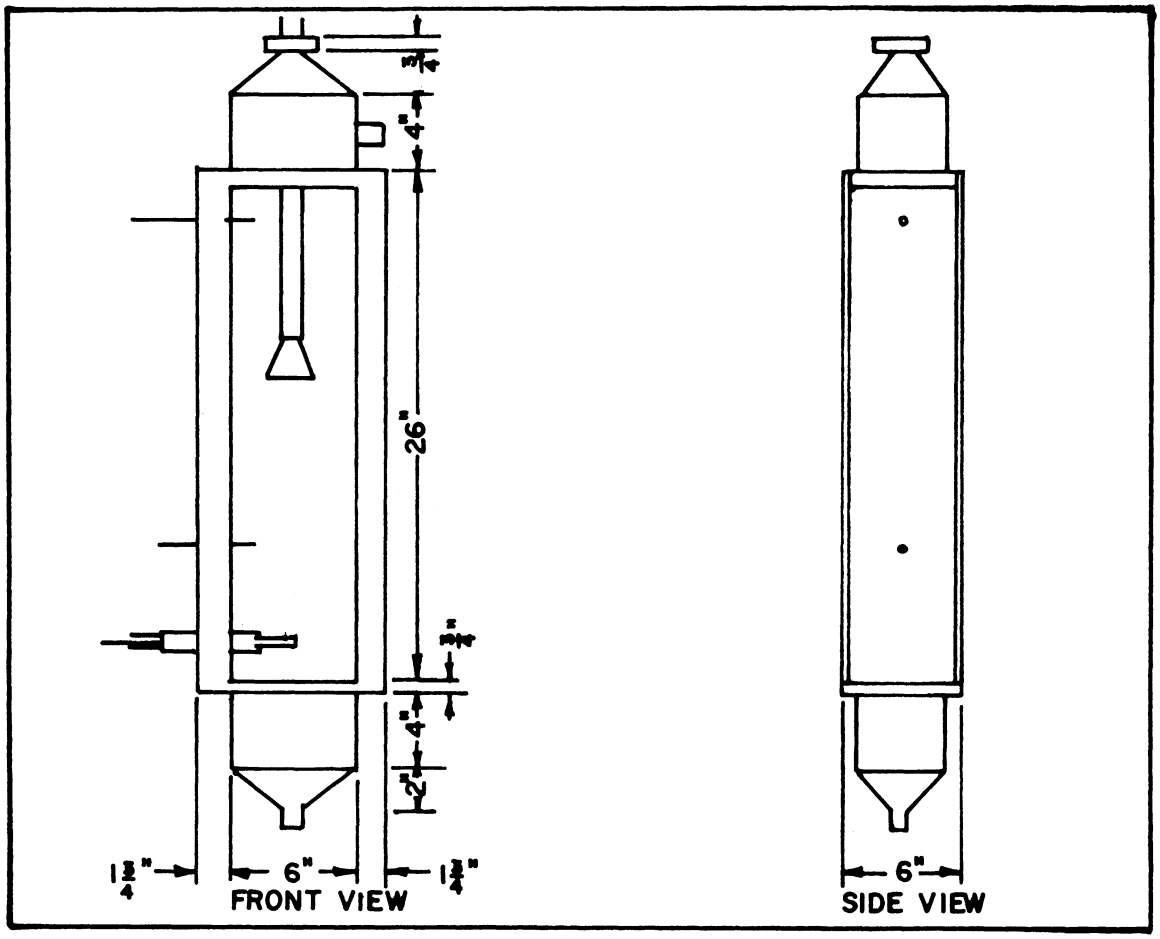

Figure 6. Details of Test Section

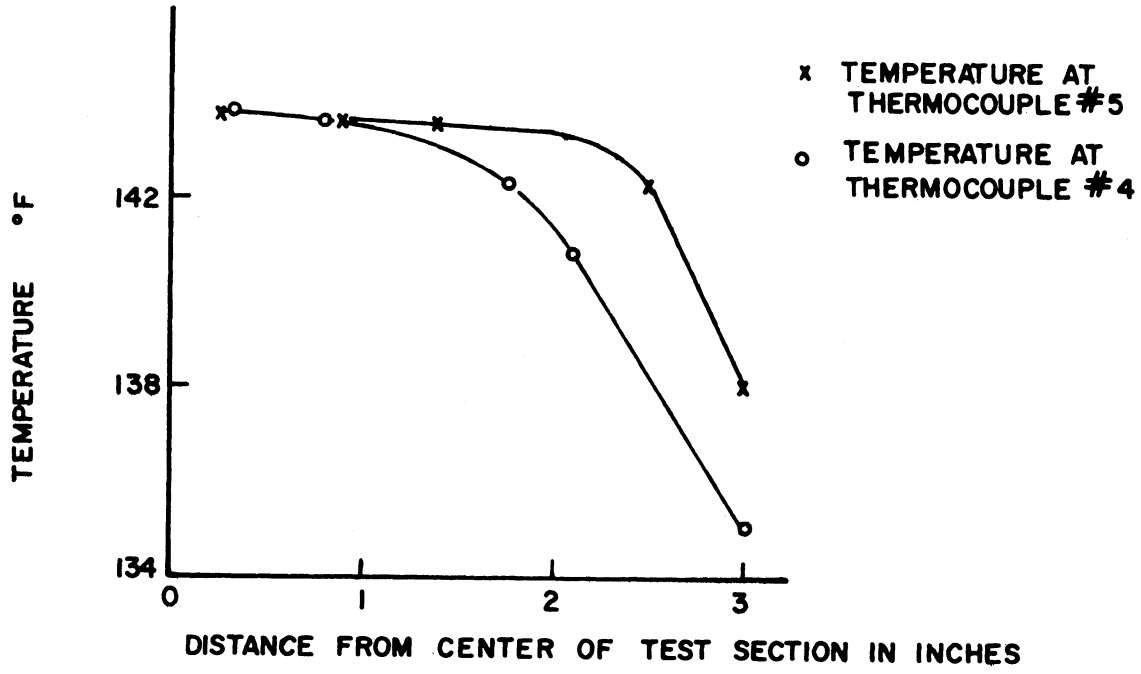

Figure 7. Temperature Distribution in Test Section

Temperatures in the test section were measured with two copper-constantan thermocouples located, for most of the runs, about six inches above and below the center of the section and about two inches from the left hand wall. The thermocouple wells were 1/8-inch stainless steel hypodermic tubing which entered the test section in such a way that the temperature could be read at any point from the center to the wall of the equipment. Using these thermocouples, a study was made of the temperature profile which existed in a horizontal section of the test apparatus with the continuous phase at operating temperature and circulating, but with no drops present. In this test, the continuous-phase liquid entered through the top of the test section and the drop collector was raised so that the bottom of the funnel was even with the upper thermocouple, No. 5. Figure 7 gives the results of this test. In this figure, the measured temperature is plotted against the distance from the center of the test section. Since the drops were always observed to rise or fall within the center two inches of the test section, it is easily seen from Figure 7 that there is very little change in temperature along the drop path due to heat losses from the test section.

Photography: Photographs of the drops were used to obtain drop dimensions and drop velocities. They were also found helpful in other phases of the work.

The camera used had a f3.5 lens with a four-inch focal length. The lens was mounted along with a standard ground-glass camera back, so as to be easily adjustable to give a wide range of magnification. In particular, it was desired to take pictures of the whole test section as well as close ups of single drops. The light source was a high intensity mercury arc, which was produced by discharging a 1/2 microfarad capacitor through a tube of mercury vapor. The duration of the flash

was estimated at ten microseconds, and was more than sufficient to stop the drop motion. A complete description of the mercury arc and power supply is given in Appendix I. Picutres were taken with the arc mounted behind a piece of opal glass to the rear of the test section, and with the camera in front of the test section. Photographs taken in this manner show the drop as a dark object in a light background which gave very good definition to the drop surface.

Shadowgraphs were made of the drops in some runs. To produce these, the mercury arc was replaced by a very small air gap, and the piece of opal glass was removed. Discharging the condenser across this gap produced sufficient light to expose a piece of film held against the front window of the test section. The results gave a fairly clear shadow of the drop and indicated the nature of the flow around the drop and in its wake. Motion pictures were also taken in some of the runs to determine the acceleration period for the drops.

The film used for the still pictures and shadowgraphs was four inch by five inch Kodak Contrast Process Ortho sheet film. The film was developed according to the manufacturers directions in Kodak developer D 11 and fixed in Kodak F 6 fixer. Glossy prints were made on Kodak AZO photographic paper, the grade used depending upon the contrast of the negative. For reproduction in the final form of the thesis, half tone negatives were made from these prints so that some of the orig-al contrast was lost.

Temperature Measurement and Control: All temperatures were measured using number 30 AWG copper-constantan thermocouples. The ice point of water was used for the cold junction and the e.m.f. produced was read with a Leeds and Northrup portable precision potentiometer, graduated in 0.01 millivolts.

The temperature of the continuous phase was controlled by using a variable transformer to vary the voltage across the electric heater. During the course of any one run, the temperature of the continuous phase did not change by more than one degree Fahrenheit.

EXPERIMENTAL PROCEDURE

The procedure used to obtain the data required for determining heat transfer rates and film coefficients for the drops is described in the following paragraphs. Briefly, the experimental measurements made consisted of data from which the following information could be obtained: The temperature change in a stream of drops along the length of the test section measured under conditions of constant drop size and frequency; the velocity of drops as a function of drop size for each liquid-liquid system; and finally, visual and photographic observations on the behavior of the drops.

Preliminary: Before starting a run, liquid from storage tank 2, was forced into the system using compressed air. Filling was continued until the liquid level reached the top of the test section. A vent line at the top of the test section indicated when the system was full, and also served to prevent the build up of pressure during filling or while making a run. After filling, circulation of the continuous phase was started and the desired flow rate set by observing the rotameter 8, and adjusting the bypass valve on the centrifugal pump 4. The flow rate used, varied from three to five gallons per minute. A small amount of the liquid was allowed to pass through the silica gel drier 9, which served to keep the water concentration down in the runs where water was used as the dispersed phase. The drier was also found to be effective in removing small amounts of rust or other suspended material which collected in the system. To bring the system up to the desired operating temperature, the auxilliary steam heater 6, used. This heater consisted of a piece of four inch pipe around a section of one-inch pipe, two feet long, through which the continuous phase was circulating. Low pressure

steam condensing in the annulus between the two pipes served as the heating media. After reaching the desired operating temperature, the steam was shut off and heat was supplied by the electric heater 5. This heater was a 1500-watt, 220-volt, knife type heater inserted in a length of three-inch pipe. The voltage to this heater was adjusted with a variable transformer to maintain the desired operating temperature. Thermal equilibrium was attained after a period of three or four hours, evidence of this being given by the constancy of temperature in the test section as recorded by a recording potentiometer.

The liquid to be dispersed was stored in the small tank 3. A low nitrogen pressure forced this liquid to flow through the rotameter 7, and control valve 12, and from there either to the sample point or to the nozzle 11. The flow rate was maintained constant by observing this rotameter and adjusting the control valve. The flow rate ranged from 0.02 to 0.40 grams per second, depending upon the size and frequency of the drops. No attempt was made to calibrate the small rotameters used, but instead, samples were collected over a measured time interval just prior to making a run. To do this, the desired frequency was first obtained by observing the drop stream in the test section and adjusting the control valve: The reading on the rotameter was then noted and the valve leading to the nozzle closed at the same time opening the valve at the sample point. With the drop material running from the sample point, the rotameter was adjusted to agree with the value read previously. Five to ten gram samples were collected and weighted to the nearest hundredth of a gram. The drop material was then allowed to flow through the nozzle to produce a stream of drops in the test section. The final preliminary step to be taken was to adjust the liquid-liquid interface in the drop

collector to the correct position. This interface could be observed through the glass at the intersection of the funnel and the jacketed portion of the collector. The interface was held at the desired position by adjusting the flow leaving the collector. This adjustment was repeated frequently during the course of a run.

Measurements Made During Run: An experimental run consisted of obtaining the temperature of the drops at seven or eight positions in the test section for a particular liquid-liquid system, drop size and frequency. The collection of drops for temperature measurement was usually started at a point two or three inches from the nozzle, and then moved progressively away from the nozzle. Sufficient time was allowed at each point for the collector to adjust to the change in temperature. The nozzle tip was used as a reference point and distances from this point to the interface in the collector were measured with a cathetometer. The e.m.f.'s produced by the thermocouple in the collector, (No. 2) as well as the two in the continuous phase, (No. 4 and 5), and the one in the nozzle (No. 3), were recorded for each point. From these data, the drop temperature could be determined along the length of the test section.

The drop frequency was recorded several times during the run. This frequency was determined for frequencies up to two drops per second, by measuring the time for fifty drops to form at the nozzles. Higher frequencies were obtained from motion pictures or indirectly as explained in another section. The time required for a number of drops to travel between two points, a known distance apart, was also measured and recorded. One or two pictures showing the drop at approximately natural size were taken during the run. From these, the dimensions of the drop could be measured, and in most cases, the point of separation of the boundary

layer from the drop could be seen. Several pictures were also taken showing the whole test section. From these, the average number of drops per unit length could be obtained. In most runs, shadowgraphs of the conditions existing along the drop path were also made. If motion pictures were taken, these were usually made just prior to the run.

To summarize the preceding description, the data obtained during a run consisted of the following measurements and observations.

1. The temperature of the drops along the length of the test section.
2. The continuous-phase temperature.
3. The dispersed phase inlet temperature.
4. The flow rate of drop material.
5. The drop frequency.
6. The drop dimensions and the number of drops per unit length.
7. A number of observations on the behavior of the drops.

A series of runs was made for each liquid-liquid system. In most cases, the only variable changed between runs in a system, was the drop diameter. However, in one system, the drop frequency and the continuous phase temperature were also varied. Periodically, throughout the experimental work, samples of both liquid phases were withdrawn from the equipment and their physical properties determined.

SYSTEMS STUDIED

Two major prerequisites had to be satisfied by each system studied: The first of these was low mutual solubility of the two phases, the second was low corrosiveness of the continuous phase. Low mutual solubility was required so that mass transfer would not appreciably effect the heat transfer rates. The continuous phase had to be fairly non-corrosive because of the materials used in the construction of the experimental equipment. These, along with the desirability of studying as wide a range as possible in the physical properties, led to the selection of the systems used. The systems finally selected are given in Table II, along with the interfacial tension and the letter designation used for the system.

TABLE II

SYSTEMS STUDIED

Dispersed Phase	Continuous Phase	Interfacial Tension dynes per cm. at 25°C	Designation
water	Dowtherm E	39.5	A
water	Dowtherm E + Dowtherm A	38.5	B
ethylene glycol	Dowtherm E + Dowtherm A	9.0	C
ethylene glycol	Dowtherm E	8.5	D
water	Finol	50.5	E
ethylene glycol	Finol	19.5	F

Dowtherm E, and Dowtherm A, are heat transfer media, manufactured by the Dow Chemical Company. Dowtherm E, is primarily o-dichlorobenzene with some p-dichlorobenzene, while Dowtherm A, is a eutectic mixture of diphenyl and diphenyl oxide. The ethylene glycol used was

commercial grade, manfuctured by Carbide and Carbon Chemicals Company. Finol is a light mineral oil, and that used was manufactured by the Standard Oil Company (Indiana). Distilled water was used in all runs where water was required. Table III, gives the values of important physical properties at 25° Centigrade for each liquid. All physical properties are given as a function of temperature in Appendix A, along with the method used to obtain these values.

TABLE III

RANGE OF PHYSICAL PROPERTIES AT 25°C

Material	Density g/cc	Viscosity Centipoises	Heat Capacity cal/g°C	Thermal Conductivity cal/sec. cm°C
water	0.997	0.893	0.999	0.00145
ethylene glycol	1.109	17.5	0.565	0.000597
Dowtherm E	1.300	1.27	0.278	0.000306
Dowtherm A+E	1.186	1.85	0.326	0.000323
Finol	0.845	24.0	0.469	0.000339

THEORETICAL ANALYSIS OF DROP MOTION AND HEAT TRANSFER PROCESS

The theory of the transfer of heat, mass and momentum, between phases where the phases may be liquid, gas or solid, is a subject that has been dealt with extensively. In this section, only those topics important in the heat transfer process occurring in drops will be discussed. The heat transfer mechanism, with respect to drops, could not be examined without an understanding of the mechanics of the drop motion. Therefore, the mechanics of drops will be discussed first, followed by a section on the heat transfer process.

Mechanics of Drop Motion

In an experimental study, such as this, there is no way of preventing heat or mass transfer from occurring during the formation period of the drop. For this reason, the mechanics of the drop formation should be discussed briefly.

Drop Formation: Three regions of drop formation are distinguishable experimentally. The first of these is the region of static drop formation, in which the drops are formed at a low enough rate so that they behave as though they were static drops. The second, is the region in which drop size is greatly dependent upon flow rate but the drops are still formed separately at the orifice. In the third region, liquid is emitted from the orifice in a jet, and drops are formed by the break up of this jet. The drops formed in the latter case are not uniform in size, and tend to rise in swarms rather than in a single stream.

In the static region of drop formation, simple theory predicts a relationship between the drop size, the diameter of the orifice or tip at which the drop is formed and the interfacial tension. The relation

can be derived by equating the buoyant force of the drop to the force exerted, due to interfacial tension, by the film connecting the drop to the orifice. Performing this operation gives the following relation for the drop volume.

$$V = \frac{\pi D_o \gamma F}{g \Delta\rho} \qquad (1)$$

In this equation, D_o is the diameter of the tip at which the drop is formed, γ is the interfacial tension and $\Delta\rho$ is the absolute value of the difference between the drop density and the continuous phase density. In the present work, the absolute system of units has been followed, so g, in equation (1), is the acceleration due to gravity. F is a factor which accounts for the shape of the film connecting the drop to the tip. For the case of bubbles, this factor can, in many cases, be assumed to be unity; however, this is not true for drops in a liquid-liquid system. Harkins and Brown[21] evaluated this factor for a number of systems and found it to vary from 0.6 to 0.75. They also found that F depended only upon the dimensionless ratio $D_o/\sqrt[3]{V}$, and was independent of any of the physical properties of the system. Equation (1), predicts a constant drop size for a particular liquid-liquid system and orifice size. In actual practice, this condition can only be approached at very low flow rates. Hayworth and Treybal[22], in their work, show a region in which the drop size increases only very slowly with increasing flow rates. This increase in drop size is due to the necessity of overcoming the additional force imposed on the drop by the accelerating continuous phase surrounding the drop. At still higher flow rates, the additional force acting in the direction of the buoyant force, due to the kinetic energy of the entering liquid, becomes important and the drop size decreases as the flow rate increases. By considering the various forces acting on the

forming drop, Hayworth and Treybal[22], were able to predict drop sizes for a wide range of physical properties and for flow rates which include the region of decreasing drop size.

Drop Rise or Fall: After separation of the drop from the forming tip, there existes a period of acceleration which ends when the drop reaches terminal velocity. Very little work has been done on the mechanics of drops in this region, and what has been done applies mostly to drops of liquid in gases. Hughes and Gilliland[25] summarize most of the work of this nature, and present a relationship by which the acceleration period can be predicted. This relationship is based upon assumptions which are valid only in the Stokes law region; and so it is not strictly applicable in the usual range of Reynolds numbers. More recently, experimental work has been done on the acceleration of small particles and drops in air streams[27] at Reynolds numbers up to 400.

The acceleration period, although important, is relatively short compared with the period during which the drop moves at a fairly constant velocity. It is felt that the best method of discussing the velocity data for drops is by comparing their drag coefficients with those for solid spheres and disks. For this reason, a short summary of drag on spheres and disks is given. In this discussion, the drag coefficient is defined as the ratio of the buoyant force of the sphere or drop divided by the cross sectional area of the sphere (equivalent sphere in the case of drops) and the impact pressure of the continuous phase.

Theoretical attempts to calculate the drag on spheres and disks have failed except for Reynolds numbers less than one. Ideal fluid theory predicts that there will be no drag on spheres or disks since these are symmetrical with respect to the direction of flow. For actual liquids, by assuming that the viscous forces are much larger

than the inertia forces, the momentum equations for flow around solid spheres and disks can be linearized and solved to yield the following relations[35].

For spheres: $$C_D = \frac{24}{Re} \quad (2)$$

For disks: $$C_D = \frac{64}{\pi\ Re} \quad (3)$$

These relations are accurate, to within a few percent, for Reynolds numbers less than about 0.7, and are shown graphically in Figure 8. By treating the inertia terms in an approximate manner, Oseen[35] was able to extend the range in which drag coefficients could be computed out to a Reynolds number of 2. Goldstein[16] solved Oseen's equation and obtained a solution which is somewhat more accurate. Since, in many applications, the Reynolds numbers encountered are much higher than this, these relations are of little help. At higher Reynolds numbers, the drag is due not only to viscous forces, but also to form drag due to the separation of the boundary layer from the surface of the sphere or disk.

Another approach to the prediction of drag coefficients is by dimensional analysis. Applying this method to the case of spheres, it predicts that there should be a functional relationship between three dimensionless groups, composed of the terminal velocity, the two densities, fluid viscosity, acceleration due to gravity and the diameter of the sphere or disk. The exact nature of the function can not be predicted by this method: However, for the case of solid spheres and disks, experimental results show that the drag coefficient is a function of the Reynolds number. Castleman[6] has summarized much of the early experimental work on drag coefficients for spheres. The experimental curve for spheres in Figure 8, was taken from these data. The experimental data for disks were taken from reference 19. The drag coefficient for spheres at

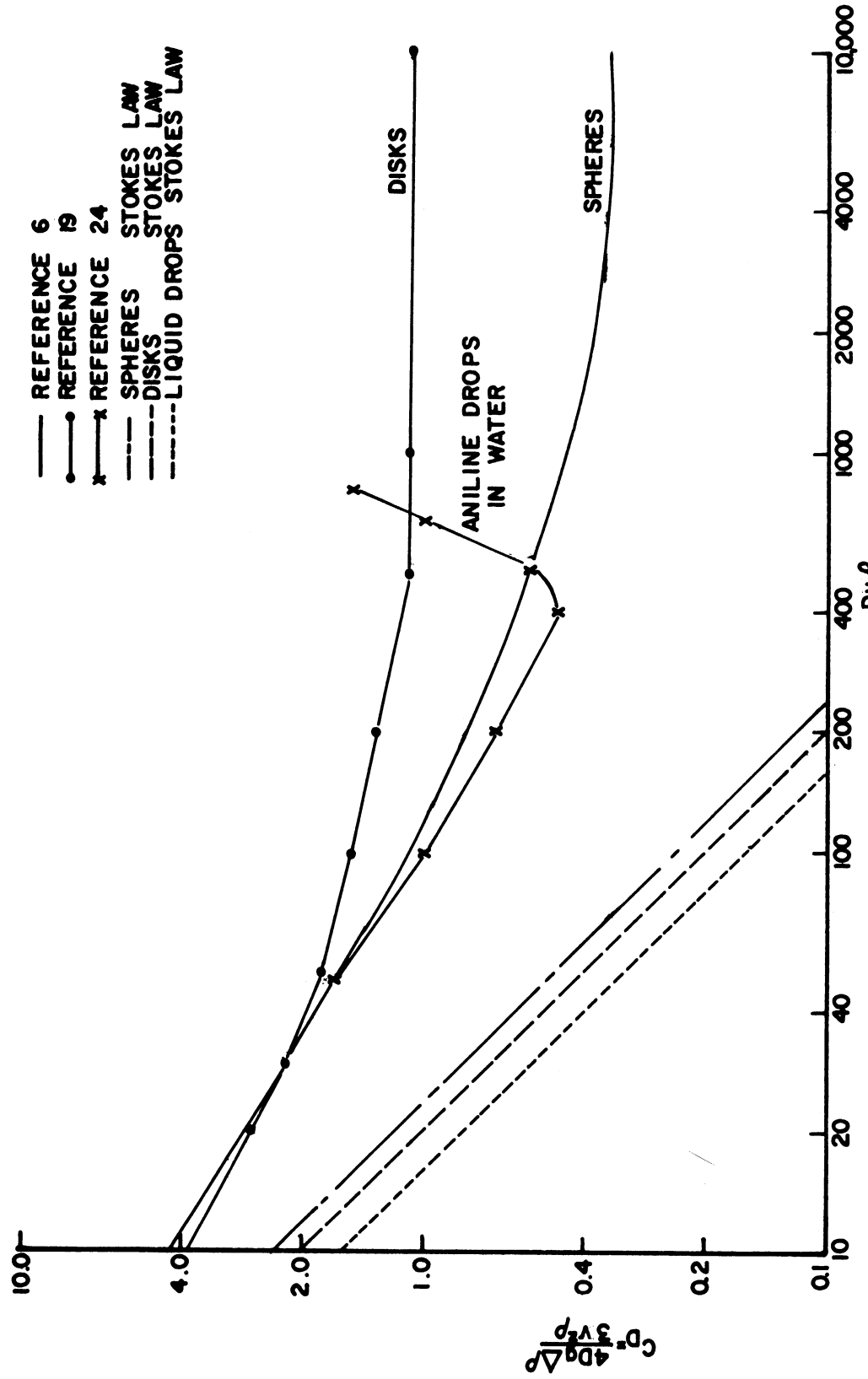

Figure 8. Drag Coefficients for Spheres and Disks

Reynolds numbers higher than those shown in Figure 8, at first approaches 0.3 and then increases slightly until a Reynolds number of around 10^5 is reached. At this Reynolds number, the drag coefficient suddenly decreases to a value of less than 0.1. This sudden drop in drag is due to the transition from a laminar to a turbulent boundary layer on the sphere. With turbulent flow persisting, the fluid in the boundary layer has a higher kinetic energy and is, therefore, more able to overcome the adverse pressure gradient occurring near the equator of the sphere. For this reason, the point of separation of the boundary layer is moved from a point on the front half of the sphere to a point just behind the equator. This shift in boundary layer streamlines the drop and thus reduces the form drag. The critical Reynolds number for spheres has no distinct value, but depends upon the roughness of the surface of the sphere and the degree of turbulence in the surrounding fluid.

Theoretical attempts to predict the drag at terminal velocity for liquid spheres and drops, like similar attempts for solid spheres, have been successful only for very low Reynolds numbers. Linearizing the momentum equations for the material inside and outside the drop yields, in the case where the drop material has zero viscosity,[35] the following relation for the drag coefficient.

$$C_D = \frac{16}{Re} \tag{4}$$

At higher drop viscosities, the value of the constant in equation (4) increases and approaches the value for solid spheres as the drop viscosity approaches infinity. Equation (4), is also plotted in Figure 8. The reduction in drag coefficient is due to the circulation occurring inside the drop which decreases the shearing forces of the continuous

phase on the drop surface. At higher Reynolds numbers, it is possible that internal circulation could have an even larger effect, for it could forestall the point at which separation occurs by increasing the average velocity in the boundary layer. Therefore, the drop would tend to be more streamlined than for the corresponding solid sphere. At still higher Reynolds numbers, viscous drag becomes less and less important and, as is shown later in the present work, the internal circulation probably effects the drag only indirectly.

Experimentally determined drag coefficients for liquid drops are not nearly so numerous as those for spheres The first systematic experimental work was done by Bond[2] and by Bond and Newton[3]. Their results were for low Reynolds numbers and indicated that circulation did not take place in some drops and bubbles due to interfacial tension. Briefly, their results can be summarized by saying that the drop diameter, at which internal circulation starts, decreases with decreasing interfacial tension and with increasing drop velocity. At higher Reynolds numbers, Hughes and Gilliland[25] have presented the existing data for liquid drops in various gases. They find that an additional dimensionless group is necessary and conclude that for these systems, the drops are probably not circulating and that the only difference between drops and solid spheres in gases is in their shape. Bubbles of air in various liquids have been studied recently by Peebles and Garber[46] and by Haberman and Morton[18]. In these systems, additional complicating factors enter due to extreme distortion and oscillation of the bubbles. For the liquid-liquid systems,Hu and Kintner[24] have recently studied the drag on drops of various organic materials in water. They were able to correlate their results empirically for a relatively wide range of Reynolds numbers.

The motion of drops through an immiscible liquid can be divided into four stages, which are:

(1) small spherical drops moving in nearly straight lines,

(2) medium size drops, flat on top, moving with a slight rocking motion,

(3) large size drops, oscillating between oblate and near prolate spheroids,

(4) drops so distorted that they tend to break up.

In the first two stages, a plot of drop velocity versus drop diameter shows that the velocity increases linearly with the diameter. At the onset of stage (3), the curve goes through a maximum and then usually decreases slightly until finally the drops are so large that they break up. The corresponding plot of the drag coefficient versus Reynolds number shows that the value of the drag coefficient follows or is slightly below the curve for solid spheres for stage (1). In stage (2), the slope increases due to the distortion of the drop and in some cases the drag coefficient may become larger than those for spheres. For stage (3), the slope of the curve becomes positive and the value of the drag coefficient rapidly approaches those corresponding to disks. The data for aniline drops in water [24] plotted in Figure 8, illustrates this behavior. Hu and Kintner[24] found that the data for the first three stages could be represented by a single curve according to equation (5), where the term, We, is the dimensionless Weber number and P is a dimensionless physical properties group.

$$C_D We P^{0.15} = \text{function of} \left(\frac{Re}{P^{0.15}} \right) \qquad (5)$$

The discussion to this point has been concerned with single spheres and drops flowing through a quiescent liquid. In the present research, a slightly different situation existed, since a whole stream of drops was studied instead of a single drop. Probably, the most obvious factor which might effect the velocity is the increase in turbulence of the continuous phase due to the passage of the drops. Another condition which could be of importance, is the circulation set up in the continuous phase due to the tendency of the drops to associate themselves with a portion of this phase. Both of these factors would tend to increase the apparent velocity above that for single drops. For the viscous region, Smoluchowski[48] has derived the following relation for the ratio of the velocity of two spheres to that of a single sphere,

$$\frac{v^1}{v} = \frac{2}{2 - 3\frac{D}{z}\left(1/2 - 3/8\,\frac{D}{z}\right)}, \qquad (6)$$

where v^1 is the velocity of the two spheres, D is the sphere diameter and z is the distance between spheres. For Reynolds numbers larger than one, equation (6) can have only qualitative significance. Other conditions in the present work which could influence the velocity are: The degree of turbulence in the continuous phase due to pumping this phase through the system, the method of forming the drops, and the presence of a temperature gradient around the drop.

Distortion and Oscillation of Drops: When discussing the drag coefficients for liquid drops, it was seen that as the Reynolds number increased beyond a certain point, the value of the drag began to increase and in some instances became larger than that for the corresponding solid sphere. This increase is due to the distortion of the drop into an oblate spheroid, thereby causing the drag coefficient to approach the value

for disks. The amount of distortion depends upon the pressure distribution inside and outside of the drop surface and the interfacial tension. The relations between these quantities and the radii of curvature at a point on the drop surface are given by the equation:

$$p_i - p_o = \gamma\left[\frac{1}{r_1} + \frac{1}{r_2}\right] \qquad (7)$$

The terms, r_1 and r_2, are the radii of curvature at the point of interest and p_i and p_o are pressures inside and outside the drop surface at this point. Hughes and Gilliland[25] have derived a method for determining the amount of distortion for drops of liquid in gases. More recently, McDonald[41] has calculated the pressure distribution around falling rain drops using equation (7), and measured values of the radii of curvature r_1 and r_2. Both of these references neglect the effect of internal circulation upon p_i, and McDonald[41] shows that this is a valid assumption for drops of water in air. For other systems where the interfacial tension is appreciably lower and for liquid-liquid systems, this assumption probably no longer applies.

If distortion was the only phenomenon that occurred as the drop size was increased, the value of the drag coefficient would probably approach the value for flat disks asymptotically. However, upon increasing the Reynolds number further, the drops begin to oscillate rapidly between oblate and near prolate spheroids. The drag coefficient in this range increases rapidly until a point where break up of the drops occurs. The oscillation of moving liquid drops is undoubtably due to the periodic discharge of eddies into the wake of the drop and, as will be shown later in this work, drop break up occurs when the frequency of this discharge reaches the natural frequency of vibration for the drop. Since the frequency of vortex discharge in the wake of drops is responsible for their

oscillation, some of the previous work done on the frequency of this discharge from behind spheres and disks will be mentioned briefly. Stanton and Marshal[50] studied the wake of circular disks in water photographically. They found that for Reynolds numbers in the range of 5 to 195, there exists a permanent vortex ring behind the disk, and that increasing the Reynolds number above 195 causes pieces of this ring to discharge periodically into the wake. Moller[45] determined, from motion pictures of spheres being dragged through water, the frequency of discharge of material in the wake. He found that the frequency of this discharge depended only upon the Reynolds number.

Effect of Surface-Active Agents: Surface-active materials, if present, collect at the drop surface as a film and it would be expected that this would effect the hydrodynamics of the drop. It was found in some of the work mentioned below, that these films were capable of supporting shear at the drop surface and thereby reduced internal circulation. Garner and Skelland[14] observed visually the effect of surface-active material on internal circulation in drops of nitrobenzene falling through water. They found that circulation tended to damp out, starting at the rear pole and progressing toward the front of the drop. They also found that the drops did not start to oscillate until a much larger drop size was reached and that the velocity and distortion of the impure nitrobenzene drops was considerably less than that for pure nitrobenzene. Lindland and Terjesen[38] made similar observations with respect to the effect of surface-active agents on drop velocity. Garner and Hale[12] found that the diameter at which internal circulation first starts, increases sharply as the concentration of surface-active material is increased. All of these authors point out that these effects have been observed at concentrations of surface-active agents which are low enough

so that there is only a small change in interfacial tension. Haberman and Morton[18] found that the velocity of air bubbles rising in filtered tap water was higher than when unfiltered water was used. They attribute this to suspended solids which collect at the bubble surface, making it behave more like a solid sphere. In the latter work, there was no difference in surface tension between the filtered and unfiltered water.

Mechanism of Heat Transfer to Drops

The effect of various factors on the mechanics of drops has been discussed in the last section. In this section, the relation between the mechanics of the drop and the rate of heat transfer to the drop will be derived. A fairly complete mathematical statement of the problem will be made first, followed by several sections in which the general problem is simplified so that a solution may be obtained. The assumptions necessary to make these simplifications are discussed and the conditions under which they are valid are given.

Statement of Problem: A general solution to the problem of heat transfer to a liquid drop would give the temperature, at all points inside and outside the drop, as a function of time. To obtain this solution, the equations of motion, continuity and energy would have to be solved simultaneously along with the associated boundary conditions for both the material inside and outside of the drop. If the physical properties of the phases are not constant, then additional equations must be included to account for the variation in these properties with temperature and pressure. If the fluid is assumed incompressible, and the viscous dissipation of energy is neglected, then for one phase, the principle equations to be solved are:

the three equations of motion of the type,

$$\rho \frac{Du}{D\theta} = \frac{\partial p}{\partial x} + \rho X + \frac{\partial}{\partial x}\left(\mu \frac{\partial u}{\partial x}\right) + \frac{\partial}{\partial y}\left(\mu \frac{\partial u}{\partial y}\right) + \frac{\partial}{\partial z}\left(\mu \frac{\partial u}{\partial z}\right) \tag{8}$$

the equation of continuity,

$$\frac{\partial u}{\partial x} + \frac{\partial v}{\partial y} + \frac{\partial w}{\partial z} = 0 \tag{9}$$

and the energy equation,

$$\rho C_p \frac{DT}{D\theta} = \frac{\partial}{\partial x}\left(k \frac{\partial T}{\partial x}\right) + \frac{\partial}{\partial y}\left(k \frac{\partial T}{\partial y}\right) + \frac{\partial}{\partial z}\left(k \frac{\partial T}{\partial z}\right) \tag{10}$$

For equations 8, 9, 10, the velocities u, v, and w are in the x, y and z directions respectively, X is the body force in the x direction, μ is the viscosity, C_p is the liquid specific heat and k is the thermal conductivity. The viscosity and thermal conductivity are assumed to vary not only with temperature, but also if the flow is turbulent; they are assumed to contain the eddy viscosity and conductivity to correct for the turbulent transfer of momentum and heat. Writing a similar set of equations for the other phase gives a total of ten equations which must be solved along with the equations giving the variation of the physical properties with temperature and the boundary conditions. The solution of such a set of equations would be extremely difficult, particularly due to the nonlinearity in the equations of motion. This, along with the uncertainty of the values of the eddy terms and the nature of the flow after the point of separation, makes a regorous solution, at the present time at least, impossible. If it is assumed that the physical properties are independent of temperature, or if the correct average value of each property is known, then the hydrodynamic equations may be studied independently of the temperature equations.

If the above assumption with respect to physical properties is made, then numerically it should be possible to obtain the temperature

distribution in the low Reynolds number range, where the solution of the linearized equations of motion is valid. However, the accuracy of any attempt of this nature would depend, to a great extent, on the values assumed for the various physical properties. In view of these difficulties, no attempt was made to solve even this vastly simplified problem.

The method of describing the problem which was finally decided upon is as follows: it was first assumed that one of several possible types of flow patterns existed inside the drop. This flow pattern was then used, along with an energy equation, to obtain the temperature distribution in the drop. Finally, it was assumed that the heat flux at the surface of the drop was the same at each point and was given by the following equation.

$$\text{Flux} = Q/A_d = h(t - T_s) \tag{11}$$

In this equation, T_s is the temperature of the drop surface, t is the bulk temperature of the continuous phase and h is the heat transfer coefficient in the fluid surrounding the drop. In the general case, T_s would vary over the surface of the drop. However, in this work due to the assumed flow patterns and other assumptions, it is independent of location and varies only with time. If an energy balance is now made around the drop, the following relation is obtained.

$$\rho_d C_{p_d} \int (T - T_i)\, dV = hA_d \int_0^{\theta} (t - T_s)\, d\theta \tag{12}$$

The temperature T_i is the initial drop temperature and T is the drop temperature at time, θ. The suscript d refers to drop properties. Equation (12) may be thought of as the defining equation for the heat transfer coefficient, h. This equation was chosen as the definition of h rather than equation (11), because it clearly shows the dependence of h upon the assumed temperature distribution inside the drop. To evaluate

the coefficient h, the temperature distribution inside the drop is required. This temperature distribution was obtained by assuming that the conditions inside the drop can be approximated by one of the three models described below.

Completely Mixed Drops: In this model, it was assumed that the motion of the material inside the drop was so turbulent that it could be considered completely mixed, or in other words, the resistance to heat transfer inside the drop is negligible. This being the case, no temperature gradients would exist inside the drop and, therefore, the drop temperature would vary only with time. A differential heat balance around the drop yields the following relation for the temperature of the drop as a function of time.

$$\frac{t - \overline{T}}{t - \overline{T}_i} = \exp\left[-\frac{hA_d\theta}{Cp_d V_d \rho_d}\right] \tag{13}$$

A complete derivation of equation (13), is given in Appendix C.

The assumption of complete mixing is not the only manner in which an equation similar to equation (13) may be obtained. For example, if h is considered to be an overall heat transfer coefficient based upon the difference between the continuous phase temperature and the average temperature of the drop, then the relation between temperature and time is still given by equation (13). This latter method was used by Garner and Skelland[13] to analyze mass transfer results for the extraction of acetic acid from nitrobenzene drops in water. Another example, is the case of a stagnant drop composed of a material whose thermal conductivity is extremely high. For this case, it would be possible for the temperature gradient inside the drop to be small enough, in comparison to the gradient outside the drop, to be considered uniform. This would probably be the case for drops of a liquid metal in water or an organic material.

Because of the number of ways to arrive at equation (13), it would be expected that it would satisfactorily describe most experimental data on heat or mass transfer to drops. The reason for this becomes more obvious after discussing the other drop models considered.

Internally Circulating Drops: In the discussion on the mechanics of drops, it was mentioned that a solution existed for the velocity distribution for the material inside and outside of a liquid drop. It was pointed out that this solution was valid only in the Stokes law region and that it could not be expected to predict drag coefficients for Reynolds numbers larger than one. The differences between the calculated and actual drag coefficients at higher Reynolds numbers is primarily due to the increasing effect of inertia forces which, in combination with the separation of flow from the surface of the drop, cause an additional drag on the drop. Therefore, the departure from Stokes law is primarily a phenomenon associated with the continuous phase and it is possible that conditions inside the drop would remain approximately as calculated up to a higher range of Reynolds numbers. That this is the actual case is shown by the results of two investigators, whose work will be described.

The velocity distribution for the material inside the drop was obtained[35] by simultaneously solving the linearized equations of motion with the boundary condition that the velocity, and tangential and radial forces should be continuous at the surface of the drop. This solution gives rise to equation (14), for the streamlines inside the drop.

$$\psi = \frac{g\Delta\rho}{6(2\mu + 3\mu_d)} (a^2 - r^2) r^2 \sin^2 \varphi \qquad (14)$$

In this equation, ψ is the stream function for the flow inside the drop, a is the drop radius, r is the distance measured radially from the center of the drop, and φ is the polar angle. Figure (9) shows a few of these

streamlines for one half of a drop. The stream surfaces are given by revolving this figure around the vertical axis. Even though this flow pattern was derived for flow in the Stokes law region, Spells[49] and Garner and Skelland[14] have shown that it exists at much higher Reynolds numbers. Spells[49] used drops of a glycerin-water mixuture in mineral oil, the internal flow pattern being made visible by the effect of shear on the glycerine-water system. Pictures taken of these drops show very clearly that the flow is of the type predicted by equation (14). These pictures also show that the effect of separation and of drop distortion is to shift the "dead zone" inside the drop towards the forward stagnation point. On the basis of these observations, it seems reasonable to assume that the streamlines for circulation inside spherical drops are given by an equation similar to (14), in which the physical property group is replaced by a constant whose exact value is not known. To obtain the temperature distribution or the average temperature of the drop, the partial differential equation for the conduction of heat under the conditions which exist inside the drop must be solved.

A general solution for conduction in a system as described above would give the temperature in terms of two space variables and time, the third space variable not being required because the system is symmetric about the vertical axis. The general differential equation applying to this case was derived by Kronig, van der Veen and Ijzerman[34]. These authors also obtained an approximate solution for the equation where it was assumed that the temperature at the surface of the drop was at all times equal to the continuous-phase temperature. This solution was not found applicable to any of the heat ransfer results in the present work. A solution to the problem of circulating drops which was found more applicable to the present work, makes the assumption that the circulation

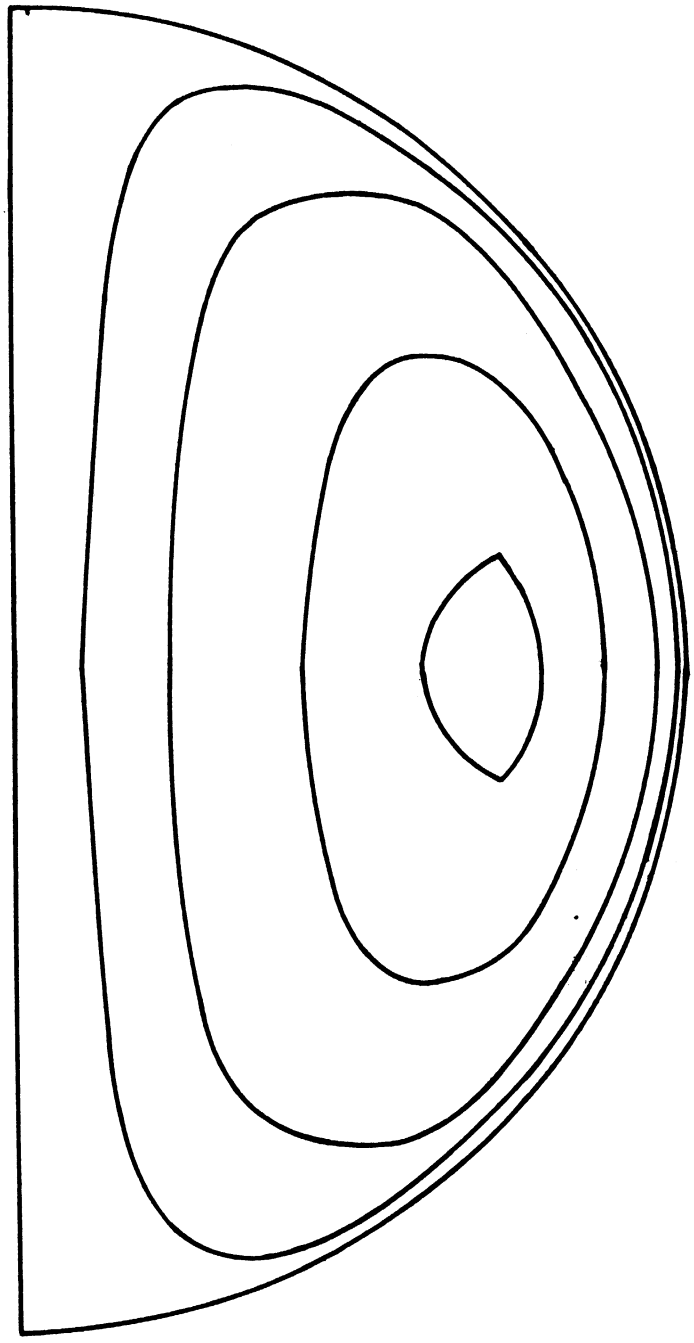

Figure 9. Streamlines for Circulating Drops

time of the material inside the drop is short compared to the time required for heat to be conducted in the drop. With this assumption, the change in temperature along a streamline is small and the streamlines are, to a good approximation, the isotherms for the conduction inside the drop.

Kronig and Brink[33] made this latter assumption and reduced the problem to one in which the drop temperature was a function of time and one space variable. These authors obtained their solution by a numerical method and only for the case where the drop surface is at all times at the temperature of the continuous phase. In the present work, a slightly more accurate solution was obtained using an electronic differential analyzer, and the solution was extended to include the cases where the value of the heat transfer coefficient at the drop surface is finite. The equation for the solution obtained by Kronig and Brink[33], which is also in the form used in the present work, is given by equation (15).

$$\frac{t - \bar{T}}{t - T_i} = 3/8 \sum_{n=1}^{\infty} B_n 2 \exp \left[-\lambda_n \frac{16 \alpha_d}{a^2} \theta \right] \qquad (15)$$

In this solution, the bar above the drop temperature indicates that this is an average value. The values of the coefficients B_n and the eigenvalues λ_n depend upon the value of the heat transfer coefficient h. This dependence is shown plotted in Figure 10, for λ_1. Table X (appendix D) gives the first three eigenvalues and constants for a wide range of the film coefficient. Appendix D contains a brief summary of Kronig and Brink's derivation of equation (15), and the extension of this work to account for a finite value of the film coefficient. This appendix also contains the computer program for obtaining the coefficients, B_n and the eigenvalues λ_n.

In equation (15), the first eigenvalue varies from about 0.2 to 1.7 in the range investigated, the second eigenvalue varies from 4 to 10 in the same range, and the third eigenvalue varies from 10 to 25. Therefore, after a very short time, all terms after the first term become negligible and equation (15) takes the same form as equation (13). It should be emphasized that this similarity does not exist in the region of zero time and for this reason, extrapolation of experimental results back to zero time using a relation of the form of equation (13), is not in all cases valid.

Stagnant Drops: The final model used to represent the temperature distribution inside the drops was conduction in a solid sphere. The work of Bond and Newton[3], which has been mentioned earlier, showed that very small drops did not circulate because of the lack of the energy required to overcome the surface forces. Larger drops which did not circulate due to the presence of surface active agents, were observed by Garner and co-workers. For these reasons, the existence of a completely stagnant drop could not be overlooked.

In this case, as in the case of circulating drops, the general solution would yield a function expressing the temperature of the drop in terms of time and two space variables. However, with the assumption that the heat transfer coefficient is constant over the surface of the drop, one of the space variables can be eliminated. The resulting surfaces of constant temperature are concentric about the center of the sphere. The solution of the corresponding differential equation, along with the associated boundary conditions, yields the following relation for the average temperature of the drop.

$$\frac{t - \bar{T}}{t - \bar{T}_i} = 6 \sum_{n=1}^{\infty} C_n \exp \left[- \psi_n^2 \frac{\alpha_d \theta}{a^2} \right] \qquad (16)$$

In equation (16), as in equation (15), the value of the coefficients C_n and the eigenvalues ψ_n depend upon the heat transfer coefficient. The method of obtaining equation (16), and the determination of C_n and ψ_n are given in Appendix E. Table XI gives the values of C_n and ψ_n for a range of values of a dimensionless group containing the heat transfer coefficient. The eigenvalue ψ_1 is shown graphically in Figure 10. Equation (16) also reduces to the form of equation (13) after a sufficient length of time. The time required for the remaining terms to become negligible is somewhat longer in this case than for circulating drops due to the relative closeness of the eigenvalues.

The preceding paragraphs have discussed three possible models which would describe the temperature distribution inside a drop. The model used, depends upon whether the drop is assumed to be completely mixed, circulating or stagnant. It has been shown that in all cases after a sufficient length of time, the relations reduce to the form of equation (13). The importance of this is that, in evaluating experimental data by using a plot of $(t - \overline{T})$ versus θ, nothing whatsoever can be told about the conditions existing inside the drop unless data are available for the region near zero time, and experimental difficulties make accurate data of the latter type impossible to obtain. Therefore, it can be concluded that in most cases, some independent method is required through which the conditions existing inside the drop can be determined.

Heat Transfer Coefficient Outside Drop: The discussion up to this point has been concerned primarily with the mechanism of heat transfer inside the drop. To describe this transfer, three models were postulated which approximated the conditions that could exist in actual drops. The conditions in the fluid outside the drop are even more

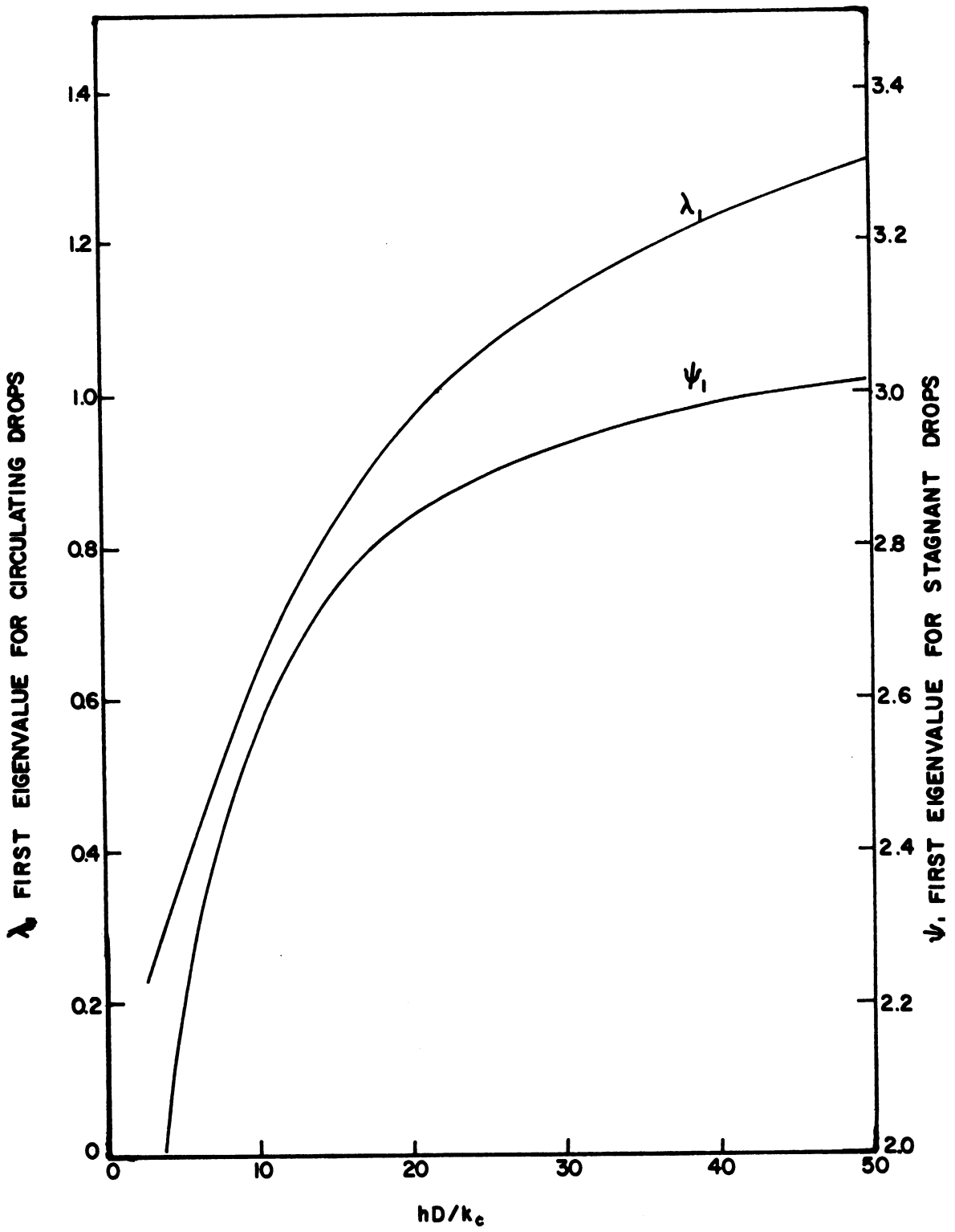

Figure 10. First Eigenvalues for Circulating and Stagnant Drops Versus System Properties

complex, and are not subject to treatment by a simple model. For this reason, the present section will be devoted to existing theories and experimental work which contribute to the knowledge of the mechanism of heat transfer through the fluid surrounding the drop. The discussion will at first be limited to solid spheres and will then be generalized as much as possible to include liquid drops.

Treating the problem of heat transfer to solid spheres by dimensional analysis, shows that the Nusselt number is a function of the Prandtl number and the Reynolds number as given by equation (17).

$$Nu = f(Pr, Re) \tag{17}$$

The exact nature of the function in (17), must be obtained either experimentally or from some theoretical consideration. Before a theoretical attempt can be made to evaluate equation (17), some assumption must be made as to the nature of velocity distribution around the sphere.

One such assumption is to assume that the fluid surrounding the drop is non-viscous and incompressible. Making this assumption, Johnstone and co-workers[30] modified the Boussinesq equation for flat plates to obtain the following relation for spheres:

$$Nu = 0.714\sqrt{Pr\ Re} \tag{18}$$

These authors also obtained an entirely different functional relation for the Nusselt number by assuming that the motion of the fluid at the surface of the sphere is tangential with a velocity equal to the velocity of the free stream. These equations were applied with some success to the transfer of heat to clouds of very fine drops.

If it is assumed that the heat is transferred through a laminar boundary layer surrounding the drop, then boundary layer theory can be used to predict the nature of equation (17). Neglecting the effect of temperature on physical properties, laminar boundary layer theory predicts

the following relation for the average value of the Nusselt number on a flat plate.

$$Nu = 0.664\ Pr^{1/3}\ Re^{1/2} \tag{19}$$

The extension of boundary layer theory to surfaces of revolution by Millikan[44] permitted Tomotika[51] to determine the boundary layer thickness on a sphere. The results of this show that the thickness up to the point of separation is given by:

$$\delta = \frac{D}{\sqrt{Re}} f(\varphi).$$

In this equation, φ is the angle from the forward stagnation point. For laminar flow, it can be shown[11] that the thickness of the thermal boundary layer is $(Pr)^{-1/3}\ \delta$. Therefore, it would be expected that the Nusselt number would vary over the surface of the sphere as shown in the following equation.

$$Nu = C\ Pr^{1/3}\ Re^{1/2}\ f(\varphi) \tag{20}$$

Although the derivation of this equation is somewhat intuitive, the form has been satisfactorily established by Cary[5]. This author measured point heat transfer coefficients on spheres in air, and found that the Nusselt number varied as the square root of the Reynolds number on the front half of the sphere. On the rear half of the sphere, after the point of separation, boundary layer theory is no longer applicable, and he found that the Nusselt number varied as the Reynolds number to the 0.59 power. Integrating these point values over the surface gives the following relation for the average value of the Nusselt number for spheres in air.

$$Nu = 0.37\ Re^{0.53} \tag{21}$$

For fluids other than air, the constant in this equation varies with the Prandtl number in some undetermined fashion. By comparison with the

numerous experimental results for cylinders in normal flow, this constant might be expected to vary as the Prandtl number to the 1/3 power. At lower Reynolds numbers, Kramers[32] correlated experimental data for spheres in air, water and oil. His relation for the Nusselt number is:

$$Nu = 2.0 + 1.3Pr^{0.15} + 0.66Pr^{0.31} Re^{0.5}. \qquad (22)$$

In equation (22), the first two terms are usually small compared with the third term, so that the Nusselt number does vary approximately as predicted previously. This equation preducts values which are approximately twenty percent higher than those predicted by Cary[5].

The relations predicted so far, have been based on laminar boundary layer theory and therefore, are applicable for Reynolds numbers below the critical value. In the present work, the Reynolds numbers encountered were well below the critical values for spheres. Therefore, it would be expected that the above discussion would apply here. However, in those cases where the drops were observed to oscillate rapidly, the existence of anything resembling a laminar boundary layer cannot be imagined and therefore, these cases would be expected to deviate from the above theory.

A slightly different approach to the problem of determining the Nusselt number is through use of the penetration theory first proposed Higbie[23]. This theory is based on the premise that in many two-phase contact operations, the contact time is so short that the transfer of heat or mass is comparable to that of conduction or diffusion into a material which is semi-infinite in extent. This theory was used successfully by Higbie[23] to correlate data for the diffusion of carbon dioxide into a surrounding liquid. It has also been applied successfully to absorption data for wetted wall columns and wetted spheres by Lynn and

co-workers[39]. The relation for the Nusselt number is:

$$Nu = 1.13\sqrt{\frac{\rho C_p D^2}{k\theta_c}} \tag{23}$$

In this equation, θ_c is the contact time which is the length of time an element of liquid in the continuous phase is in contact with the surface of the drop. It is interesting to note that if θ_c is assumed equal to the time required for the drop to travel one drop diameter, that is:

$$\theta_c = \frac{D}{\bar{v}} \quad , \tag{24}$$

then equation (23) reduces to:

$$Nu = 1.13\sqrt{Pr\ Re} \tag{25}$$

which is the Boussinesq equation for heat transfer for potential flow over flat plates. For the actual case, the contact time would always be greater than that predicted by equation (24). In any case, it appears that the exponent on the Reynolds number should be close to one half and that the exponent on the Prandtl number should be somewhere between one third and one half. The exact value of the exponent to be used here is in some doubt, but for stagnant drops, since these approximate solid spheres, the value would probably be close to one third. For circulating drops, the conditions at the drop surface approach that of zero traction which is the boundary condition used for nonviscous fluids and for this case, the exponent would probably be close to one half. If this latter statement is correct, then the exponent on the Prandtl number would depend, in some manner, on the amount of circulation inside the drop. Another point that is in doubt, is the calculation of the contact time by using the drop velocity. A better approximation to the contact time could be obtained by using the surface velocity of the fluid inside the drop, since this velocity, when used in equation (24), would give the

average contact time between the drop surface and an element of the continuous phase. This velocity not only depends upon the drop velocity, but as an examination of the equations of motion for the fluid inside the drop will show, it also depends upon the drop viscosity and density. Including these in the analysis for the Nusselt number would introduce the ratio of the drop viscosity to that of the continuous phase and the ratio of densities as additional dimensionless groups. If the form of equation (25) is maintained, then the new dimensionless groups may be considered as coefficients which adjust the drop velocity to give the correct value for the contact time in equation (24).

Another factor which must be considered, is the distortion of the drop due to the forces exerted by the fluid inside and outside the drop. The additional variable of importance here is the interfacial tension. With the system of units used so far in this analysis, the dimensionless interfacial tension group becomes:

$$M = \frac{D\gamma\rho}{\mu^2}$$

If this group is considered as a coefficient which adjusts the drop diameter in equation (24) to give the correct contact time, then the complete relation for the Nusselt number would have the following form:

$$Nu = m\left(\frac{\mu_d}{\mu}\right)^n \left(\frac{\rho_d}{\rho}\right)^o \left(\frac{D\gamma\rho}{\mu^2}\right)^q \sqrt{Pr\ Re} \qquad (26)$$

where the exponent on the Prandtl number is taken as one half on the supposition that the drops circulate.

Although the above analysis takes into account most of the important variables, there are other factors which may effect the heat transfer rates. One of these factors is the turbulence in the continuous phase

due to the motion of the drops and the circulation of this phase through the system. It would be difficult without actual experimental measurements to determine what effect the continuous phase turbulence has on the heat transfer rates, especially since there is no way to foretell the turbulence level in the equipment. Comings and co-workers[9] determined experimentally the effect of turbulence on heat transfer from a heated cylinder normal to an air stream. Although the turbulence level was shown to have some effect at higher Reynolds numbers, there was no measurable effect at Reynolds numbers below 1800, when the turbulence level was increased from between one to three percent up to seven to eighteen percent. These authors also state that a turbulence level of one to three percent is about the normal amount of turbulence for an unobstructed duct at Reynolds numbers between 4000 and 200,000. In the present work, the Reynolds number for the test section never exceeds 4500, and even though the level of the turbulence is not known, it is not expected to be large enough to appreciably affect the heat transfer.

In the discussion of the mechanics of drops, it was mentioned that the presence of a temperature gradient in the neighborhood of the drop would change the physical properties in this region and therefore, would effect the drop mechanics. In heat transfer, there would not only be the influence of the effect on drop mechanics, but also the effect of natural convection could be important. Kramers[32] has determined experimentally where the effect of natural convection became measurable and therefore, the conditions under which it might be measurable, in the present work, could be estimated. Another factor of lesser importance is the effect of mass transfer to or from the drop on the heat transfer. In

the present work, the mutual solubilities of the phases are low and computations have shown that mass transfer effects are negligible, for most of the systems tested.

In the present section, various factors affecting the heat transfer rate to drops have been discussed, and it has been shown that models can be set up which should predict the conditions existing inside completely mixed drops, circulating drops, and stagnant drops. Also in this section, theory and previous experimental work has been used to determine the form of the equation for the heat transfer coefficient on the outside of the drop. Some of the factors mentioned briefly in this section will be mentioned again in more detail in the discussion of experimental results.

DATA PROCESSING

This section will discuss the reduction of the experimental data to a form in which it can be used for final analysis and correlation. All of the reduced experimental data, except for a few preliminary runs are given in Table IV. Each item in this table will be discussed briefly.

Run Number: The first column in Table IV gives the run numbers. This number is composed of three parts. The capital letter prefix designates the system used and is the same as the letter used to designate each system in Table II. Runs for a single system were numbered consecutively and these numbers appear next in the run number. The small letter at the end denotes which nozzle was used and is the same as the letter assigned to each nozzle in Table I. An asterisk preceding the run number indicates that the drops were observed to oscillate during the run.

Continuous Phase Temperature: The continuous phase temperature is the average of the temperatures given by thermocouples four and five.

Average Drop Temperature: This temperature was calculated by taking the time average of the drop temperature over the length of the test section, these temperatures having been corrected by means of the drop collector calibration curves (Figure 30). In most cases, this average is only slightly higher than the average of the inlet and final drop temperature.

Drop Diameter: The drop diameter was defined as the diameter of a sphere having the same volume as the drop. It was computed using the measured flow rate of the drop material in grams per second, the drop density and the drop frequency.

Drop Velocity: In most runs, this was computed from still pictures of the whole stream of drops in the test section, and the drop

frequency. The drop velocity is the product of the drop frequency and the average distance between drops determined from the pictures. In most runs, two or three pictures of this type were taken and the average used, however, in the first twenty runs of system A, only one picture was taken so these are slightly less reliable. Motion pictures taken at 32 frames per second, were used to obtain the velocity in runs B4 to B14. From these motion pictures, the period of acceleration could also be observed. From an analysis of the results from the motion picture study and those from still pictures, it was found that only one fourth of the still pictures gave a velocity which was within two percent of the average velocity as determined by motion pictures. However, ninety percent of the still pictures gave velocities which were witnin four percent of the average velocity. Therefore, in runs where only one still picture was taken, the error could be higher than four percent but in most cases is less than this. For runs in which two or three pictures were taken, the error was most likely always less than four percent. In all systems, the time required for several drops to rise a known distance was also measured. Since the time of rise for many drops was about 0.2 seconds, the velocity computed from these may have errors up to seven percent.

Drop Frequency: The drop frequency was obtained, in most cases, by measuring the time interval for twenty five to fifty drops to emerge from the nozzle. In those runs where motion pictures were taken, the frequency was obtained directly from these pictures. The higher frequencies reported in the A system runs were obtained indirectly from the still photographs, and a velocity determined from a plot of Reynolds number versus drag coefficient for the system. This procedure is based on the premise that the frequency has no effect on the velocity. This latter

was found to be true from the motion picture data and by actually timing rising drops at different frequencies.

Drop Drag Coefficient: The density of the drop material used in calculating this quantity was taken at the average drop temperature reported in column three. Likewise, the continuous phase density was taken at the temperature reported in column two. The calculation of the ratio of drop volume to drop area was made on the basis that the drop was spherical, so that this ratio becomes proportional to the drop diameter described above. The square of the drop velocity is used in determining the drag coefficient, so that any error in velocity is considerably magnified here.

Drop Reynolds Number: This quantity was determined using densities and viscosities at the temperature of the continuous phase reported in column two. The equivalent spherical diameter was used along with the drop velocity to complete the calculation.

Ratio of Maximum Diameter to Minimum Diameter: This ratio was computed directly from measurements made on photographs of individual drops taken during each run.

Drop Surface Area: Since most of the drops observed in this work were deformed in the shape of oblate spheroids, their surface area was obtained from a plot of surface area versus drop volume for oblate spheroids with the difference between the major and minor axis as a parameter. The data for these curves were taken from reference[53]. For oscillating drops, the area of the equivalent sphere was used if the drops were observed to oscillate between an oblate and prolate spheroid, otherwise, average values of the major and minor diameters taken from several photographs were used in conjunction with the curve mentioned previously. This method of determining surface area was checked for a greatly deformed

non-oscillating drop by numerical integration of dimensions taken from a projected image of the drop. The integrated value was found to agree with the value read from the above curves to within two percent.

Slope of $\log_{10}(t - \bar{T})$ versus z: The details of computing this slope from the experimental data are given in the sample calculations, Appendix F. However, some of the less obvious points will be discussed here. The quantity $(t - \bar{T})$ is the difference between the continuous-phase temperature and the average drop temperature, and z is the distance the drops have traveled to the point of collection. A quantity which is proportional to $(t - \bar{T})$, was computed from the experimental data by differencing the e.m.f. representing the average continuous-phase temperature, and that produced by the thermocouple in the drop collector. This procedure was valid, since it was found that the temperature was a linear function of e.m.f. to an approximation well within the experimental error in temperature measurements, and since the correction factor for the drop collector, as explained in Appendix B, is a constant for any one run. The logarithm of this difference in e.m.f. may be used directly to compute the desired slope, since its derivative is equal to the derivative of the logarithm of $(t - \bar{T})$. The best slope for each run was determined from the experimental data by the method of least squares.

Figure 11, is a plot of the logarithm of the difference in e.m.f. versus distance, taken from the original data for one run from each of the six systems studied. The data shown in this figure are all for approximately the same size drop. This figure shows not only the scatter of the data, but also shows that the data are well represented by a straight line.

Nusselt Numbers for Each Run: The last three columns in Table IV, contain the Nusselt numbers computed for each run. In general, there

will be three of these quantities for each run. The first Nusselt number assumed that the drop was completely mixed and therefore, was computed from the slope, discussed above, in conjunction with equation (13), and the drop velocity. The Nusselt number, assuming the drop to be circulating, was determined by first computing the first eigen value λ_1, using the above slope, the first term of equation (15) and the drop velocity. The first eigen value λ_1 was then used on a graph, similar to Figure 10, only on an expanded scale, to determine the quantity $h\ D/k_d$, from which the corresponding Nusselt number could be found simply by multiplying by the ratio of the thermal conductivity of the drop material to the thermal conductivity of the continuous phase. The Nusselt number, assuming the drop to be stagnant, was computed in a similar manner using equation (16), and the curve for ψ_1 on Figure 10.

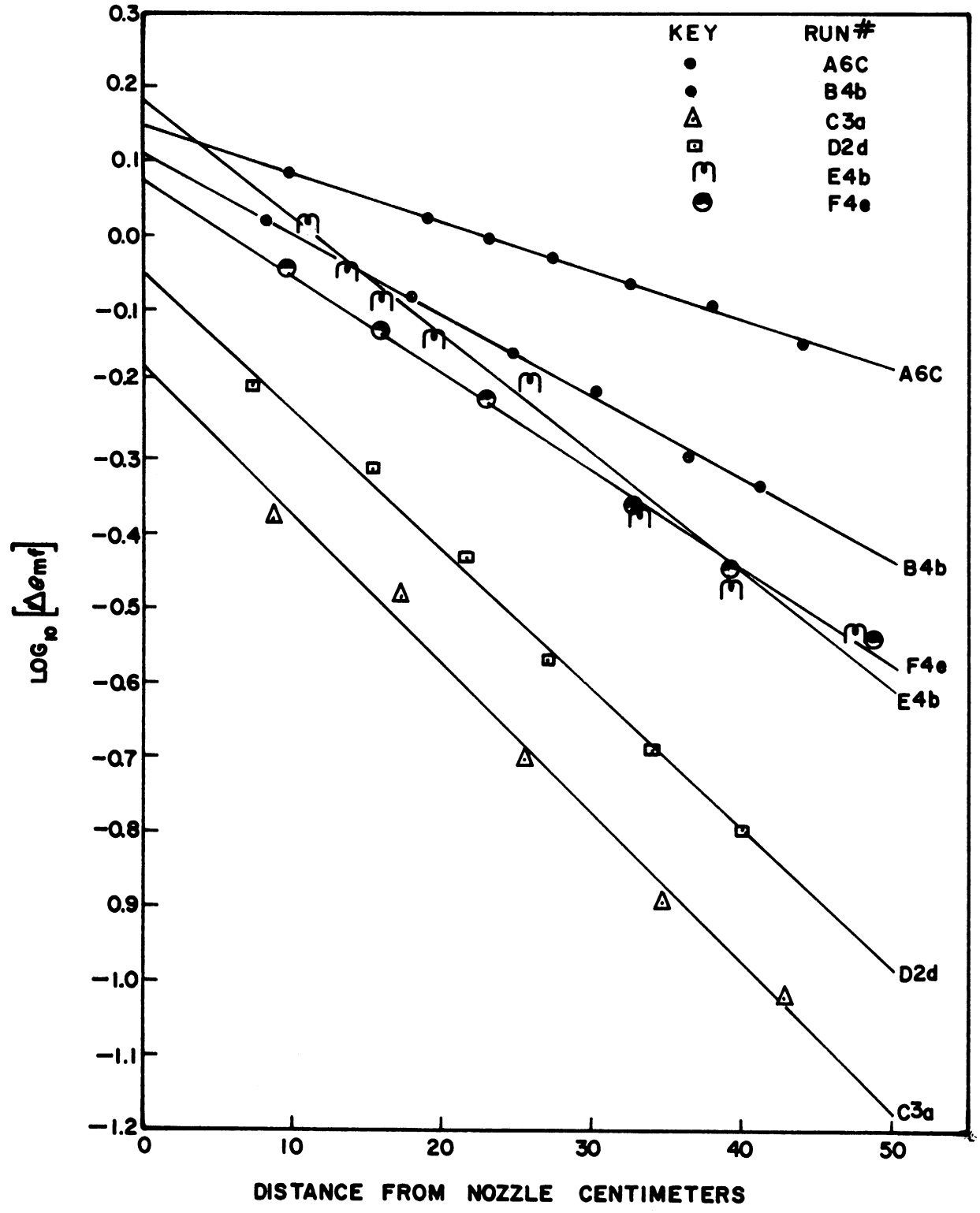

Figure 11. Typical Experimental Data from Each System

TABLE IV

QUANTITIES COMPUTED FROM EXPERIMENTAL DATA

Run No.	Continuous Phase Temperature °C	Average Drop Temperature °C	Drop Diameter Cm.	Drop Velocity cm/sec	Drop Frequency $(sec)^{-1}$	Ratio of Diameters	Drop Drag Coefficient	Drop Reynolds Number	Drop Surface Area $(cm)^2$	Slope of $\log_{10}(t-\bar{T})$ versus Z $(cm)^{-1}$	Nusselt Number = $\frac{hD}{k}$ Completely Mixed Drop	Circulating Drop	Stagnant Drop
A1b	57.2	48.0	0.361	12.0	2.57	1.10	0.729	636	0.413	-0.0141	28.3	39.0	105
A2b	57.0	45.5	0.367	12.1	1.43	1.22	0.732	647	0.428	-0.0113	23.5	29.3	49
A3b	77.3	60.0	0.353	13.3	2.80	1.15	0.565	775	0.396	-0.0162	35.1	50.4	
A4b	77.3	63.7	0.364	13.6	1.39	1.16	0.566	815	0.420	-0.0188	44.3	69.0	
A5c	58.5	37.2	0.475	13.0	5.84	1.22	0.807	915	0.719	-0.00812	30.5	43.7	250
A6c	59.5	37.8	0.508	13.2	2.86	1.27	0.832	1000	0.823	-0.00652	28.4	40.3	131
A7c	59.7	41.1	0.505	13.2	1.16	1.27	0.830	997	0.817	-0.00726	31.1	45.8	296
A8c	78.8	48.5	0.500	14.4	2.95	1.25	0.673	1189	0.814	-0.00783	36.2	53.9	
A9c	79.5	55.6	0.493	14.4	1.19	1.22	0.667	1177	0.791	-0.00875	39.2	60.7	
A10d	58.2	33.0	0.607	13.6	1.66	1.29	0.909	1221	1.16	-0.00593	37.9	58.1	
A11d	58.2	32.1	0.624	13.7	3.08	1.33	0.936	1260	1.24	-0.00418	28.5	40.4	149
A12d	58.2	32.1	0.609	13.7	4.91	1.26	0.916	1231	1.18	-0.00571	37.2	56.3	
A13d	80.6	42.6	0.604	13.7	5.06	1.37	0.910	1379	1.16	-0.00630	41.1	64.2	
A14d	80.9	42.0	0.648	13.2	1.42	1.34	1.01	1428	1.34	-0.00605	43.7	71.4	
A15e	58.2	33.0	0.671	13.4	2.08	1.32	1.07	1323	1.44	-0.00545	41.9	68.4	
A16e	58.0	30.7	0.644	13.6	4.25	1.28	0.967	1290	1.32	-0.00494	35.6	53.1	
A17e	80.1	42.8	0.597	13.8	5.26	1.18	0.855	1361	1.14	-0.00610	39.0	58.6	
A18e	81.0	42.0	0.659	12.9	1.75	1.34	1.08	1417	1.39	-0.00633	46.4	78.3	
A19e	60.3	45.0	0.616	13.3	0.996	1.19	1.01	1229	1.21	-0.00707	45.3	77.1	
A20d	59.2	37.1	0.590	13.6	1.12	1.30	0.907	1192	1.11	-0.00582	35.0	51.7	
A21c	59.0	41.0	0.504	13.6	1.38	1.19	0.779	1019	0.804	-0.00699	31.1	44.2	250
A22b	59.1	49.0	0.420	12.5	0.984	1.15	0.777	781	0.560	-0.0105	29.8	42.2	148
*A23e	58.2	40.1	0.649	14.4	2.00	1.26	0.900	1377	1.34	-0.00819	63.2	166	
A24b	59.0	50.2	0.401	14.6	1.45	1.08	0.549	871	0.509	-0.0155	47.1	79.4	
B1b	58.9	45.1	0.445	11.5	1.68	1.10	0.631	528	0.628	-0.0116	32.0	46.2	
B2b	59.0	44.8	0.459	11.2	1.58	1.09	0.683	533	0.667	-0.00964	27.6	38.8	133
B3b	57.2	46.0	0.453	11.8	1.74	1.10	0.618	538	0.651	-0.00886	25.8	35.7	91.2
B4b	58.1	43.2	0.442	10.7	1.95	1.12	0.731	482	0.620	-0.0109	27.4	38.4	126
B5c	58.0	35.0	0.600	11.7	1.44	1.22	0.811	713	1.14	-0.00686	35.0	52.0	
B6d	58.0	33.1	0.695	11.9	1.41	1.25	0.892	847	1.54	-0.00595	41.3	70.0	
B7e	58.7	32.2	0.765	12.1	1.57	1.39	0.962	951	1.88	-0.00673	56.7	294	
*B8f	58.2	33.0	0.890	12.1	1.01	1.67	1.11	1097	2.61	-0.00562	62.6	436	
*B9c	57.9	43.1	0.556	14.3	2.69	1.41	0.513	810	1.04	-0.0129	65.1	260	
*B10c	76.2	52.0	0.604	14.1	1.58	1.89	0.538	1029	1.22	-0.0128	77.1	662	
*B11c	59.0	43.2	0.533		2.72	1.34			0.956				
*B12c	56.3	41.1	0.565	14.5	1.59	1.57	0.517	810	1.07	-0.0137	72.0	522	
*B13c	59.0	45.1	0.560	14.6	1.83	2.24	0.492	844	1.05	-0.0146	76.5	1000	
*B14c	71.0	52.0	0.612	12.4	1.31	2.09	0.726	892	1.26	-0.0144	76.9	702	
*B15d	59.1	43.8	0.682	14.3	1.84	2.08	0.633	1009	1.55	-0.0104	79.4	1830	
B16a	58.8	47.9	0.380	13.3	1.97	1.60	0.409	521	0.49	-0.0194	42.3	77.2	
*B17f	58.9	38.0	0.927	12.8	0.906		1.05	1224	2.88	-0.00741	93.3		
C1f	59.0	42.0	0.881	6.95	0.449	2.08	1.20	632	2.44	-0.00891	38.0		
C2d	59.3	45.9	0.673	7.75	0.622	1.52	0.777	539	1.47	-0.0103	27.9	140	
C3a	59.0	53.9	0.464	7.00	0.600	1.21	0.716	335	0.682	-0.0200	24.0	65.4	
D1b	58.1	56.0	0.288	9.31	1.60	1.31	0.617	396	0.245	-0.0383	26.7	66.2	
D2d	59.0	51.3	0.437	9.28	1.32	1.49	0.931	604	0.628	-0.0187	26.9	97.4	
D3c	58.8	53.8	0.369	10.4	1.78	1.57	0.637	570	0.443	-0.0216	25.2	72.6	
E1c	60.1	42.0	0.645	16.2	0.583	1.23	0.657	121	1.32	-0.0104	80.2	2970	
E2c	60.0	44.1	0.655	16.8	0.769	1.27	0.612	128	1.36	-0.00875	71.9	458	
E3a	61.0	51.8	0.450	9.65	1.08	1.06	1.27	51.0	0.642	-0.0238	53.2	120	
E4b	59.4	47.8	0.523	13.8	0.729	1.14	0.718	82.8	0.862	-0.0158	68.6	294	
E5d	60.0	45.5	0.729	18.1	0.691	1.57	0.586	153	1.73	-0.00770	82.2		
E6e	59.1	38.3	0.804	18.2	0.712	1.61	0.652	167	2.12	-0.00727	94.5		
*E7f	61.0	38.0	0.964	18.3	0.579	1.86	0.782	207	3.14	-0.00543	99.0		
F1b	59.2	53.8	0.330	9.03	1.77	1.11	1.70	34.1	0.345	-0.0310	22.9	63.6	
F2c	59.0	52.1	0.376	11.1	1.19	1.24	1.29	47.7	0.446	-0.0236	27.9	170	
F3d	60.4	50.0	0.423	12.5	1.11	1.33	1.16	61.3	0.574	-0.0167	27.7	176	

DISCUSSION OF RESULTS AND CORRELATION

The experimental results will be discussed in two parts, following the same procedure as was used in the theoretical analysis section. The first part of this section is devoted to the drop mechanics, and the second part to the heat transfer results and correlation. The range of variables covered by this investigation is shown in Table V. This table includes the extreme values of the physical properties as well as those for the mechanical properties and the important dimensionless groups.

Observations on Mechanics of Drops

It should be emphasized that most of the results pertaining to drop mechanics can only be applied qualitatively to other systems. The reason for this is that the conditions under which the results were obtained are much different than the conditions under which most published data were taken. The most important factor, in this respect, is the change in drop density as the drop rises through the test section. This change in density is enough, in extreme cases, to cause the difference in densities to change by thirty percent. Another factor which does not exist in other data on the mechanics of drops, is the fairly large temperature gradient surrounding the drop, which makes the selection of values for the physical properties rather indefinite. Even though these uncertainties are present, it is thought that the data are general enough to show some interesting phenomena characteristic of most systems.

Drop Formation: The size of the drops formed at the nozzles used in this research was fairly uniform. Measurements from photographs

TABLE V

RANGE OF VARIABLES STUDIED

Variable	Lowest Value	Highest Value
Density (g/cc)		
Dispersed Phase	0.988	1.098
Continuous Phase	0.823	1.271
Viscosity (Centipoises)		
Dispersed Phase	0.562	9.05
Continuous Phase	0.480	7.20
Heat Capacity (Cal/g °C)		
Dispersed Phase	0.60	1.00
Continuous Phase	0.288	0.502
Thermal Conductivity (Cal/sec. cm. °C)		
Dispersed Phase	0.00059	0.00156
Continuous Phase	0.00029	0.00033
Interfacial Tension (dynes/cm.)	8.2	48.1
Drop Diameter (cm)	0.288	0.964
Drop Velocity (cm/sec.)	7.00	18.3
Reynolds Number (Re)	34.1	1428
Drag Coefficient (C_D)	0.40	1.70
Prandtl Number (Pr)	7.80	110
Interfacial Tension Group (M)	0.10	52.6
Nusselt Number (Nu)	23	100

of individual drops showed about a five percent variation in drop volume for drops of a single run. Attempts to duplicate the average drop size of one run in another run were not usually successful, even though other conditions were identical. The variation in the average drop volume between these runs was as high as ten percent. In all cases, the drop size versus nozzle velocity plots show that the drop size increases to a maximum and then decreases. This trend agrees with the results of Hayworth and Treybal,[22] however, the correlation given by these authors predicts drop sizes which are on the average fifteen percent lower than those found in this work.

Drop Velocity: After forming and breaking away from the tip, there is a short period in which the drops accelerate to their terminal velocity. From the motion pictures taken in the B series of runs, it was found that the drops had always reached at least 95 percent of their terminal velocity after traveling a distance of two inches.

The drop velocity, after this initial period of acceleration, was constant enough so that no variation could be detected during the remainder of the drop rise. Figure 12 shows the variation of velocity with drop diameter for two sets of runs in the same system. The upper curve shows the characteristic maximum associated with the start of drop oscillation. The lower curve in this figure is for drops in the same system, but with a surface-active powder present. In this case, the point at which oscillation occurs is not so obvious, and there does not seem to be a noticeable maximum in the curve. The difference in these two curves is due to a surface-active powder which was present in the latter case. This behavior will be discussed in greater detail later in this section.

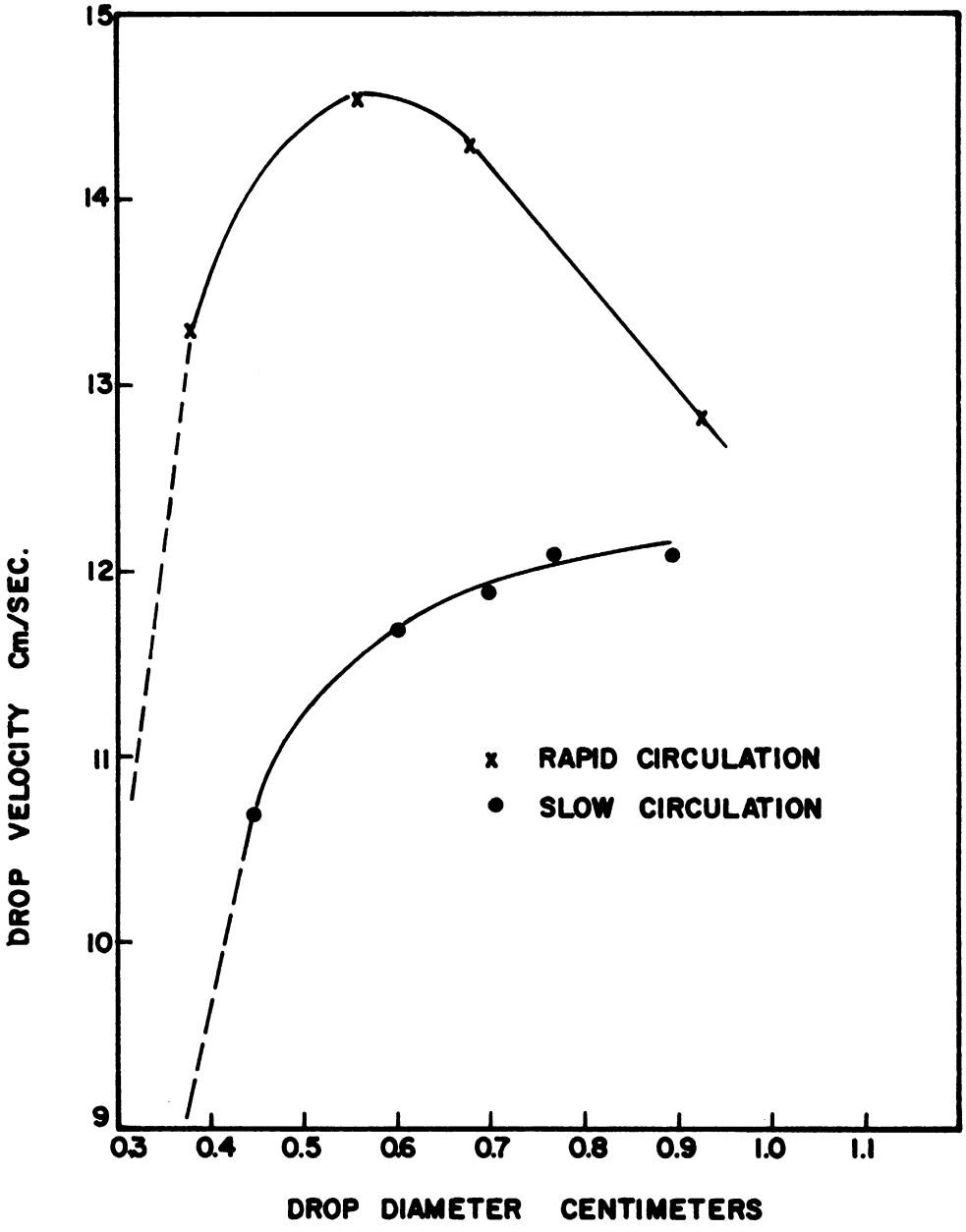

Figure 12. Velocity Versus Diameter for Water Drops in Dowtherm A + E.

The drop velocity data for this work is compared to that of solid spheres and disks in Figure 13, by means of a plot of drag coefficient versus Reynolds number. The drag coefficient for solid spheres, predicted by Stokes law, is also shown for comparison in this figure. The general shape of these curves agree well with previously mentioned work,[18,24,46] on bubbles and drops. However, some of these curves differ in one respect from the work of Hu and Kintner[24] on the velocity of drops in liquid-liquid systems. Whereas these authors found that only one of the ten systems they studied showed the drag coefficient curve lower than that for solid spheres, the present work shows that in all runs where a small enough drop size was obtained, the drag coefficients were lower than those for solid spheres. This behavior is especially predominant in the runs with water or ethylene glycol in Finol (systems E and F).

While some of the disagreement between this work and that of Hu and Kintner may be explained on the basis of the temperature gradients existing near the drops in the present work, most of the disagreement is probably due to the method by which the drops were formed. Hu and Kintner formed their drops by pouring the drop material into the continuous phase, so that the drop is essentially stagnant at the start. In the present work, the drops were formed at an orifice which imparts a motion to the fluid inside the drop similar to that of circulating drops. Therefore, in the former work, the drops were stagnant, at least initially, while in the present work, the drops were initially circulating and the reason for the lower drag coefficients in this work was due to the presence of internal circulation. Although the drops formed by Hu and Kintner were not initially circulating, skin

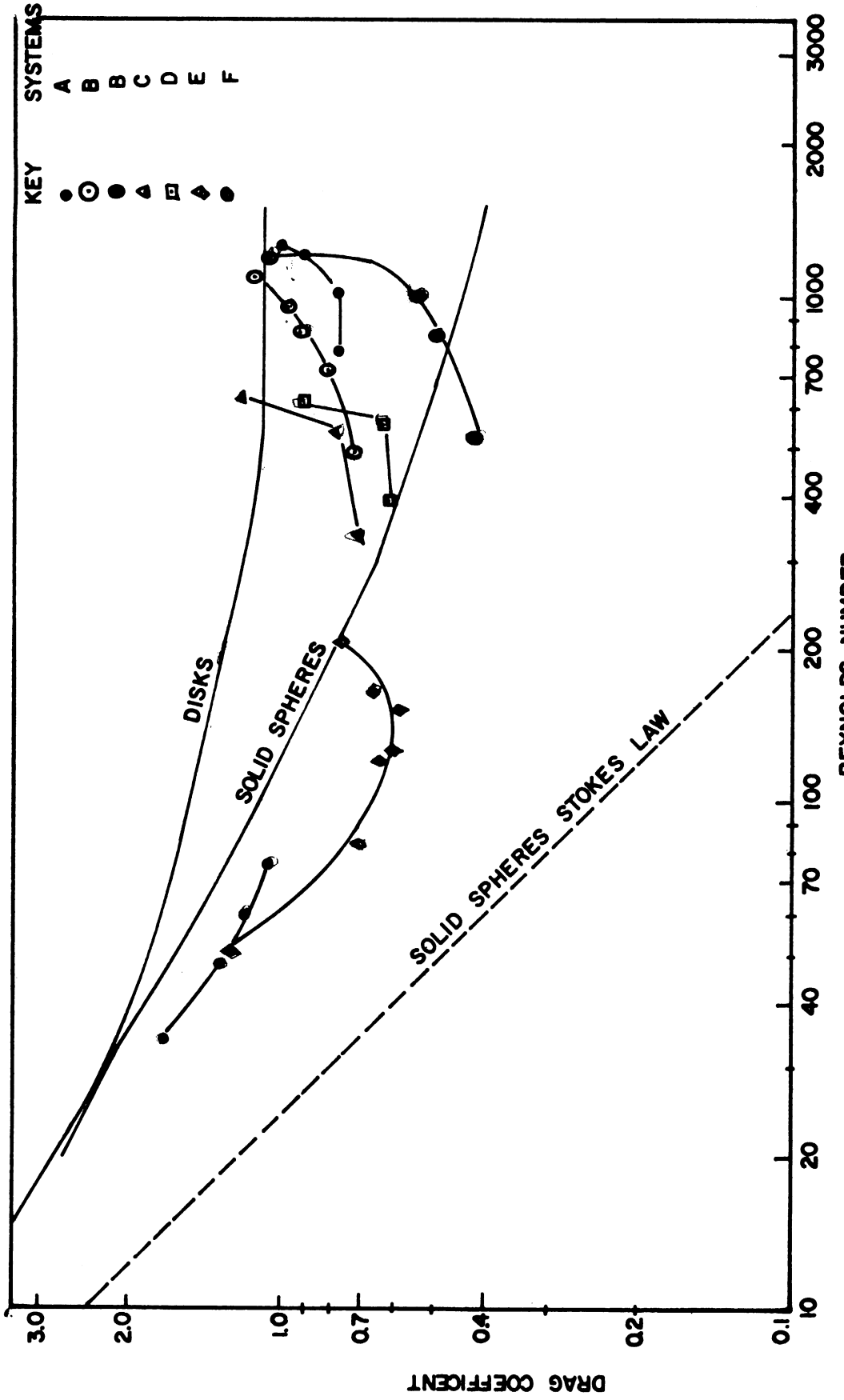

Figure 13. Drag Coefficients for All Systems Studied.

drag could cause these drops to circulate after traveling a short distance. This is evidently the case for the aniline-water system, which was the one system found by these authors in which the drag coefficient was substantially lower than that for solid spheres. The drag coefficient for this system is shown in Figure 8, and it can be seen from this plot that there is a Reynolds number at which the curve departs from the curve for solid spheres. This point corresponds to the drop size at which circulation starts for drops in this system, and is, therefore, the Reynolds number at which the forces acting on the drop become large enough to overcome the surface forces and initiate internal circulation as postulated by Bond and Newton.[3] The other systems studied by Hu and Kintner all had interfacial tensions ten to twenty times higher than that of the aniline-water system, so that circulation is nonexistant in these cases, and therefore, the drag coefficient followed those for solid spheres.

Internal Circulation of Drops: Since the internal circulation has been shown to have an important influence on the drag coefficient and velocity of the drop, and thereby also affects the heat transfer, a more detailed account of its role will be given here.

The most obvious way that internal circulation could influence the drop velocity and drag coefficient, is by reducing the shear at the surface of the drop. This is probably the primary effect in the low Reynolds number range of this work. Figure 14, a, b, c, and d, shows some photographs made of drops of ethylene glycol (a and b) and water (c and d) in Finol (systems E and F, respectively) for Reynolds numbers from about 30 to 80. In this range, the drops are nearly spherical and except for internal circulation, should behave like solid

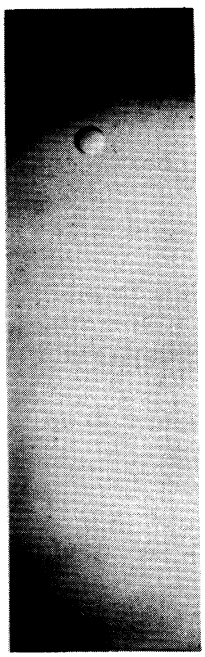

(a)
x 1.2
Run No. F1b
Re = 34.1

(b)
x 1.4
Run No. F1b
Re = 34.1

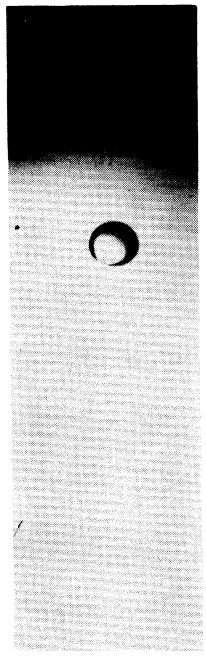

(c)
x 1.2
Run No. E4b
Re = 82.8

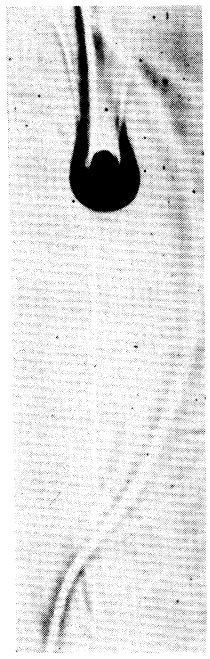

(d)
x 1.4
Run No. E4b
Re = 82.8

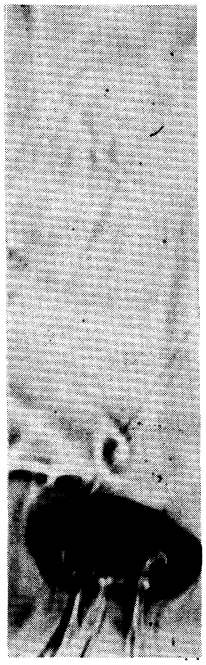

(e)
x 1.4
Run No. E7f
Re = 207

(f)
x 1.4
Run No. B16a
Re = 521

(g)
x 1.4
Run No. B13c
Re = 844

(h)
x 1.4
Run No. B8f
Re = 1097

Figure 14. Drop Photographs

spheres. The reduction in drag for this Reynolds number range due to internal circulation can be seen in Figure 13.

At higher Reynolds numbers, an additional reduction in drag occurs which seems to be in some way related to the degree of circulation inside the drop. This effect is shown best by Figure 15, photographs b and f, which are both pictures of water drops in Dowtherm A and E (system B). In both cases, the Reynolds number is the same, however in one case, photograph b, circulation was reduced by the presence in the water of a surface-active powder. Photograph f shows that in the case of the circulating drop, the wake behind the drop is much smaller despite the fact that the drop is even more deformed than the drop in photograph b. The resulting reduction in form drag in the circulating drops can be seen by comparing the two drag curves for system B in Figure 13.

Since this reduction in the size of the wake could be due to a shift in the point of boundary layer separation towards the rear of the drop, the solution of the boundary layer equation was investigated to determine the effect of internal circulation on separation. Figure 16 gives the change in the point of separation, in degrees, caused by increasing the ratio of the liquid velocity, at the surface of the drop, to the drop velocity. The form of the boundary layer equation used and the solution is outlined in Appendix G. As can be seen from Figure 16, increasing the velocity at the drop surface changes the point of separation very little. This has been shown experimentally for rotating cylinders by Prandtl and Tietjens (reported in reference 16), where it was found that the point of separation was not shifted appreciably until the surface velocity was at least twice the free stream

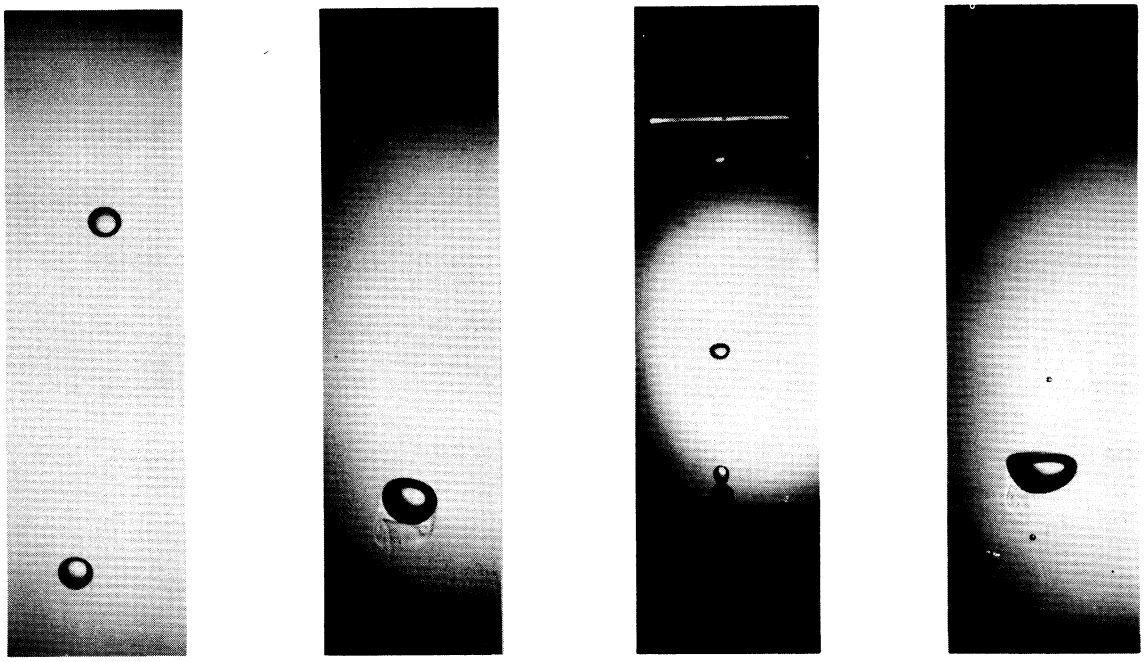

(a)
x 1.2
Run No. B4b
Re = 482

(b)
x 1.2
Run No. B6d
Re = 847

(c)
x 0.25
Run No. B7e
Re = 951

(d)
x 1.2
Run No. B8f
Re = 1097

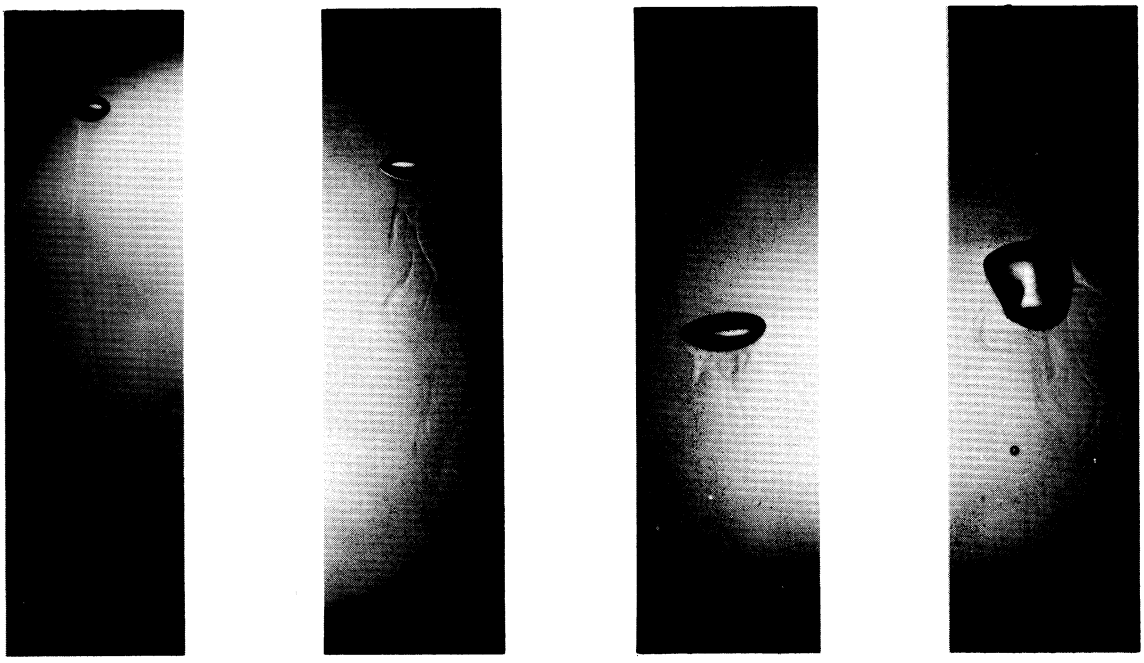

(e)
x 1.2
Run No. B16a
Re = 521

(f)
x 1.2
Run No. B13c
Re = 844

(g)
x 1.2
Run No. B15d
Re = 1009

(h)
x 1.2
Run No. B17f
Re = 1224

Figure 15. Drop Photographs

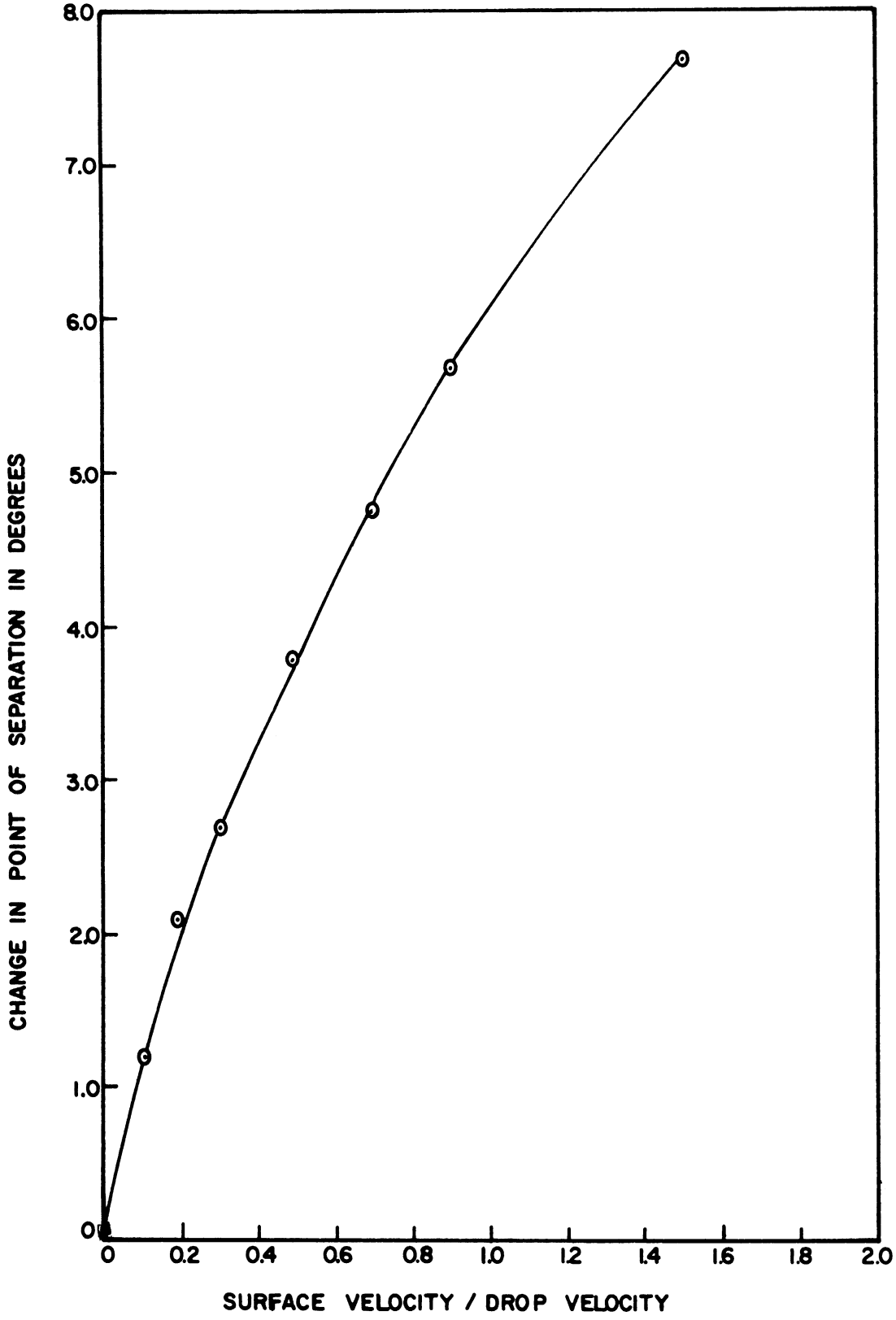

Figure 16. Effect of Circulation on Point of Separation

velocity. The conclusion seems to be that internal circulation does reduce skin drag on drops, but is only indirectly responsible for reducing the form drag.

Distortion and Oscillation of Drops: The ratio of the major diameter to the minor diameter was used to indicate the amount of distortion for a drop. It was found that the correlation of Hughes and Gilliland[25] predicted values for this ratio that were much lower than those actually measured. The reason for this was that the correlation was developed for stagnant drops, and therefore does not account for the added distortion of the drop due to internal circulation. The photographs in Figures 14 and 15 are typical of the appearance of the drops. In some of the runs, the drops were observed to oscillate after traveling two or three inches from the nozzle, and in these cases, photographs were made of the drop just before it started to oscillate. Most of the drops are seen to be deformed in a shape approximating an oblate spheroid. However, the shape of the largest drops was poorly defined and changed radically during the rise or fall of the drops. Photograph h in Figure 15 illustrates the latter type of drop. This photograph also shows the small satellite drop that was formed when these drops broke away from the nozzle.

The variables which exert the principle influence on the distortion of drops in a single liquid-liquid system, are the drop size, velocity, and the degree of internal circulation. The change in the ratio of the major diameter to the minor diameter due to increasing the degree of internal circulation and the drop velocity, is shown by Figure 17. The upper curve in this figure is for rapidly circulating drops, and is based on data from the same set of runs in which the

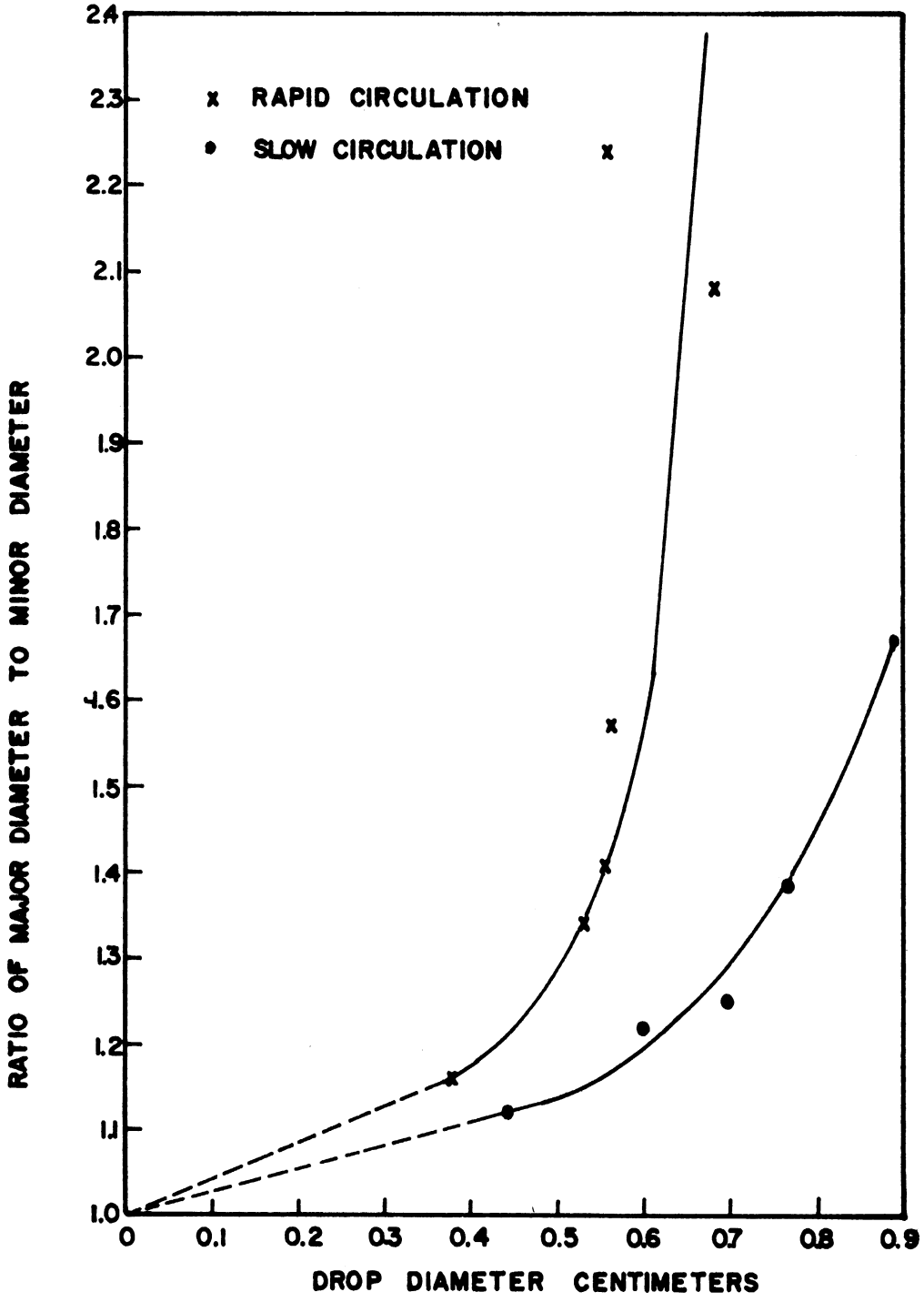

Figure 17. Distortion of Water Drops in Dowtherm A + E.

photographs e, f, g, and h, of Figure 15, and the velocity data for the upper curve in Figure 12, were taken. The lower curve in Figure 17, is for slowly circulating drops in the same system and corresponds to the remaining photographs and curve of Figures 15 and 12, respectively.

The drop size at which oscillation starts, has been shown to depend upon the value of the Weber number. Hu and Kintner[24] found that oscillations start when the Weber number reaches a value of 3.6. In the present work, this value was found to hold for the systems with the high interfacial tensions, but for lower interfacial tensions, systems C and D, this number increased to a value of 5.5. This value of the Weber number probably represents the condition where the drop surface forces become small enough, in comparison with the forces acting on the drop, so that the periodic discharge of eddies in the wake of the drop is reflected by an oscillation of the drop itself.

The nature of the flow in the wake of the drops can be seen in Figure 14, shadowgraphs b, d, e, f, g, and h. For the low Reynolds numbers, it is evident that the motion of the fluid in the wake is laminar. Shadowgraph b, in Figure 14, shows a drop which appears to be following in the path of the previous drop. This seems to be the exception rather than the rule for in no other photograph was a similar situation observed. As the Reynolds number is increased, the wake becomes progressively more turbulent. The transition to a turbulent wake seems to occur near a Reynolds number of 200, which is in fair agreement with the previously mentioned observations of Stanton and Marshall.[50] At Reynolds numbers above this value, a periodic distortion of the wake can be observed in the shadowgraphs. Figure 14, shadowgraph

g, shows this distortion as it appears directly behind the drop and a short distance downstream from the drop.

The frequency of vortex discharge from spheres, in terms of a dimensionless group, has been shown by Möller[45] to be a function of the Reynolds number. Figure 18 shows the curve drawn by Möller through his experimental data. In the present work, the discharge frequency was calculated from the drop velocity and the distance between the periodic distortions in the wake as shown by shadowgraphs. These data are also plotted in Figure 18 for those runs in which the wake was measurably periodic. Most of the disagreement between these data and those of Möller is due to the drops being nonspherical.

The periodic discharge of material into the wake of the drop gives rise to a reasonable explanation for the breakup of large drops noted by Hu and Kintner.[24] Lamb[35] has shown that the primary natural frequency of vibration of a liquid sphere is given by

$$f^2 = \frac{192\gamma}{(3\rho_d + 2\rho)D^3} \quad . \tag{27}$$

This equation shows that the natural frequency of vibration decreases with increasing drop size. Figure 18 shows that the frequency of vortex discharge increases with increasing Reynolds numbers. Therefore, at some Reynolds number, the frequency of discharge will be the same as the natural frequency of the drop and could cause the amplitude of the drop oscillations to increase to such an extent that the drop would break up. This reasoning has been used by Gunn[17] to explain the break-up of rain drops and can be shown to apply to liquid-liquid systems, using the drop breakup data of Hu and Kintner. These authors give the

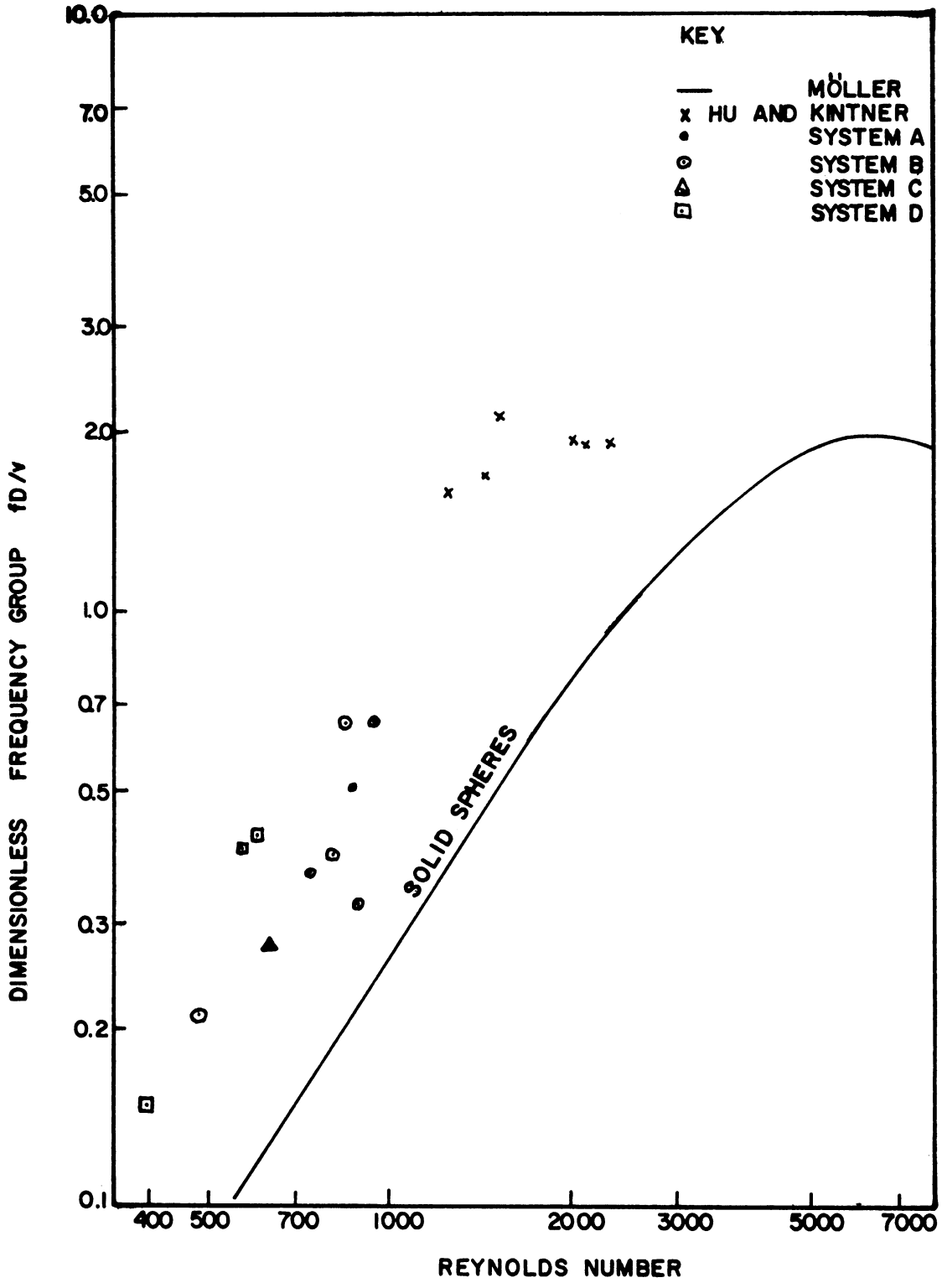

Figure 18. Frequency of Periodic Discharge in Wake of Drops Showing Relation to Drop Break Up Data of Hu and Kintner

critical size of drops for a number of systems. Using equation (27) and the critical drop size, the natural frequency of the drops can be computed. If this frequency matches the vortex discharge frequency, then, when it is plotted in the manner of Figure 18, it should agree with the vortex discharge data of the present work. That this is the case can be seen by noting, in Figure 18, where the data of Hu and Kintner fall with respect to the present data and that of Möller.

Surface-Active Materials: Several times during the course of this discussion, mention has been made of the two sets of runs made with the same system, in which entirely different results were obtained. These two sets of runs were obtained using water as the dispersed phase and a mixture of Dowtherm A and Dowtherm E as the continuous phase (system B). The runs made with this system were made consecutively over a period of two months. The difference between the data taken prior to and including run B8f, and that taken after this run can be seen by comparing the drop velocities, drag coefficients and distortions shown in Figures 12, 13 and 17. The difference in appearance of the drops is clearly shown in the photographs of Figure 15.

At first it was thought that the difference was due to a soluble surface-active material in either the distilled water or the continuous phase used for the early runs in the system. However, numerous attempts to detect this material by measuring a change in interfacial tension were inconclusive, since this factor had changed by less than 0.5 percent. The contaminating material was finally identified as a fine white powder, when it was noted that the bottom of the glass receiver for the used drop material was coated with this substance. This powder was proven to be the contaminating material by injecting a

dilute slurry of it into the water stream at the inlet to the nozzle. When this slurry reached the tip of the nozzle, the character of the drops changed back to the form noted for the initial eight runs. It was also found that this slurry had no measurable effect on the interfacial tension. No attempts were made to analyze this powder. Most probably it was aluminum oxide, since it was similar to a powder which was found adhering to the inside walls of the aluminum tubing used to carry the drop material from the storage container to the nozzle. Further evidence that aluminum oxide was the material is given by Alexander and Johnson,[1] who report that aluminum oxide is surface active to the extent that it collects at oil-water interfaces and thereby helps to stabilize oil-water emulsions.

The above authors also report that aluminum oxide is hydrophilic and therefore, in these runs, it would collect on the inside of the drop surface. For this reason, the film would not tend to "wash" off the drop as would be the case if the powder were hydrophobic. Therefore, a small amount of aluminum oxide could contaminate the drop surface during the entire period of rise.

Since the water used in all of the runs previous to B8f was contaminated with this material, two additional runs were made with water in Dowtherm E (system A). The difference between these results and the earlier results can be seen by comparing the two runs A23e and A24b with the other runs in this system, as given in Table IV.

Heat Transfer

The section on theoretical analysis discussed completely mixed, circulating, and stagnant drops used as models to account for the heat transfer inside the drops. Mention was also made of how the

value of the outside film coefficient varied, depending upon the model used, and therefore, in general there would be three different values of the outside film coefficient for the drops in a particular run. Finally, it was shown that since the equations relating temperature to time for each model are of the same form except near zero time, some independent method must be used to select the model which best approximates the actual conditions existing inside the drop. The present section will discuss the selection of the best model for the drops in each system, and a correlation of the resulting film coefficients.

Selection of Most Probable Film Coefficient: There are several ways by which the selection of a particular drop model can be justified. In some cases, it was found that one or two of the three models led to impossible results. Another method would be to measure or independently calculate the initial drop temperature and compare this value with the initial values computed for each model from the intercept of a plot of log $(t-\overline{T})$ versus time. A third method is to compare the three values of the film coefficient or the corresponding Nusselt numbers with existing data on similar systems. Some possibilities can be eliminated on the basis of their disagreement with a previously established trend in a set of runs for a particular system. Finally, those selections in which the Nusselt numbers show a dependence upon the thermal properties of the drop material could be eliminated. This latter method would be difficult to apply unless data were available over a wide range of thermal properties for the drop material.

The elimination of one or two of the three possible models on the basis of their leading to an impossible solution was the simplest and most direct method to use. Unfortunately, it could not be applied

to all of the runs. This method is based on the observation that experimentally determined slopes of log $(t-\bar{T})$ versus time led to eigenvalues which exceeded the upper limits of these numbers. For example, reference to Figure 10 shows that λ_1 and ψ_1 both increase with the dimensionless group hD/k_d and Tables X and XI show that the maximum value of these numbers occurs when hD/k_d is infinite. Therefore, when the slope is large enough so that the eigenvalue exceeds the maximum value corresponding to an infinite value of hD/k_d, the corresponding model may be eliminated. The runs in which this was the case, are indicated in Table IV by the absence of a value for the Nusselt number corresponding to the excluded model. It can be seen from this table that on this basis, the existence of stagnant drops has been excluded for most of the runs, as have circulating drops for a few of the runs.

The second method mentioned above depends upon the initial temperature of the drop. In this method, a measured or independently calculated value of the initial drop temperature would be compared with the values calculated for each of the three models. This method was not used because no way was found by which the initial temperature could be determined accurately enough to choose the correct model on this basis.

After eliminating as many of the models as possible on the basis of the maximum value of the eigenvalues, the choice of the most probable model was made from those remaining by comparing the corresponding Nusselt numbers with what were considered minimum values for these numbers. The minimum value of the Nusselt number for any system was calculated using Kramers[32] correlation for solid spheres (equation 22). If any of the Nusselt numbers corresponding to the remaining

models were lower than the value calculated from this equation, these models were excluded. Due to the nature of the models, the Nusselt number assuming complete mixing always has the lowest value, while that for stagnant drops has the highest value. Therefore, this method is capable of eliminating either the completely mixed model or the circulating drop model or both.

Kramers equation was assumed to give a limiting value because of the differences existing at the interface between the continuous phase and the sphere and the continuous phase and the drop. In the case of the solid sphere this interface is rigid, while in the case of a liquid drop the interface is elastic and its resulting motion would tend to increase the rate of heat transfer. The reason for using Kramers correlation rather than one of the other correlations for heat transfer to spheres, is that it is based on data taken over the same range of continuous phase physical properties and the same range of Reynolds numbers as were used in the present research.

Kramers equation is shown plotted in Figures 19 through 24, along with the experimentally determined Nusselt numbers for each system. The experimental data are shown at each Reynolds number by a series of one, two or three points connected by a vertical line. The lowest point, in each case, is always at the Nusselt number corresponding to the assumption of completely mixed drops for that particular run. In those cases where only one point is shown at each Reynolds number, this point is also calculated assuming that the drops are completely mixed. The other Nusselt numbers are not shown in these cases, either because they have been eliminated as possibilities or their values are too high to show on the figures. For those cases

in which a Nusselt number corresponding to either circulating or stagnant drops exists but is too high to show on the figures, its presence is indicated by an extension of the vertical line for a short distance. On these figures, runs in which the drops were observed to oscillate are indicated by a circle around the plotted point. A cross indicates that the drop was circulating rapidly enough internally so that it was more closely characterized by the completely mixed drop model.

Figure 19 shows the calculated values of the Nusselt numbers for water drops in Dowtherm E (system A). These data were taken at two different temperature levels in the continuous phase, so that this factor is responsible for some of the scatter. As can be seen, Kramers correlation predicts values which are, in most cases, intermediate between circulating and completely mixed drops. This would indicate either that the drops are circulating or fall into an intermediate category between the circulating and completely mixed case. Except for the two runs marked with a cross, it was assumed that the drops were more closely characterized by the circulating drop model, or are intermediate between circulating and completely mixed drops. The two exceptions are the check runs made at a later date without the presence of the surface-active powder. These two runs are characterized by the completely mixed drop model.

The Nusselt numbers for water drops in Dowtherm A plus E mixture (system B) are shown in Figure 20, plotted against the Reynolds number. Two sets of data are shown in this figure, one set is for the runs in which the surface-active powder was present, and the other set is for the runs made in the absence of this powder. All of the latter data was characterized by the completely mixed model, and is indicated

on the figure by the crosses. It will be noticed that in this set of data, even the run in which the drops did not oscillate was better characterized by the completely mixed drop model. This seems to indicate that internal circulation of the drop can become turbulent enough to cause fairly complete mixing. The other set of data for this plot is best characterized by completely mixed drops in the run where the drops were observed to oscillate, and by the circulating drop model in the remaining runs. In this latter set, the run at a Reynolds number of 850 was considered to be transitional between the completely mixed model and the circulating model. The basis for this decision is that the Nusselt number corresponding to the circulating or completely mixed drop model does not agree with the trend established by the two runs at the higher Reynolds number.

The Nusselt numbers for ethylene glycol drops in Dowtherm A plus E and in Dowtherm E are shown in Figures 21 and 22. These systems are clearly transitional and the best estimate of the actual Nusselt number is given by Kramers correlation. The analysis of this data would have been simplified by increasing the Reynolds number to a point where the drops become completely mixed. However, this was not done because, with the type of nozzles used, a larger drop size was not obtainable.

The solubility of Dowtherm E in ethylene glycol may also have influenced these results. This solubility is about five weight percent at 25°C and increases with temperature. This factor was

estimated to have increased the Nusselt number about ten percent for the runs with the larger drop size. Table VI shows the increase in the Nusselt number (Δ Nu) due to mass transfer for ethylene glycol drops in Dowtherm A plus E. The method of estimating this effect is given in Appendix H. It should also be pointed out that ethylene glycol is soluble to some extent in Dowtherm A plus E and in Dowtherm E. This gives rise to a velocity component in the continuous phase which is normal and directed away from the drop. The effect on the Nusselt number is in the opposite direction from that due to the dissolving of the continuous phase in the drop material.

TABLE VI

INCREASE IN NUSSELT NUMBER DUE TO MASS TRANSFER

Run No.	Δ Nu	Percent of Nu Number for Completely Mixed Drops
C 1f	+ 3.02	7.9
C 2d	+ 1.58	5.6
C 3a	+ 0.489	2

Figure 23 gives the Nusselt numbers for water drops in Finol. In this case, Kramers correlation predicts values which are about sixty percent lower than those shown on the graph. These runs were best characterized by the completely mixed drop model. Again, this is an example of how the degree of circulation can increase to a point where it becomes turbulent enough to completely mix the material inside the drop. A similar graph for ethylene glycol drops in Finol is shown

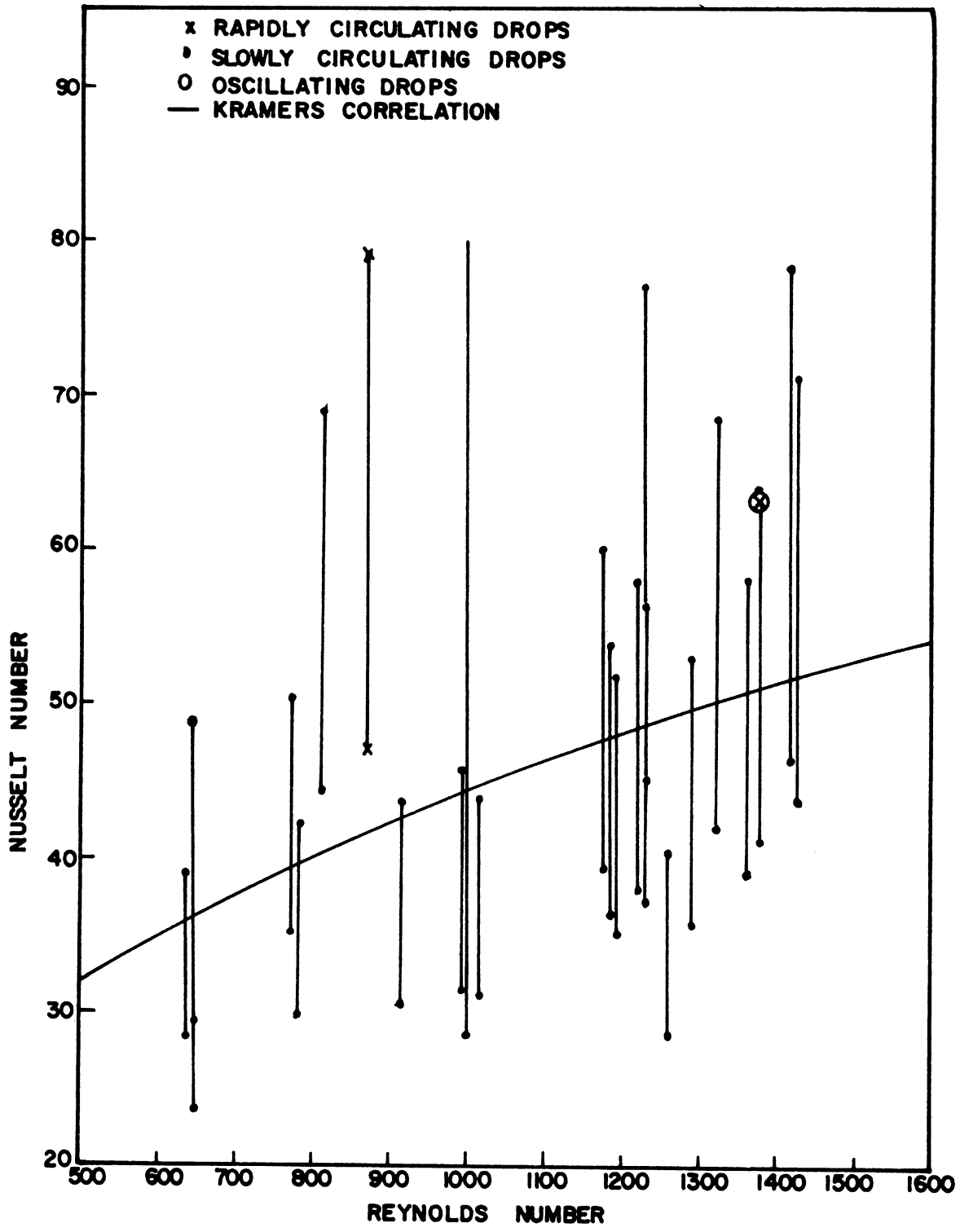

Figure 19. Nusselt Numbers for Water Drops in Dowtherm E (System A).

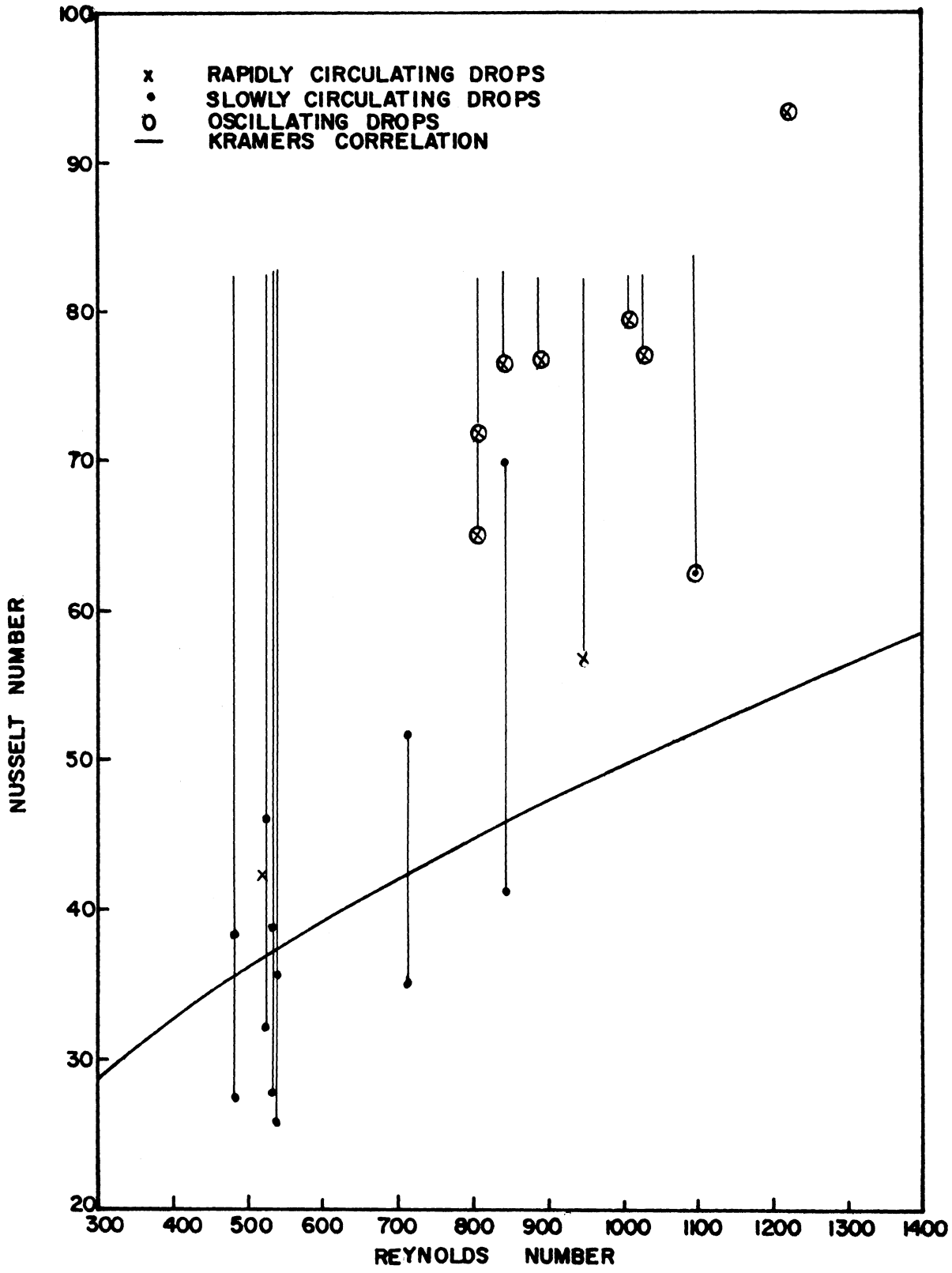

Figure 20. Nusselt Numbers for Water Drops in Dowtherm A + E. (System B)

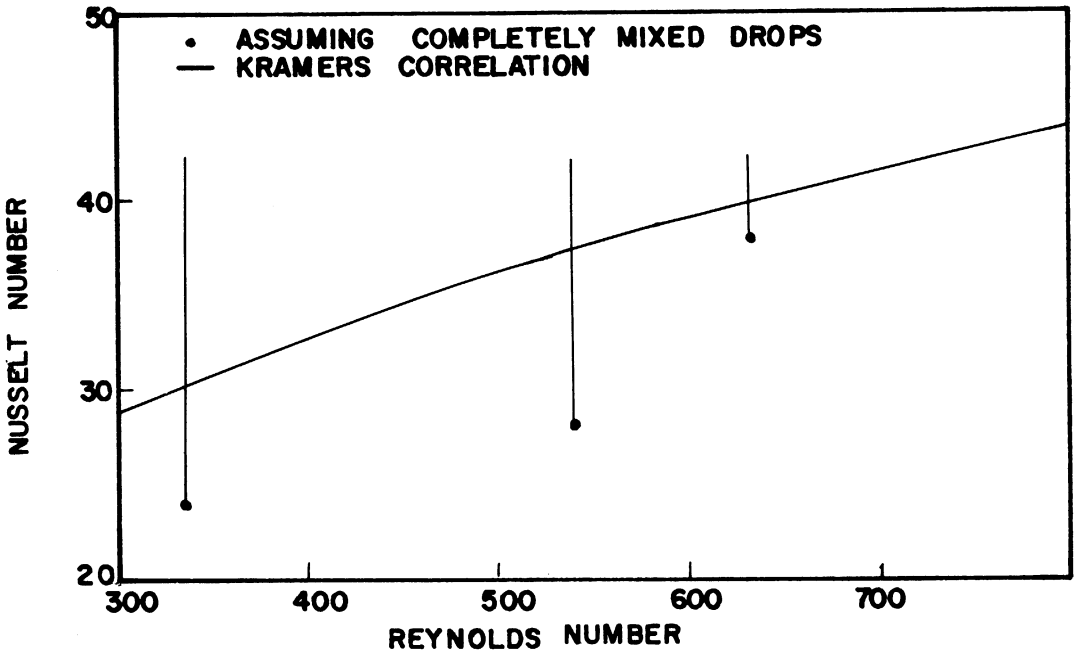

Figure 21. Nusselt Numbers for Ethylene Glycol Drops in Dowtherm A + E (System C)

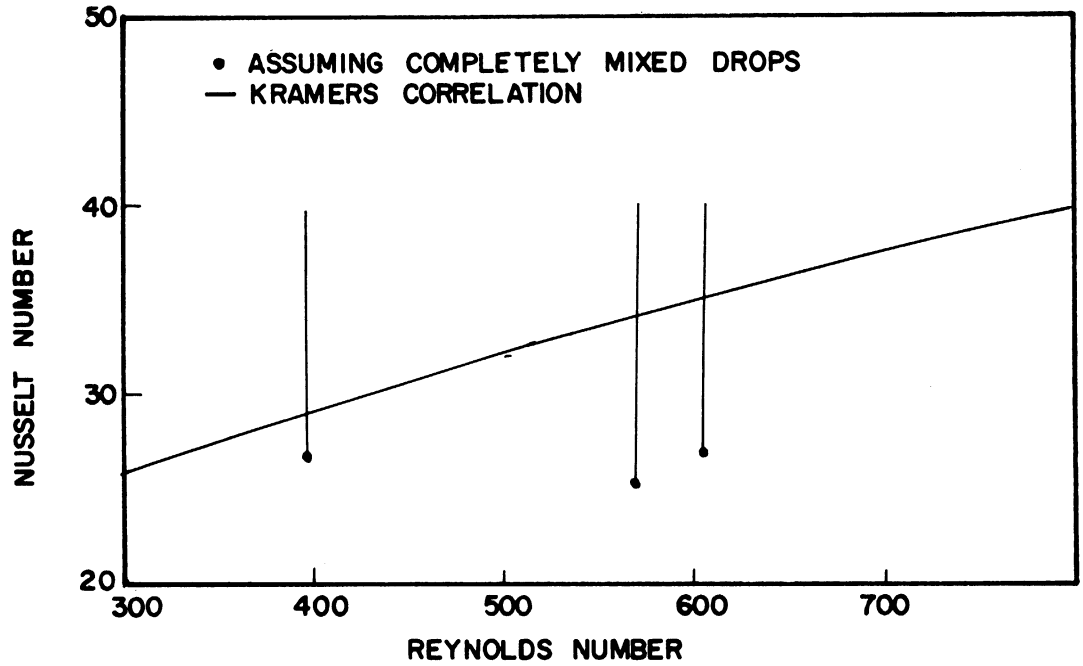

Figure 22. Nusselt Numbers for Ethylene Glycol Drops in Dowterm E (System D)

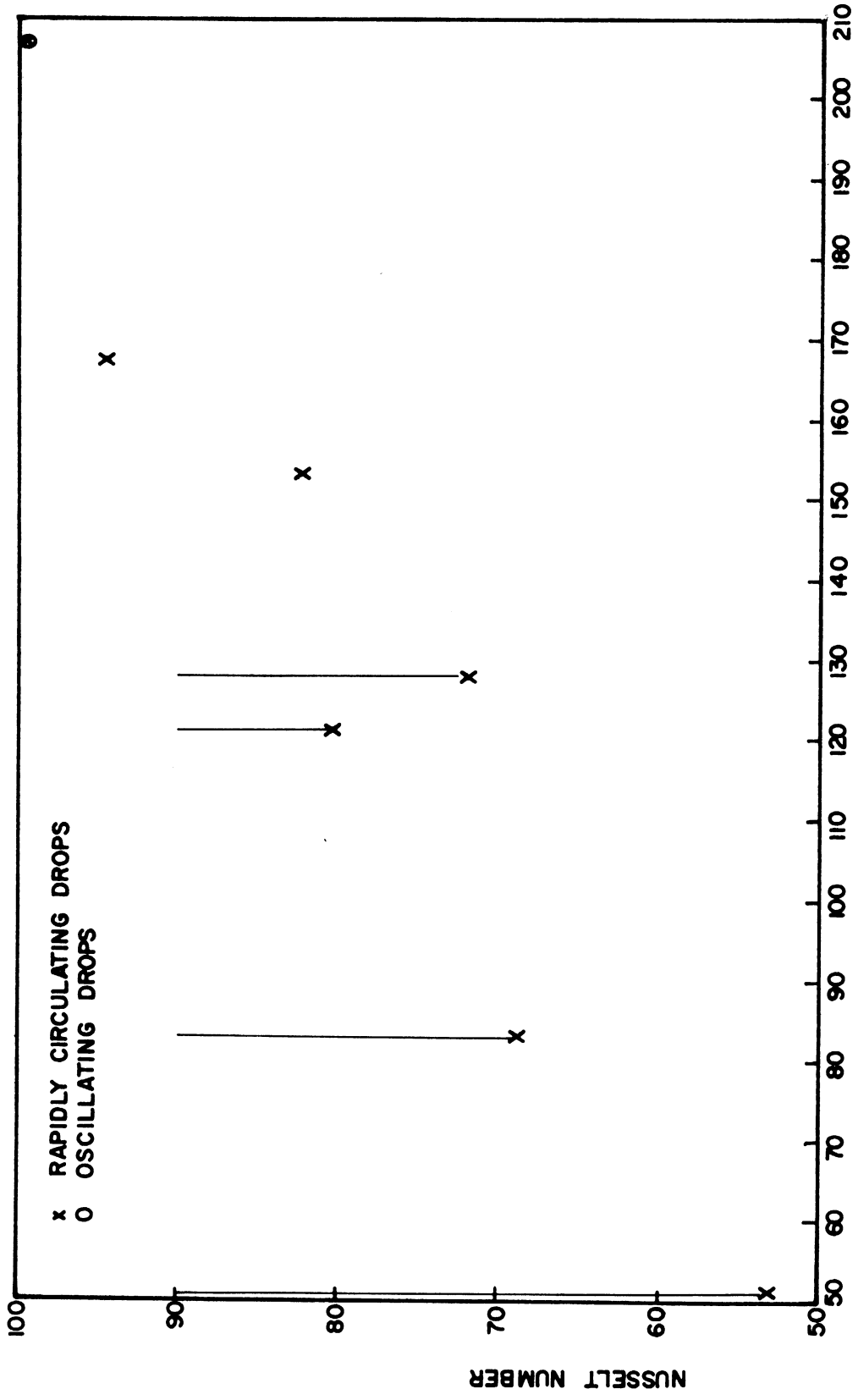

Figure 23. Nusselt Numbers for Completely Mixed Water Drops in Finol

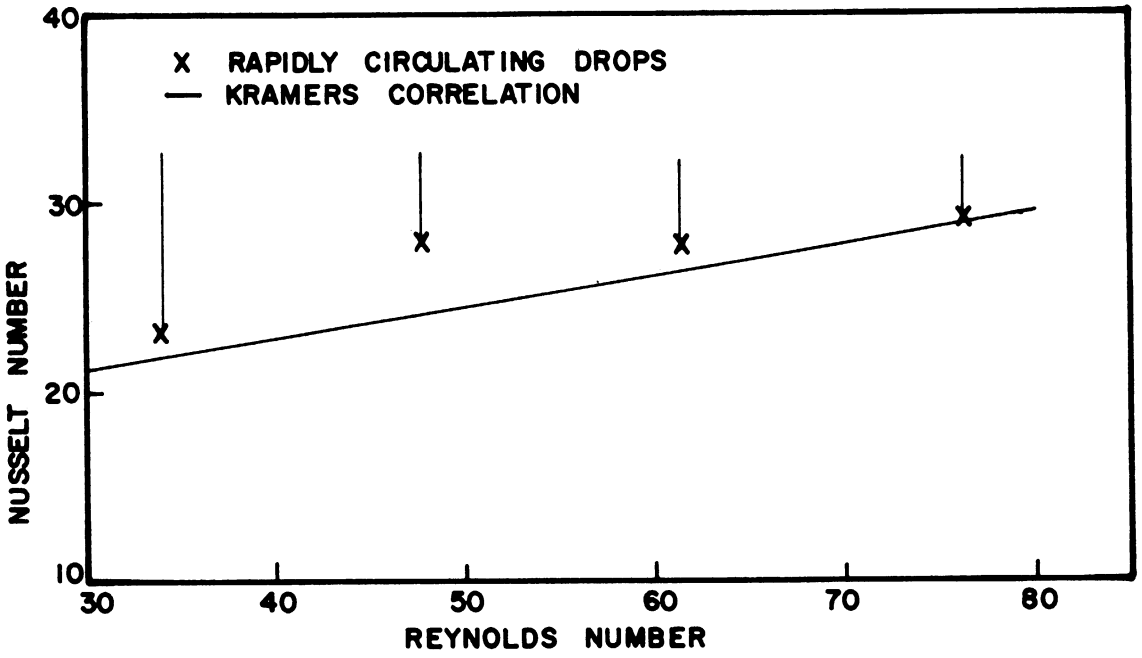

Figure 24. Nusselt Numbers for Completely Mixed Ethylene Glycol Drops in Finol

in Figure 24, and again, it was found that the drops were best characterized by the completely mixed model.

By comparing Figures 24 and 23, the effect of the ratio of drop viscosity to continuous phase viscosity can be seen. This ratio is about 0.1 for the data of Figure 23, and about 1.0 for the data of Figure 24. As was explained earlier (page 49), increasing this ratio decreases internal circulation and the drop behaves more like a solid sphere. This is illustrated by the agreement between Kramers equation and the data for ethylene glycol drops in Finol (system F) shown in Figure 24. Further examples of this effect are given by the results for ethylene glycol drops in Dowtherm A plus E and in Dowtherm E, as given in Figures 21 and 22. In these cases, the ratio of drop viscosity to continuous phase viscosity is about 7. As can be seen by comparing Figures 21, 22, 23 and 24, there seems to be a large effect of the viscosity when the ratio of drop viscosity to continuous phase viscosity is less than unity, but the effect seems to be less important when this ratio increases above one.

The model finally chosen for each run is indicated in Table IV, by underlining the corresponding Nusselt number for each run. For those cases in which it was clear that none of the models characterized the drop behavior, and that the actual behavior is intermediate between two models, the Nusselt numbers for both these models are underlined.

Effect of Drop Frequency on Heat Transfer Rates: At one time it was thought that the drop frequency would have a measurable effect on the heat transfer rates. There are a number of ways in which the frequency could affect the heat transfer rates. One way which would intend to increase the rate, is by the increased continuous phase

turbulence due to increased drop frequency. Increasing the drop frequency might also increase the heat transfer rate due to the higher initial internal circulation imparted to the drop material during formation. It is also conceivable that increasing the drop frequency might decrease the heat transfer rate by decreasing the temperature of the fluid along the drop path. To determine whether any of these effects were measurable, numerous runs were made with water drops in Dowtherm E (system A) at various frequencies and at two different continuous phase temperatures. The results of these runs are shown graphically in Figure 25, where the slope of the $\log_{10}(t-\bar{T})$ versus z is plotted as a function of the drop diameter. The drop frequency is indicated to the right of the corresponding data point. As can be seen, there is no consistent effect of drop frequency at either temperature level.

Correlation of Results: In the theoretical analysis the variables which influence the heat transfer coefficient outside the drop were discussed. By dimensional analysis, it was found that the Nusselt number should be some function of five dimensionless groups involving the other variables. One possible form for this function was given by equation (26). This equation is repeated here for reference.

$$Nu = m\left(\frac{\mu_d}{\mu}\right)^n\left(\frac{\rho_d}{\rho}\right)^o\left(\frac{D\gamma\rho}{\mu^2}\right)^q\sqrt{Pr\ Re} \qquad (26)$$

There are several features of this equation which should be discussed with respect to the present work. In the first place, the exponent on the Prandtl number has been shown to vary from 1/3 to 1/2, so that to be more general, its value in equation (26) should have been determined

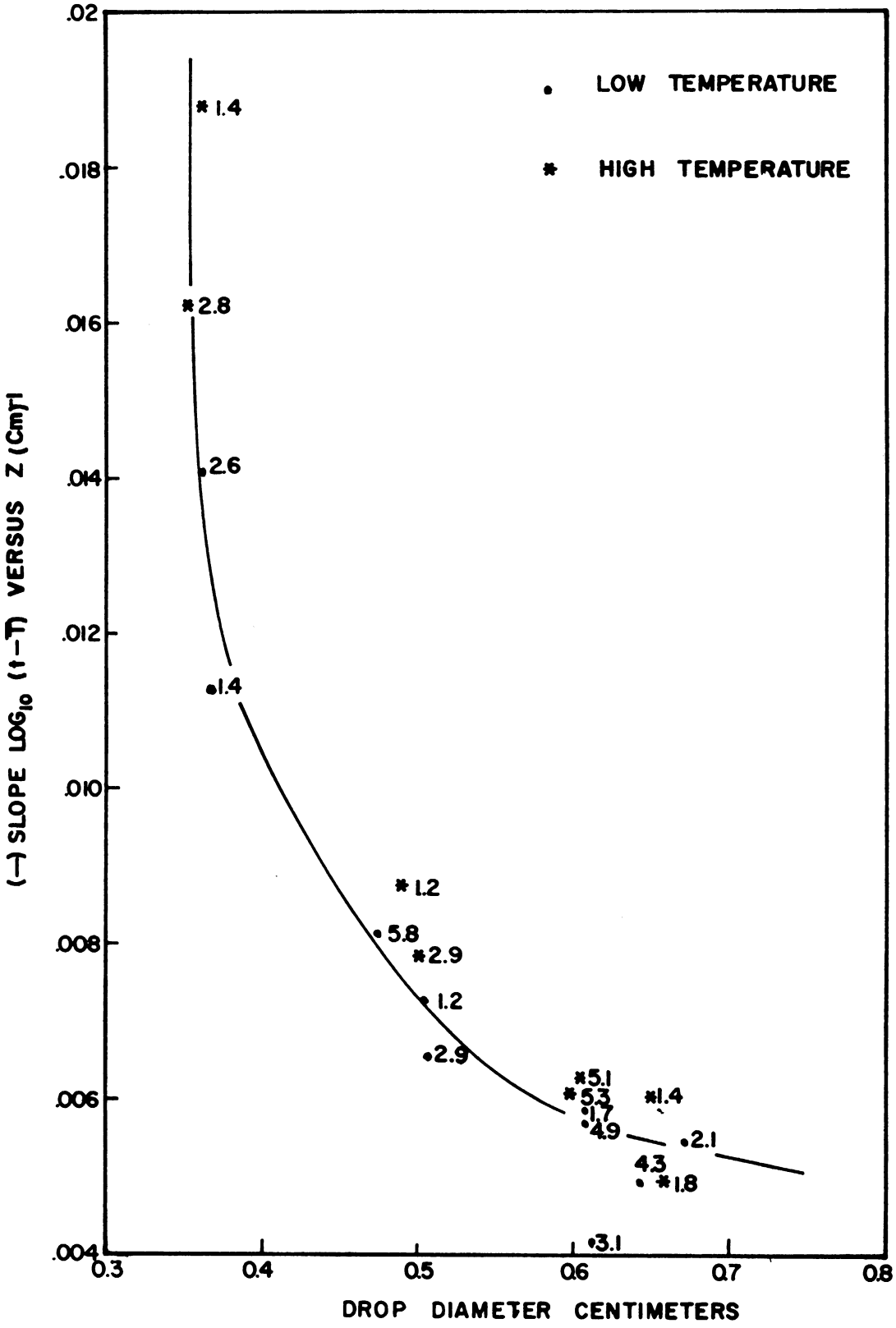

Figure 25. Effect of Drop Frequency on Heat Transfer Rates for Water Drops in Dowtherm E.

from the experimental data. This was not done because even though there was over a tenfold increase in the Prandtl number between the runs using Dowtherm as a continuous phase and those using Finol, this change was primarily due to the change in viscosity. For this reason, very little can be said about the effect of the thermal properties which are also contained in the Prandtl number. The exponent of 1/2 was used, since this seemed to be most consistent with theory for the case of circulating drops.

The density ratio is another feature which should be discussed. This ratio was not used in the final correlation because it was confined to a rather limited range by the systems used. However, this does not mean that it might not be important for systems where the density ratio is greatly different from those of the present work. The validity of omitting the density ratio, in this case, is substantiated by a comparison of the experimental data with the correlation which shows that there is no consistent effect of this variable.

The viscosity group, as shown in equation (26), appears as the ratio of the drop viscosity to continuous phase viscosity. It is desirable to change the form of this group as can be seen by noting the values of the Nusselt number in equation (26) for extreme values of the drop viscosity. For example, at infinite drop viscosity, corresponding to a solid sphere, the Nusselt number becomes infinite, while at zero viscosity, corresponding most closely to gas bubbles, the Nusselt number becomes zero. Therefore, the form of this group was changed so that it would be more consistent with the extremes of drop viscosity. The form finally decided upon for this group was

$$\frac{\mu + \mu_d}{2\mu + 3\mu_d}$$

which is the manner in which the viscosities enter the relation for the drag coefficient of liquid spheres in the Stokes law region.[35] It is obvious that any group of the above type would satisfy the requirements at the viscosity extremes, and that the only justification in selecting this form is that it enters into Stokes law for liquid spheres.

With these modifications, the form of the equation for the Nusselt number becomes

$$Nu = m\left(\frac{\mu + \mu_d}{2\mu + 3\mu_d}\right)^n \left(\frac{D\gamma\rho}{\mu^2}\right)^q \sqrt{Pr\ Re} \quad . \qquad (28)$$

The values of the exponents n and q, and the constant m, were determined from the experimental data using the method of least squares. The data from runs in which the drops were observed to oscillate and that from those runs in which the drop behavior was intermediate between two models, were not used in this determination. The data from the early runs in system A was also excluded because the velocity determinations were less accurate for these runs. To apply the method of least squares to equation (28), the logarithm of this equation was first taken. This logarithm is then linear in terms of the exponents, and the method of least squares gives rise to three linear equations which can be solved simultaneously to obtain n, q, and the logarithm of m. The resulting expression for the Nusselt number is given by equation (29).

$$Nu = 5.52\left[\frac{\mu + \mu_d}{2\mu + 3\mu_d}\right]^{3.47}\left[\frac{D\gamma\rho}{\mu^2}\right]^{0.056}\sqrt{Pr\ Re} \qquad (29)$$

The runs used for this determination are given in Table VII, and the agreement between equation (29) and the experimental data for these runs is shown graphically in Figure 26. The mean square error for this correlation is

$$\text{M. S. E.} = \left[\frac{\sum_{n}^{n} (\text{deviation})^2}{n}\right]^{1/2} = \underline{1.35}$$

As can be seen from Figure 26, there is satisfactory agreement between the data and the correlation. Although the exponent on the interfacial tension group is small, it is significant because of the wide range of values obtained for this group. Attempts to reduce the scatter of the data by including other variables such as drop frequency and density were unsuccessful.

TABLE VII

EXPERIMENTAL RUNS USED FOR HEAT TRANSFER CORRELATION

Water Drops in Dowtherm E	Water Drops in Dowtherm A+E	Water Drops in Finol	Ethylene Glycol Drops in Finol
A 20 d	B 4 b	E 1 c	F 1 b
A 21 c	B 5 c	E 2 c	F 2 c
A 22 b	B 7 e	E 3 a	F 3 d
A 24 b		E 4 b	F 4 e
		E 5 d	
		E 6 e	
		E 7 f	

Equation (29) is compared with all of the experimental data, except those runs in system B which were taken in the absence of the surface

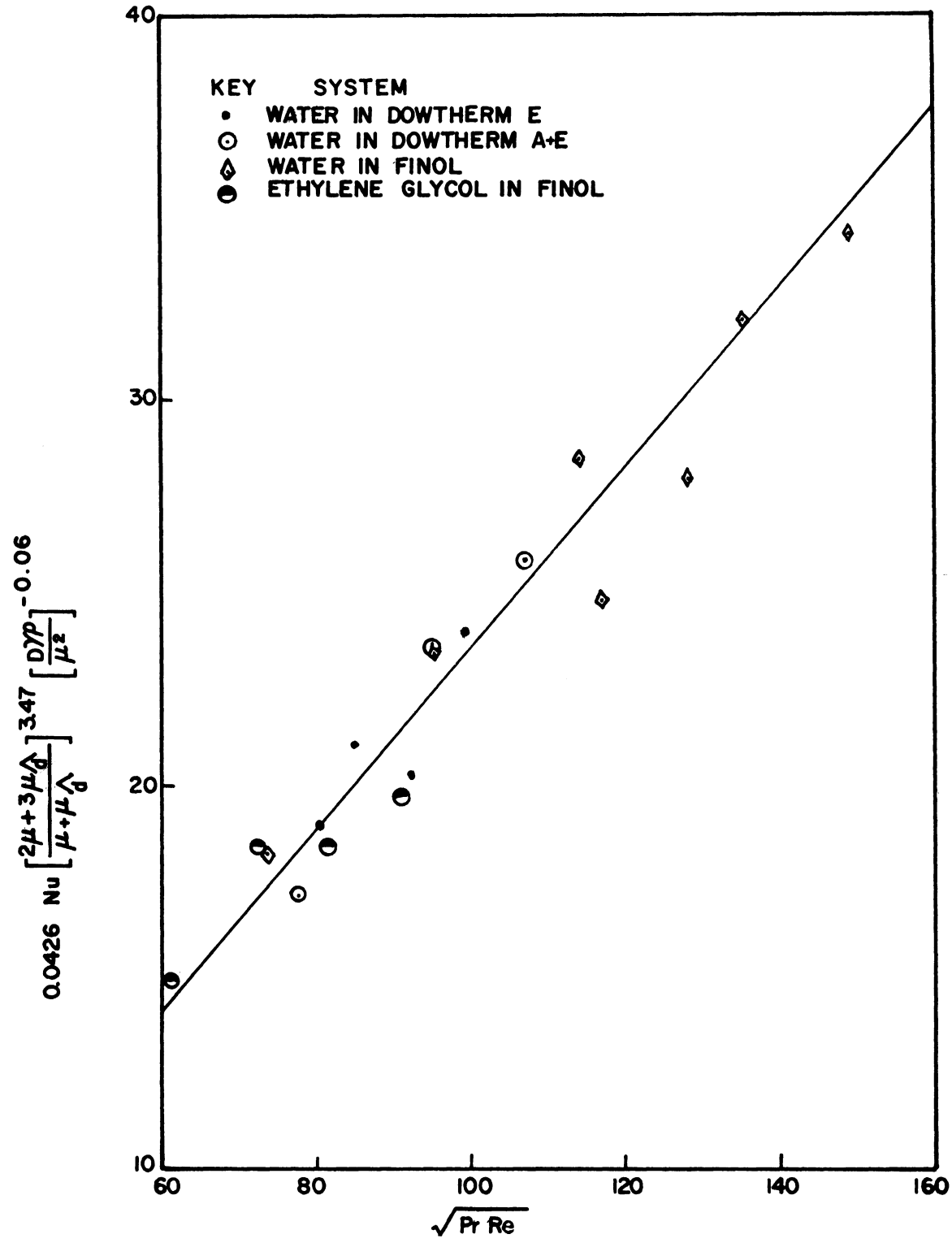

Figure 26. Heat Transfer Correlation and Experimental Values from which the Correlation was Derived

active powder, in Figure 27. The runs in which the drops behave in an intermediate manner between two drop models are indicated by drawing a vertical line through the two points corresponding to the limiting models. It can be seen that, in most cases, the limiting models for these runs fall on either side of the curve representing equation (29). However, for ethylene glycol drops in Dowtherm A + E, and in Dowtherm E, the correlation predicts Nusselt numbers which are lower than would be expected for these systems. The data points for these two systems are indicated by solid squares on Figure 27, and the vertical lines through these points indicate that these are minimum values. The reason these points are thought to be minimum values for the above two systems, is that the corresponding Nusselt numbers are lower than those predicted by Kramers correlation. The dimensionless group that seems to be the most critical here is the viscosity group, for these are the only systems in which the drop viscosity is larger than that of the continuous phase. In an attempt to remedy this situation, a number of other groups containing the viscosities were tried in equation (28). However, these attempts were abandoned when it was found that the viscosity function needed was one which possessed a maximum with respect to the viscosity ratio. For this reason, the correlation is only applicable when the ratio of the drop viscosity to the continuous phase viscosity is equal to or less than one. For higher values of this ratio, Kramers correlation, equation (22), probably gives the best estimate of the heat transfer coefficient for non-oscillating drops.

Figure 28 shows the deviation between the correlation and the data for the runs in system B made in the absence of the surface-active powder. As can be seen, the heat transfer data for the one run in this

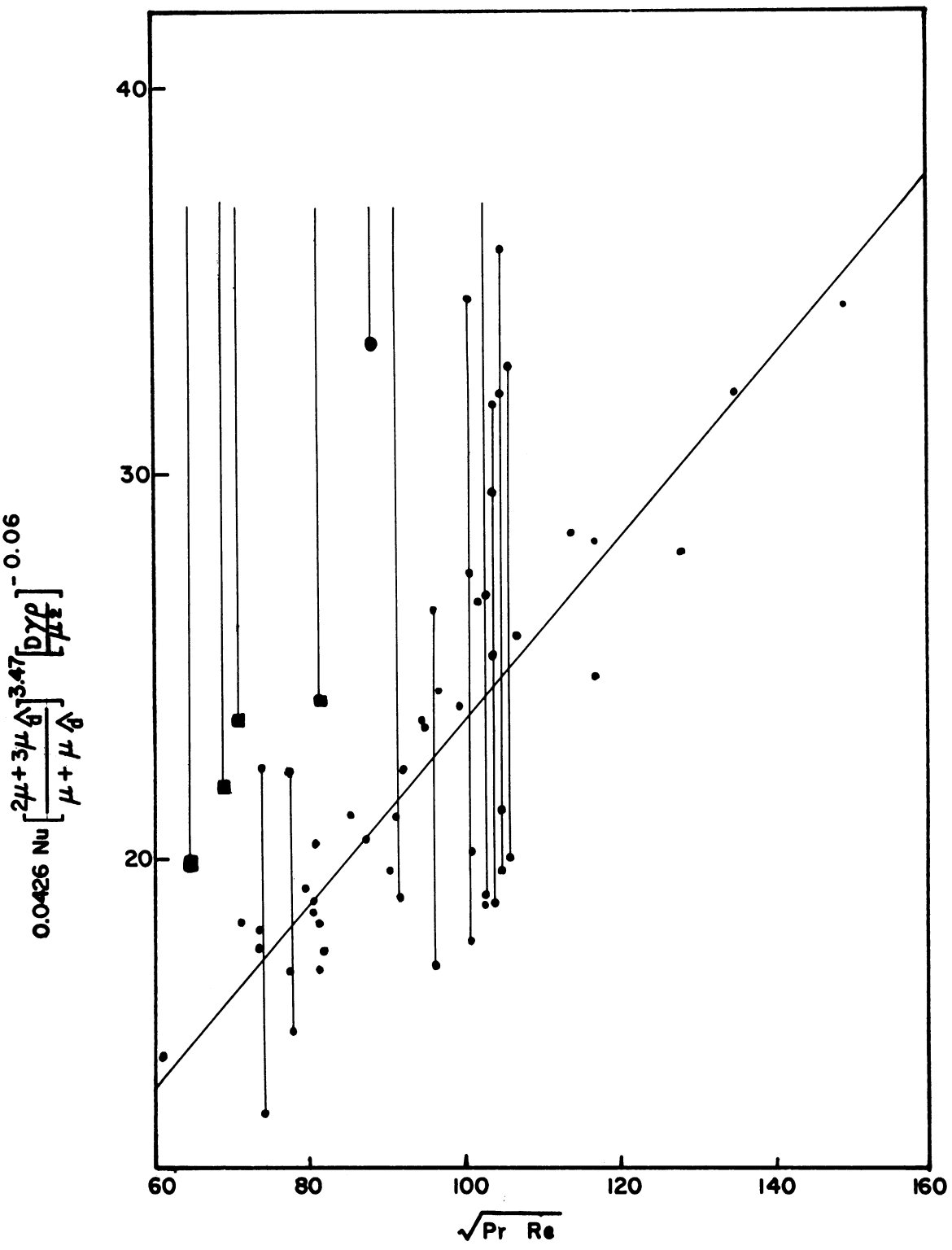

Figure 27. Heat Transfer Correlation and Experimental Values

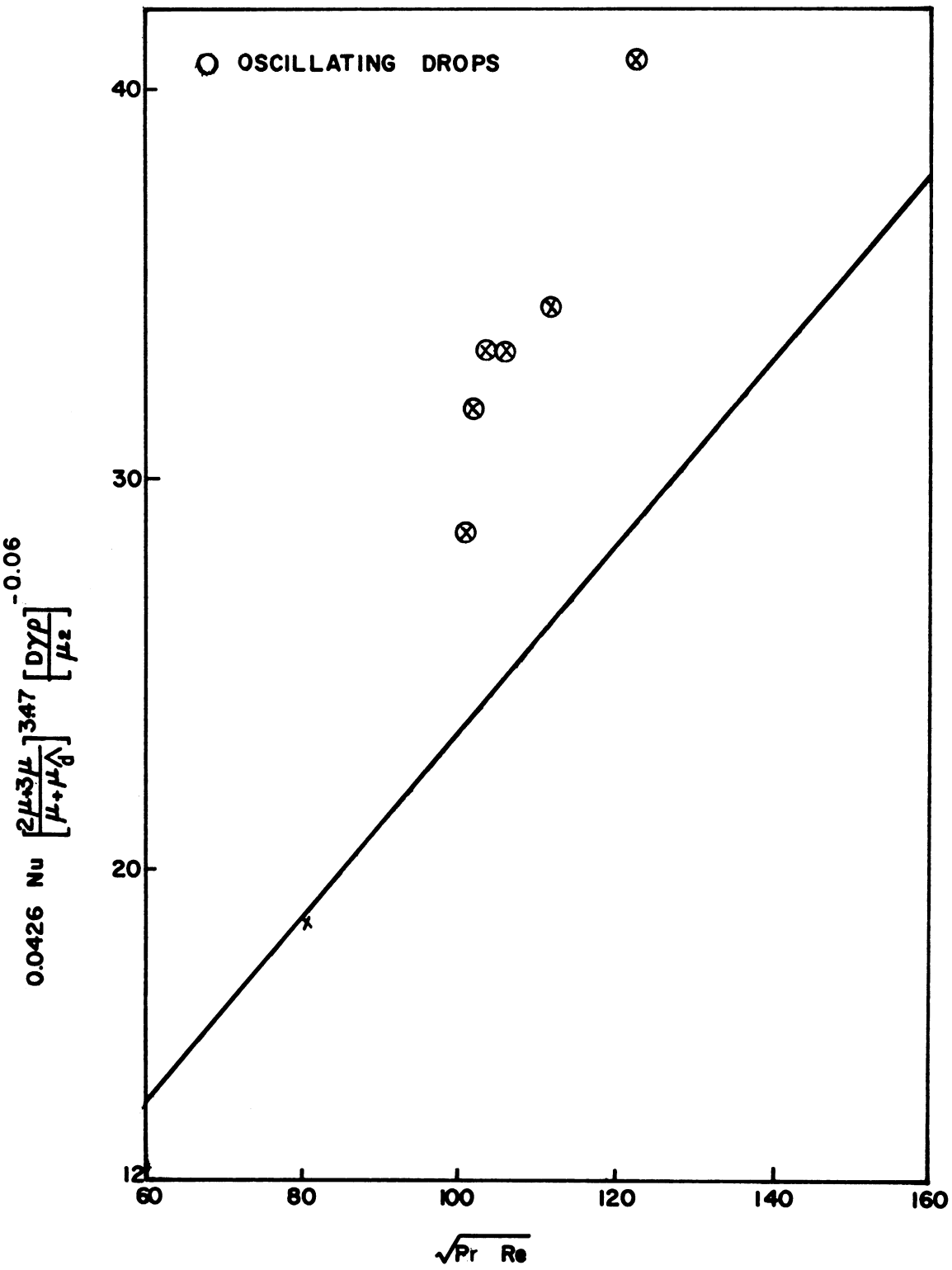

Figure 28. Heat Transfer Correlations and Results for "Clean" Water Drops in Dowtherm A + E

set during which no drop oscillation was observed, agrees well with the correlation. However, for the runs in which oscillation of the drops occurs, the experimental values increase much more rapidly than those predicted by the correlation.

Comparison of Results with Previous Work: A comparison of these results with similar work in the literature is hampered by the lack of previous work which is truly analogous. In the field of heat transfer, the results of Pierce,[47] Garwin and Smith,[15] and McDowell and Myers[42] are the most similar. Pierce studied heat transfer between swarms of mercury drops and water, flowing countercurrent to the drops in an extraction column, and his results give values for the Nusselt number which are much smaller than those found in the present work. The explanation for these low results is that the swarm of mercury drops flowing through the continuous phase sets up a circulation in this phase. This circulation causes a large portion of the water phase to bypass the central region of the column, and therefore, the average temperature of the continuous phase is not representative of the temperature of this phase which is in contact with the mercury drops. The results of Garwin and Smith for heat transfer between swarms of benzene drops rising through water in an extraction column were comparable to those of Pierce, and show a marked dependence on those variables which influence circulation in the continuous phase. A comparison of the present work with that of McDowell and Myers for heat transfer from a single stream of drops is difficult because it was not possible to correct their results for the end effects present in their apparatus.

The research of Licht and Pansing[37] on the transfer of acetic acid from a single stream of water drops to methyl isobutyl ketone was done in a manner similar to the present work and such that the end effects were eliminated. Therefore, it would be desirable to compare the work of these authors with the present results. In order to convert these mass transfer results to equivalent heat transfer results, the validity of one of the analogies between heat and mass transfer must be assumed. In the present case, the following analogy was used to convert the mass transfer results to equivalent heat transfer results.

$$\frac{h}{\rho C_p v} = \left(\frac{K}{v}\right) (Le)^{2/3} \qquad (30)$$

From an analysis of the experimental data of the above authors, it was found that the completely mixed drop model applied to these drops. Therefore, the mass transfer coefficient K, in equation (30), was calculated on this basis. The dimensionless Lewis group, Le, is the ratio of thermal diffusivity to molecular diffusivity for the continuous phase. Table VIII gives the Nusselt number, calculated using equation (30), and the corresponding Reynolds numbers for the data of Licht and Pansing. This table also contains the drop size, velocity and the Nusselt number calculated by Kramers equation. The above authors also observed that these drops were oscillating, a fact which is substantiated by the decrease in velocity with increasing drop size, so that the results cannot be compared with the correlation in the present work. However, a comparison can be made between these results and the results for the oscillating water drops in Dowtherm A plus E (system B). This comparison has been made in Figure 29, where the Nusselt numbers for

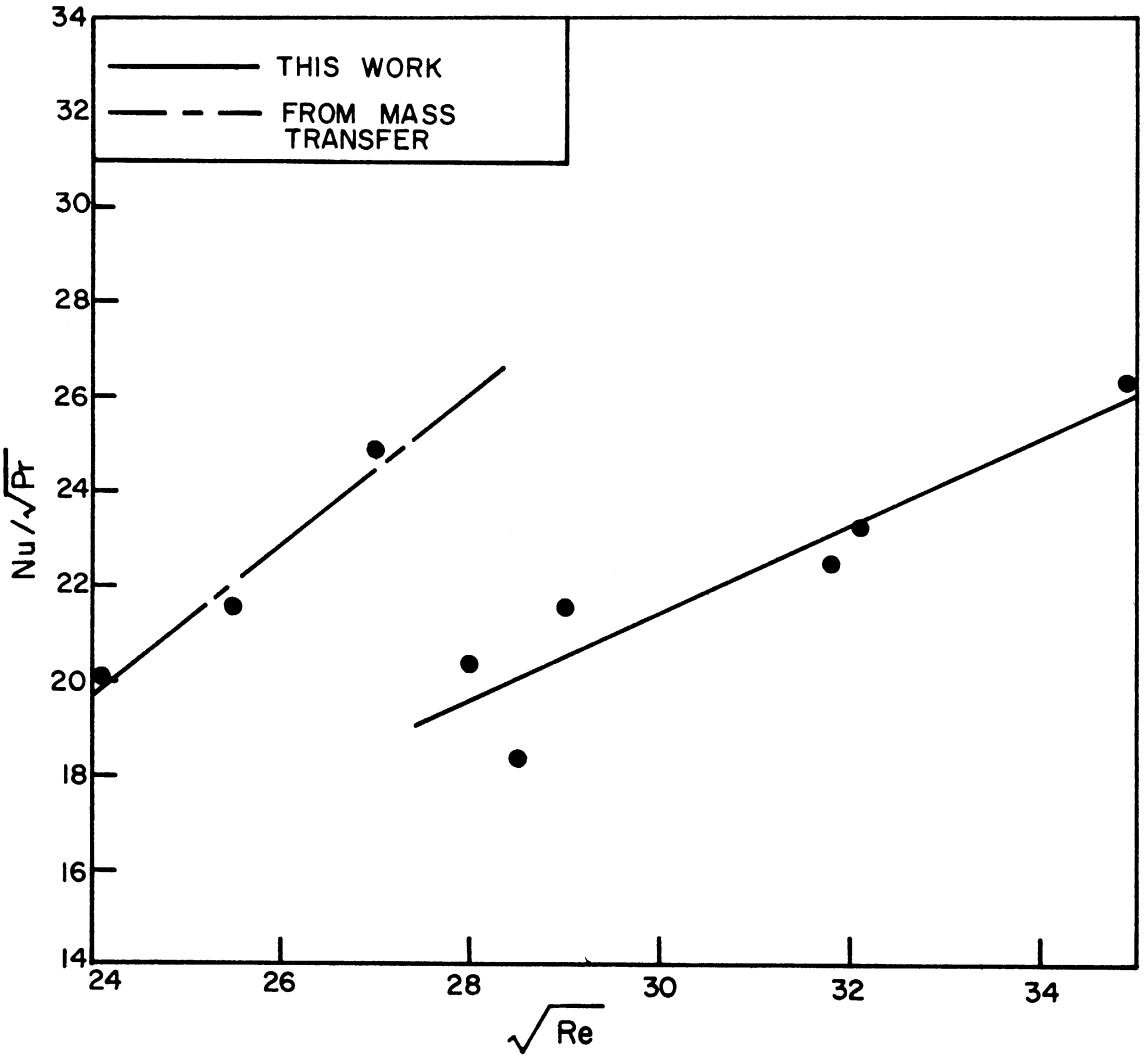

Figure 29. Comparison Between Results Calculated from Heat Transfer Data and Those Calculated from Mass Transfer Data for Oscillating Drops

TABLE VIII

NUSSELT NUMBERS FOR WATER DROPS IN METHYL ISOBUTYL KETONE
(CALCULATED FROM MASS TRANSFER DATA)

Drop Dia. cm.	Drop Velocity cm/sec.	Reynolds Number	Nusselt Number from Equation (30)	Nusselt Number Kramers Equation
0.294	13.2	569	53.4	32.9
0.355	12.5	651	58.0	35.0
0.419	11.9	731	66.6	36.8

this work, and those given in Table VIII, have been divided by the square root of their respective Prandtl numbers and plotted as a function of the square root of the drop Reynolds number. As can be seen, there is satisfactory agreement, considering the differences existing between the viscosities and interfacial tensions of the two systems.

CONCLUSIONS

From the results of this study, a number of conclusions regarding the mechanism of heat transfer to liquid drops in a liquid-liquid system can be made. These conclusions and some related observations are outlined in this section.

1. The three drop models used to describe the heat transfer inside the drops proved satisfactory in most cases. However, the results of a few runs indicated that the behavior of the transfer inside these drops was intermediate between two models.

2. Kronig and Brink's[33] analysis of the transfer rates inside circulating drops can be modified to include the effect of a finite heat transfer coefficient outside the drop.

3. In all cases where the drops were observed to oscillate, the drops were best characterized by the completely mixed drop model. This model also characterized the drops for many of the runs in which no visible oscillation occurred, and it was theorized that in these cases, the degree of internal circulation was large enough to effectively mix the drops. This rapid internal circulation was substantiated by the low values of the drag coefficients for these drops.

4. The Nusselt numbers obtained from the experimental results are correlated for most cases by a relation containing the important system variables. However, this correlation does not include oscillating drops or systems in which the drop viscosity is much larger than the continuous phase viscosity. For this latter case, Kramers correlation for solid spheres probably gives the best estimate of the Nusselt number.

5. The drop frequency does not affect the heat transfer results, at least for the range of frequencies obtainable in this work.

6. The presence of surface-active materials may exert a considerable influence on the heat transfer rates by its effect on the motion of the material inside and outside the drop surface.

7. In the low Reynolds number range, drag coefficients were obtained which were much lower than those for solid spheres. This is due to internal circulation initiated during drop formation.

8. Drop breakup can be satisfactorily explained by the action on the drop of the vortices, which are shed periodically into the wake of the drop. This substantiates the work previously reported by Gunn[17] on the breakup of raindrops.

APPENDIX A. PHYSICAL PROPERTIES OF LIQUIDS

This appendix contains a table in which the temperature dependency of the physical properties of each liquid is given. A short statement is also given on the method used to obtain each property or the literature source from which it was taken. In all experimentally determined properties, a constant temperature bath was used, in which the temperature was automatically controlled, and did not vary more than ± 0.2°C.

Density: The density of water was obtained from reference 20 and that for ethylene glycol from reference 10. The densities of the other materials were obtained using a hydrometer. A hydrometer was selected for each liquid, so that it could be read to the nearest two or three thousandths.

Viscosity: The above references were used also to obtain the viscosities of water and ethylene glycol as a function of temperature. These reported values were checked experimentally at one temperature and the agreement was found to be better than 0.5 percent. The viscosity of the other liquids were measured using calibrated Ostwald viscometers.

Specific Heat: The values for the specific heat of water were taken from reference 20, and those for ethylene glycol from reference 10. The values for the remaining materials were taken from reference 28.

Thermal Conductivity: All thermal conductivities were taken from the experimentally determined values of Woolf and Sibbitt.[55] The thermal conductivity of the Dowtherm A-Dowtherm E mixture was computed

assuming that it was a linear function of the weight percent of each component and the thermal conductivities of the two components, as recommended by Cecil and Munch.[7]

Interfacial Tension: The interfacial tensions of each system were measured by means of the drop-weight method developed by Harkins and Brown.[21] A determination of the interfacial tension of water against carbon tetrachloride checked the value reported in reference 20 to within one percent.

TABLE IX

PHYSICAL PROPERTIES OF MATERIALS USED

Material	25°C	40°C	50°C	60°C	70°C	80°C
Density: grams/cc						
Water	0.997	0.992	0.988	0.983	0.978	0.972
Ethylene Glycol	1.109	1.099	1.093	1.085	1.078	1.070
Dowtherm E	1.300	1.285	1.276	1.268	1.260	1.253
Dowtherm E + A	1.186	1.175	1.166	1.158	1.148	1.137
Finol	0.845	0.834	0.828	0.823		
Viscosity Centipoises:						
Water	0.893	0.656	0.549	0.469	0.406	0.357
Ethylene Glycol	17.5	9.65	6.90	5.17	3.95	3.05
Dowtherm E	1.27	1.05	0.938	0.843	0.779	0.758
Dowtherm E + A	1.85	1.46	1.26	1.11	0.987	
Finol	24.0	13.5	9.10	7.10		
Heat Capacity: cal/g. °C						
Water	0.999	0.999	0.999	1.000	1.001	1.003
Ethylene Glycol	0.565	0.583	0.594	0.606	0.617	0.628
Dowtherm E	0.278	0.282	0.285	0.288	0.292	0.296
Dowtherm E + A	0.326	0.336	0.342	0.347	0.351	
Finol	0.469	0.483	0.492	0.501	0.510	0.519

TABLE IX (Cont'd)

Material	25°C	40°C	50°C	60°C	70°C	80°C
Thermal Conductivity: cal/sec. cm. °C						
Water	0.00145	0.00152	0.00155	0.00158	0.00160	0.00161
Ethylene Glycol	0.000597	0.000595	0.000594	0.000592	0.000591	0.000589
Dowtherm E	0.000306	0.000301	0.000297	0.000294	0.000290	0.000287
Dowtherm E + A	0.000323	0.000318	0.000315	0.000311	0.000308	0.000325
Finol	0.000339	0.000333	0.000331	0.000329	0.000327	0.000325
Interfacial Tension: dynes/cm.						
System						
Water + Dowtherm E	39.5	38.5	37.	37.1	36.5	35.8
Water + Dowtherm A + E	38.5	37.7	37.2	36.6	36.1	35.5
Ethylene Glycol Dowtherm A + E	9.0	9.0	9.0	9.0	9.0	9.0
Ethylene Glycol Dowtherm E	8.5	8.35	8.26	8.16	8.06	7.96
Water + Finol	50.5	49.0	47.9	46.8	45.7	44.6
Ethylene Glycol + Finol	19.5	19.2	19.0	18.8	18.6	18.4

APPENDIX B. CALIBRATION OF DROP COLLECTOR

The drop material flowing from the liquid-liquid interface in the collector to the point where its temperature was measured, increased in temperature due to heat transfer through the interface and conduction through the glass collector. Since the temperature of the drop entering the liquid-liquid interface was desired, it was necessary to calibrate the collector. The drop collector was removed from the test section for the purpose of calibration and wrapped with an electrically heated jacket to simulate the surrounding continuous phase. Water entered the collector at a point corresponding to the liquid-liquid interface, and a thermocouple was also inserted at this point to obtain the water temperature. The calibration extended over a wide range of water flow rates and temperature differences. The correction factor is defined by

$$\frac{t - \bar{T}}{t - T_1}$$

where t is the surroundings temperature, $\bar{T}$ is the temperature at the point of liquid entry, and T_1 is the temperature of the water as given by the collector thermocouple. Therefore, multiplying experimentally determined temperature differences by this factor gives the actual temperature difference between the continuous phase and the average drop temperature.

A relation between the correction factor and the water flow rate can be derived by making a heat balance over the collector as follows:

$$L\, C_p\, d\bar{T} = h_c\, (t - \bar{T})\, d\, A \quad . \qquad (B\text{-}1)$$

In this equation, L is the water flow rate, h_c is a heat transfer coefficient which includes heat transfer through the interface as well as by conduction through the collector, and A is the area through which heat is transferred. Solution of this equation gives

$$\ln \frac{t - \bar{T}}{t - T_1} = \frac{h_c A}{C_p L} \quad . \tag{B-2}$$

Now h_c in general is proportional to the water rate raised to some power; therefore, this last equation can be written as

$$\ln \frac{t - \bar{T}}{t - T_1} = C L^{o} \quad , \tag{B-3}$$

where C is a function only of the physical properties of the drop material and the dimensions of the collector. This equation shows that the correction is independent of the temperature difference, a fact which was verified from the data taken during calibration, and depends only upon the water rate.

Figure 30 is a graph of the experimentally determined correction factors versus the water rate. There are two calibration curves given because after run A18e the collector thermocouple was moved farther into the collector when it was found that this location gave more uniform temperature readings. The location of the thermocouple in the collector was maintained fixed by securing it with a loop of fine wire attached to a copper ring, and drawing up on the whole assembly until the copper ring rested snugly against the constriction in the top of the collector chamber. For runs where ethylene glycol was used as a drop material, the correction factor was estimated from that for water by adjusting the value of the constant C to correspond to the change

physical properties. The correction for ethylene glycol was much less than that for water due to its higher Prandtl number.

It should be pointed out that the correction factor does not change the slope of the experimentally determined plots of log $(t - \overline{T})$ versus distance from orifice, and therefore, this factor does not enter into the computation of the Nusselt number. The correction factor is needed, however, in order to determine the actual drop temperatures for the purpose of determining average values for the physical properties of the drop material.

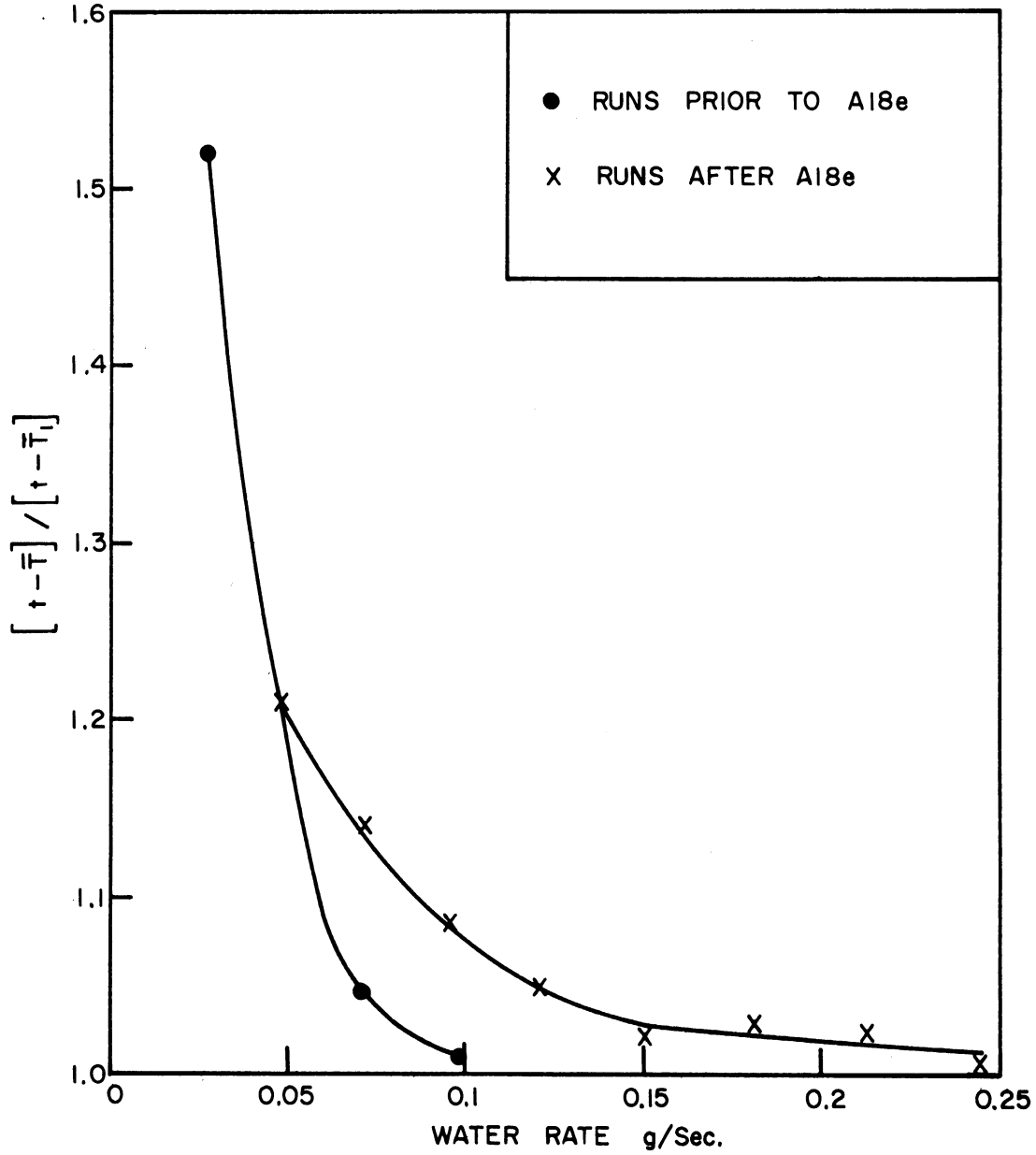

Figure 30. Calibration Curve for Drop Collector

APPENDIX C. DERIVATION AND SOLUTION OF THE DIFFERENTIAL EQUATION FOR COMPLETELY MIXED DROPS

The assumption that the drop is completely mixed gives a drop model in which there exists no internal temperature gradient, and therefore, no internal resistance to heat transfer. The temperature of the drop as a function of time can be derived by the following heat balance:

Rate of heat transfer to drop = $hA_d\ (t - \bar{T})$

Accumulation of heat energy in drop = $C_{p_d}\ \rho_d V \frac{d\bar{T}}{d\theta}$

Equating these two relations gives

$$\frac{d\bar{T}}{d\theta} = \frac{hA_d}{C_{p_d} V \rho_d}\ (t - \bar{T}) \quad . \tag{C-1}$$

The solution of this equation is

$$\frac{t - \bar{T}}{t - \bar{T}_i} = \exp\ (- \frac{hA_d\theta}{C_{p_d} V \rho_d}) \quad . \tag{C-2}$$

where T_i is the initial temperature of the drop.

APPENDIX D. DERIVATION AND SOLUTION OF THE DIFFERENTIAL EQUATION FOR CIRCULATING DROPS

This appendix contains a short summary of the derivation by Kronig and Brink[33] for transfer rates in circulating drops. It also includes the necessary modifications to account for the presence of a resistance to heat transfer outside the drop, and the method of solving the resulting boundary value problem with the aid of an electronic differential analyzer.

The major assumptions made in this analysis are:

1. The flow inside the drop is such that the flow pattern is identical to that derived for flow inside liquid spheres in the Stokes law region.

2. The drop is spherical.

3. The time of circulation inside the drop is short compared to the time of conduction.

With these assumptions, the stream lines given by equation (14) and shown in Figure 9, become lines of constant temperature. A function which is proportional to the stream function ψ, when radial distances are measured in terms of the drop radius, is given by the following equation.

$$\xi = 4\, r^2 \left(1 - r^2 \right) \sin^2 \varphi \qquad \text{(D-1)}$$

By assumption (3), these are also lines of constant temperature, and the paths along which heat is conducted are the orthogonal trajectories of (D-1), given by

$$\gamma = \frac{r^4 \cos^4 \varphi}{2r^2 - 1} \quad . \qquad \text{(D-2)}$$

Using ξ, γ, and the azimuthal angle β to form a set of orthogonal-coordinate axes, a relation for the temperature distribution in a circulating drop can be derived. Making a heat balance around a differential element in this coordinate system, and using the fact that the temperature is independent of γ, and β, gives

$$\frac{\partial}{\partial S_\xi}\left(\frac{\partial T}{\partial S_\xi} d S_\gamma d S_\beta\right) = \frac{1}{\alpha_d}\frac{\partial T}{\partial \theta} d S_\gamma d S_\beta \qquad \text{(D-3)}$$

where S_ξ, S_γ and S_β are distances measured in the ξ, γ, and β directions respectively. The relation between the distance and the corresponding direction can be derived from equations (D-1) and (D-2) and the definition of the azimuthal angle. The final relations are shown by equation (D-4).

$$d S_\xi = \frac{a\, d\, \xi}{8r \sin\varphi \sqrt{\Delta}}$$

$$d S_\gamma = \frac{a(2r^2 - 1)^2\, d\, \gamma}{4r^3 \cos^3\varphi \sqrt{\Delta}} \qquad \text{(D-4)}$$

$$d S_\beta = a\, r \sin\varphi\, d\, \beta$$

where

$$\Delta = (1 - r^2)^2 \cos^2\varphi + (1 - 2r^2)^2 \sin^2\varphi \,.$$

Substituting these relations in (D-3) gives

$$\frac{\partial}{\partial \xi}\left[\frac{\partial T}{\partial \xi}\frac{2a \sin^2\varphi\,(2r^2 - 1)^2}{r \cos^3\varphi}\right] = \frac{1}{\alpha_d}\frac{a^3 (2r^2 - 1)^2}{32 s^2 \cos^3\varphi\, \Delta}\frac{\partial T}{\partial \theta} \,. \qquad \text{(D-5)}$$

Multiplying (D-5) by $d\gamma$ and integrating over γ yields a relation for the drop temperature as a function of time and the space variable ξ. This equation is

$$\frac{\partial}{\partial \xi}\left[p(\xi)\,\frac{\partial T}{\partial \xi}\right] - \frac{a^2}{16\alpha_d}\,q(\xi)\,\frac{\partial T}{\partial \theta} = 0 \quad , \tag{D-6}$$

where

$$p(\xi) = \int \frac{(2r^2 - 1)^2 \sin^2 \varphi}{r \cos^3 \varphi}\, d\gamma$$

and

$$q(\xi) = \int \frac{(2r^2 - 1)^2}{4r^3 \cos^3 \varphi\, \Delta}\, d\gamma \quad .$$

The integrals p and q have been solved in terms of elliptic integrals by Kronig and Brink and are shown graphically in Figure 31. In these equations, ξ varies from zero on the outside surface of the drop and along the vertical axis, to a value of one at the point of symmetry for the isotherms and stream lines located on the horizontal radius of the drop.

The boundary conditions needed to solve equation (D-6) are the initial temperature distribution in the drop and a relation involving the heat flux or temperature at $\xi = 0$. It is also necessary to restrict the temperature to finite values or to require that

$$\left[\frac{\partial T}{\partial \xi}\right]_{\xi = 1} = 0 \quad . \tag{D-7}$$

The boundary conditions used by Kronig and Brink for a continuous phase temperature of zero degrees are

$$[T]_{\theta = 0} = T_i \tag{D-8}$$

and

$$[T]_{\xi = 0} = 0 \quad . \tag{D-9}$$

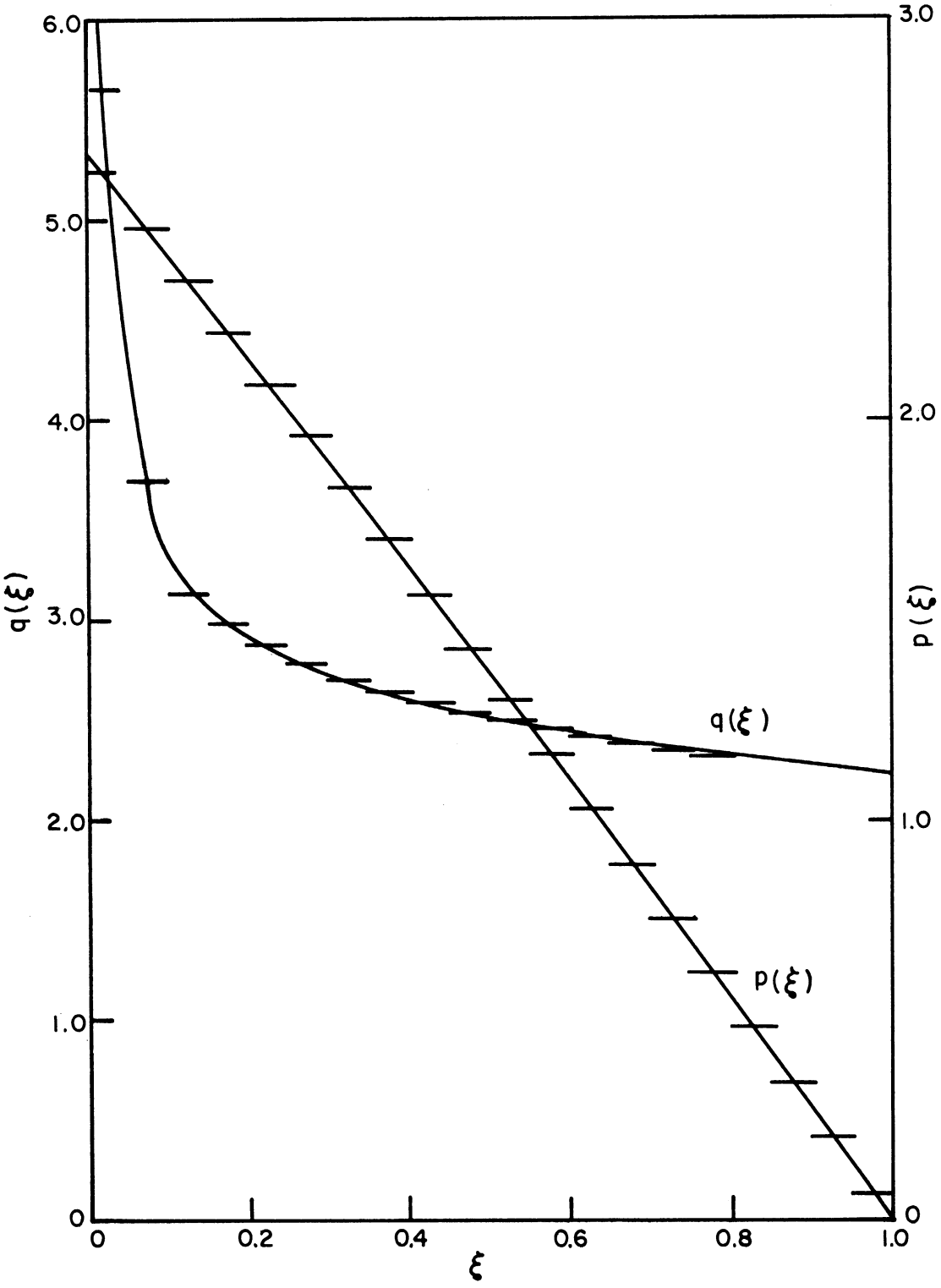

Figure 31. Functions p, and q, for Circulating Drops

The equation (D-8) is the condition of uniform initial temperature. Boundary condition (D-9) states that the surface and vertical axis of the drop are at all times equal to the temperature of the continuous phase. The latter condition is equivalent to stating that the heat transfer coefficient is infinite or that there is zero resistance to heat transfer around the drop. This condition is easily realized in the field of mass transfer to drops, but is not too realistic in the case of heat transfer.

In the present work, the boundary condition (D-9) was generalized to include the effect of a finite value of the heat transfer coefficient. To do this, the total amount of heat entering the drop surface by convection per unit time, was set equal to the heat leaving the surface per unit time by conduction on the inside of the drop. In equation form this becomes

$$\int_A k_d \frac{\partial T}{\partial S_\xi} \, d S_\gamma \, d S_\beta \Big]_{\xi=0} = A_d \, h \, T\Big]_{\xi=0} \qquad \text{(D-10)}$$

where it has been assumed that the continuous phase temperature is zero. This equation can be changed to a more usable form using equation (D-4) and the condition that the temperature is independent of γ, and β, which reduces (D-10) to

$$\frac{\partial T}{\partial \xi}\Big]_{\xi=0} \int_\beta \int_\gamma \frac{2 \sin^2 \varphi (2r^2 - 1)^2 \, a}{r \cos^3 \varphi}\Big]_{\xi=0} d\gamma \, d\beta = \frac{4\pi \, h \, a^2}{k_d} \, T\Big]_{\xi=0} \qquad \text{(D-11)}$$

Because of symmetry, (D-11) need be integrated only over $0 = \beta = \pi/2$ and multiplied by 4, and then integrated over $0 = \gamma = 1$ and multiplied by 2. The integral along the vertical axis of the drop need not be considered, since the integrand is zero here. Also, the integration with respect to β may be performed directly, since the integrand is independent of β. Carrying out the indicated operations gives the following equation:

$$\left.\frac{\partial T}{\partial \xi}\right]_{\xi=0} \int_0^1 \left.\frac{2 \sin^2 \varphi (2r^2 - 1)^2}{r \cos^3 \varphi}\right]_{\xi=0} d\gamma = \left.\frac{h\, a}{k_d} T\right]_{\xi=0} \qquad \text{(D-12)}$$

Equation (D-2) is a relation from which $d\gamma$ may be obtained in terms of φ and r. Differentiating (D-2) shows that for the surface of the drop,

$$d\gamma = -4 \cos^3 \varphi \sin \varphi \, d\varphi \quad .$$

Substituting this in equation (D-12) and integrating gives

$$\left.\frac{\partial T}{\partial \xi}\right]_{\xi=0} = \left.\frac{3\, h\, a}{16\, k_d} T\right]_{\xi=0} \qquad \text{(D-13)}$$

as the generalized boundary condition. The complete boundary value problem is given by the following system of equations.

$$\frac{\partial}{\partial \xi}\left[p(\xi) \frac{\partial T}{\partial \xi}\right] - \frac{a^2}{16 \alpha_d} q(\xi) \frac{\partial T}{\partial \theta} = 0$$

$$\left.\begin{aligned} T]_{\theta=0} &= T_i \\ \left.\frac{\partial T}{\partial \xi}\right]_{\xi=0} &= \left.\frac{3\, h\, a}{16\, k_d} T\right]_{\xi=0} \\ \left.\frac{\partial T}{\partial \xi}\right]_{\xi=1} &= 0 \end{aligned}\right\} \qquad \text{(D-14)}$$

The system (D-14) may be solved by the method of separation of variables. This gives rise to the following set of ordinary differential equations and boundary conditions.

$$\frac{d}{d\xi}\left[p(\xi)\frac{d\Xi}{d\xi}\right] + \lambda q(\xi)\Xi = 0$$

$$\frac{d\Xi(1)}{d\xi} = 0 \tag{D-15}$$

$$\frac{d\Xi(0)}{d\xi} - \frac{3\,a\,h}{16\,k_d}\Xi(0) = 0$$

$$\frac{d\Theta}{d\theta} + \lambda\frac{16\alpha_d}{a^2}\Theta = 0 \tag{D-16}$$

The equations (D-15) are of the Sturm-Liouville type and therefore, their solution gives rise to a set of orthogonal functions. The solution of (D-16) is

$$\Theta = \exp\left[-\lambda\frac{16\alpha_d\,\theta}{a^2}\right]$$

and combining this with the solution of (D-15) in terms of the orthonormal functions and corresponding eigenvalues gives the following general solution to (D-14).

$$\frac{T(\xi,\theta)}{T_i} = \sum_{n=1}^{\infty} B_n \Xi_n(\xi)\exp\left[-\lambda_n\frac{16\alpha_d\,\theta}{a^2}\right] \tag{D-17}$$

In this equation, the coefficients (B_n) must be such that the boundary condition at zero time is satisfied, that is

$$\sum_{n=1}^{\infty} B_n \Xi_n(\xi) = 1 \quad . \tag{D-18}$$

Using the properties of orthonormal functions gives

$$B_n = \int_0^1 \overline{\overline{=}}_n (\xi)\, q\,(\xi)\, d\,\xi \quad . \tag{D-19}$$

An alternate expression for B_n can be obtained by solving (D-15) for $\overline{\overline{=}}_n (\xi)\, q\,(\xi)$ and substituting this in D-19). This integral can then be solved using the values of p at $\xi = 0$ and at $\xi = 1$, to obtain the following expression.

$$B_n = \frac{8}{3\lambda_n} \frac{d\,\overline{\overline{=}}_n(0)}{d\xi} \tag{D-20}$$

The average temperature of the drop can be found at any time, θ, by integrating (D-17) over the volume of the drop and dividing by the total drop volume. Carrying out this operation, and removing the restriction of zero continuous phase temperature yields equation (15).

$$\frac{t - \overline{T}}{t - T_i} = \frac{3}{8} \sum_{n=1}^{\infty} B_n^2 \exp\left[- \lambda_n \frac{16\alpha_d\, \theta}{a^2} \right] \tag{15}$$

The eigenvalues λ_n and the coefficients (B_n) must be found by solving equations (D-20) and (D-15). Kronig and Brink solved these equations using the Rayleigh-Ritz method. The method used in the present work will be explained below.

The electronic differential analyzer was used to solve the differential equations (D-15) to obtain the eigenvalues which were used in equation (D-20) to find B_n. In this computer, voltages are used to represent the dependent variable and the independent variable is set proportional to time. Setting twenty seconds of computer time equal to one unit of ξ, the equation (D-15) became

$$p(\tau)\frac{d^2\overline{\overline{=}}}{d\tau^2} + p(\tau)\frac{d\overline{\overline{=}}}{d\tau} + \frac{\lambda q(\tau)\overline{\overline{=}}}{400} = 0$$

$$\frac{d\overline{\overline{=}}(20)}{d\tau} = 0 \qquad \text{(D-21)}$$

$$\frac{d\overline{\overline{=}}(0)}{d\tau} = \frac{3Dh}{640\ k_d}\overline{\overline{=}}(0)$$

In these equations, τ is the computer time in seconds. A schematic diagram of the computer circuit used to solve (D-21) is shown in Figure 32. The integrators and summers shown are high gain amplifiers, with capacitance feed back for the integrators and resistance feed back for the summers. The numbers preceding each amplifier in the figure are the values in megohms of the input resistors. The feed back resistances on the summers are in each case one megohm, unless otherwise indicated. In all cases, the value of the feed back capacitors on the integrators is one microfarad. The functions p and q appear as input and feed back resistances, respectively. These functions were simulated in a stepwise manner by automatically changing the resistance each second of operation. The stepwise approximation to the actual functions is shown in Figure 31. A solution was started by setting the initial values of $\frac{d\overline{\overline{=}}}{d\tau}$ and $\overline{\overline{=}}$ on their respective integrators. This was done by impressing an initial voltage on the feedback capacitors of these integrators such that these voltages satisfy the second boundary condition in (D-21). The solution was completed by adjusting the value of the input resistor (y) so that the first boundary condition in (D-21) was satisfied. Since there is one solution for each eigenvalue, the solutions were numbered according to the number of

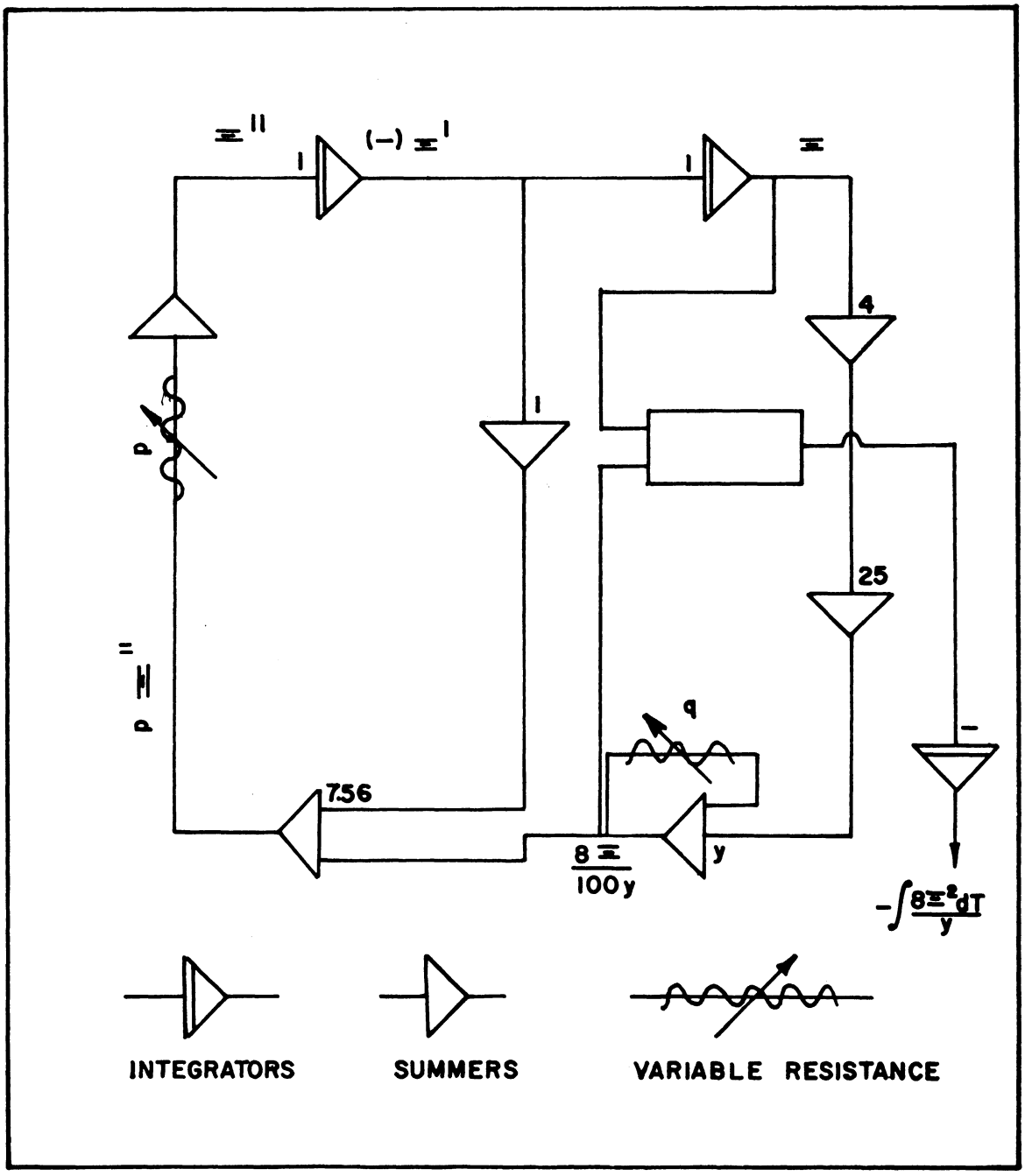

Figure 32. Electronic Differential Analyzer Circuit for Boundary Value Problem in Circulating Drops

times $\frac{d\,\overline{\overline{\Xi}}_n}{d\tau}$ passed through zero. The eigenvalues are related to the value of the input resistance (y) by the relation $\lambda_n = 4/y$. Using this relation for the eigenvalues, the corresponding constants for equation (14) can be found through equation (D-20). However, since the magnitude of the voltage representing $\overline{\overline{\Xi}}$ is arbitrary, the condition that $\overline{\overline{\Xi}}_n$ be normalized must also be used. This condition is given by

$$\int_0^{20} \frac{\overline{\overline{\Xi}}^2 (\tau)\, q\, (\tau)\, d\tau}{20} = 1 \quad . \qquad \text{(D-22)}$$

Therefore, the value of $\frac{d\,\overline{\overline{\Xi}}_n}{d\xi}$ as given by the computer must be multiplied by a factor, calculated from equation (D-22), before it is used in equation (D-20) to find B_n. The computer was used to obtain the solution to the integral appearing in equation (D-22). The above procedure was repeated for a wide range of values for hD/k_d. The results giving λ_n and B_n for various values of hD/k_d are tabulated in Table X.

The values for $hD/k_d = \infty$, can be compared to those computed by Kronig and Brink. These authors found the following values for λ_n and B_n.

$$\lambda_1 = 1.678 \quad ; \quad B_1 = 1.32$$

$$\lambda_2 = 9.85 \quad ; \quad B_2 = 0.73$$

TABLE X

EIGENVALUES AND COEFFICIENTS FOR CIRCULATING DROPS

hD/k_d	λ_1	λ_2	λ_3	B_1	B_2	B_3
3.20	0.262	4.24		1.49	0.107	
5.33	0.386					
8.00	0.534					
10.7	0.680	4.92		1.49	0.300	
16.0	0.860	5.26		1.48	0.382	
21.3	0.982	5.63		1.47	0.428	
26.7	1.082	5.90	15.7	1.49	0.495	0.205
53.3	1.324	7.04	17.5	1.43	0.603	0.298
107	1.484	7.88	19.5	1.39	0.603	0.384
213	1.560	8.50	20.8	1.31	0.588	0.396
320	1.600	8.62	21.3	1.31	0.583	0.391
∞	1.656	9.08	22.2	1.29	0.596	0.386

APPENDIX E. DERIVATION AND SOLUTION OF DIFFERENTIAL EQUATION FOR STAGNANT DROPS

The conduction of heat in a solid sphere was used as the model for stagnant drops. The methods of setting up and solving the temperature equations for this case are well summarized by Carslaw and Jaeger[4] so that only a brief outline will be given in this appendix.

The differential equation and boundary conditions for the temperature inside the stagnant drop with an outside film coefficient are

$$\frac{\partial T}{\partial \theta} = \alpha_d \left[\frac{2}{r}\frac{\partial T}{\partial r} + \frac{\partial^2 T}{\partial r^2}\right]$$

$$\left.\frac{\partial T}{\partial r}\right]_{r=0} = 0$$

$$\left.\frac{\partial T}{\partial r}\right]_{r=a} + \frac{h}{k_d} T\Bigg]_{r=a} = 0 \qquad \text{(E-1)}$$

$$T]_{\theta=0} = T_i$$

The solution of these equations integrated over the volume of the drop gives the following relation for the average drop temperature.

$$\frac{t - \bar{T}}{t - T_i} = 6 \sum_{n\ 1} C_n \exp\left[-\psi_n^2 \frac{\alpha_d \theta}{a^2}\right] \qquad (15)$$

For this case, the coefficients C_n are given by

$$C_n = \frac{(\sin \psi_n - \psi_n \cos \psi_n)^2}{\psi_n^3 \left(\psi_n - \sin \psi_n \cos \psi_n\right)} \quad . \qquad \text{(E-2)}$$

The eigenvalues ψ_n depend upon the dimensionless group hD/k_d and are the roots of the following equation.

$$\tan \psi \quad \frac{2\psi}{2 - \frac{hD}{k_d}} \tag{E-3}$$

The first six roots of equation (E-3) are given in reference 4. Some of these roots and the values of the corresponding coefficients are given in Table XI for various values of hD/k_d.

TABLE XI

EIGENVALUES AND COEFFICIENTS FOR TEMPERATURE DISTRIBUTION IN STAGNANT DROPS

hD/k_d	ψ_1	ψ_2	ψ_3	ψ_4	C_1	C_2	C_3	C_4
4	2.029	4.913	7.979	11.086	0.159	0.00634		
6	2.289	5.087	8.096	11.173	0.153	0.0109		
8	2.456	5.233	8.205	11.256				
10	2.570	5.354	8.303	11.335	0.142	0.0179	0.00408	
12	2.654	5.454	8.391	11.409				
14	2.717	5.538	8.470	11.477	0.134	0.0220	0.00600	
16	2.765	5.608	8.541	11.541				
18	2.804	5.667	8.603	11.599	0.129	0.0242	0.0119	0.00291
20	2.836	5.717	8.659	11.653				
22	2.863	5.761	8.708	11.703	0.125	0.0255	0.00858	0.00359
32	2.948				0.118			
42	2.993							
62	3.041				0.111			
82	3.065							
102	3.080				0.107			
∞	3.142				0.101			

APPENDIX F. SAMPLE CALCULATION

A sample of the original data and calculations is given in this section, using run E4b as an example. In this run, Finol was the continuous phase and water was the dispersed phase. Table XII gives the original data taken during the run.

TABLE XII

ORIGINAL DATA FOR RUN E4b

Run No. E 4 b

Date: 7-13-56

Continuous phase rotameter reading, 15

Dispersed phase rotameter reading, 3.21

Net weight of sample of drop material, 7.96 gms.

Time interval during which sample was collected, 147.2 sec.

Drop frequency, 0.729 drops per sec.

Four photographs and two shadowgraphs of drops in test section.

Distance from Nozzle to Interface in Collector. (cm)	Thermocouple Readings in Millivolts				
	No. 1	No. 2 Collector	No. 3 Nozzle	No. 4 Cont. Phase	No. 5 Cont. Phase
11.1	1.160	1.589	0.848	2.448	2.451
16.7	1.160	1.753	0.841	2.451	2.451
18.2	1.160	1.833	0.843	2.451	2.457
25.5	1.160	1.932	0.842	2.458	2.458
32.8	1.160	2.081	0.840	2.459	2.459
38.7	1.160	2.167	0.839	2.455	2.455
47.3	1.160	2.210	0.841	2.451	2.459

From this data, the following computations were made.

1. Dispersed phase flow rate = $\frac{7.96}{147.2}$ = 0.0541 gm/sec.

   From the photographs, the average distance between drops in the test section was found to be 19.0 cm/drop.

2. Drop velocity: v = 19 x 0.729 = 13.8 cm/sec.

3. Drop weight = 0.0541/0.729 = 0.0742 gms.

4. Average continuous phase temperature, by averaging all the readings for T. C. No. 4 and T. C. No. 5 = 59.4°C.

5. Time average drop temperature = 47.8°C.

   This quantity is computed using the following relation:

$$(t - T)_{av} = \frac{\int_0^{\theta} (t - \overline{T})d\theta}{\theta} = 0.434 \frac{(t - \overline{T} - \text{antilog}_{10}\, i)}{b\ z}$$

   Then using the values at the point z = 75.3 gives

$$(t - T)_{av} = - \frac{0.434 \times (0.292 - 1.500)}{0.01578 \times 47.3} = 0.655 \text{ millivolts}$$

   Therefore, the time average drop temperature is = 2.455 - 0.655 = 1.800 millivolts or 47.8°C.

6. Physical properties:

	Continuous Phase	Dispersed Phase
ρ g/cc.	0.8234	0.9888
μ centipoises	7.20	0.565
C_p cal/g °C	0.500	0.999
k cal/sec. cm. °C	0.000330	0.00155
γ dynes/cm.	47.5	47.5

7. Drop volume: V = 0.0742/0.9888 = 0.0750 cc/drop.

8. Drop diameter (Spherical based on volume).

   $D = (0.0750 \times 3/4\ \pi)^{1/3}$ = 0.523 cm.

9. Drop area (assuming oblate spheroid).

Major diameter/minor diameter = 1.14

$A_d = 0.862\ (cm)^2$

10. Drop Reynolds Number.

$$Re = \frac{D\ v\ \rho}{\mu} = \frac{(0.523)(13.8)(0.823)}{(0.0720)} = 82.8$$

11. Drag coefficient.

Cross sectional area of drop $= \frac{\pi D^2}{4} = 0.215\ (cm)^2$

$$C_D = \frac{V\ \Delta\rho\ 2g}{\rho\ v^2\ A_{c_s}} = \frac{0.075 \times 0.165 \times 2 \times 980}{0.823 \times (13.8)^2 \times 0.215} = 0.718$$

12. Slope of $\log_{10}(t - \bar{T})$ versus z.

Assuming that $\log_{10}(t - \bar{T}) = bz + i$, then the constant b and i can be determined from the experimental data by the method of least squares. This method gives (for t and $\bar{T}$ in millivolts):

$$b = \frac{\Sigma z_n \Sigma y_n - n \Sigma z_n y_n}{(\Sigma z_n)^2 - n \Sigma z_n^2}$$

$$i = \frac{\Sigma y_n - b \Sigma z_n}{n}$$

where y is a corrected value of $\log_{10}(t - \bar{T})$. The computation of y_n was as shown below.

z_n	$t - \bar{T}$	$t - \bar{T}$ Corrected*	$t - \bar{T}$ Corrected & Adjusted**	$y_n = \log_{10}(t-\bar{T})$
11.1	0.866	1.028	1.036	0.0154
16.7	0.702	0.834	0.835	-0.0783
18.2	0.622	0.739	0.742	-0.1296
25.5	0.523	0.621	0.623	-0.2055

(Continued)

z_n	$t - \bar{T}$	$t - \bar{T}$ Corrected*	$t - \bar{T}$ Corrected & Adjusted**	$y_n = \log_{10}(t-\bar{T})$
32.8	0.374	0.444	0.444	-0.3526
38.7	0.288	0.342	0.341	-0.4672
47.3	0.245	0.291	0.292	-0.5346

* Corrected for temperature gain in the collector. In this case, the correction factor was 1.19 as shown on Figure 30 for a water rate of 0.0541 g/sec.

** Adjusted to a water temperature of 0.840 millivolts at the drop nozzle.

From these data, the slope b and the intercept i were calculated to be

$$b = \frac{-334.36 + (446.10)}{36,404.6 - 43,486.1} = -0.01578$$

$$i = \frac{-1.7524 - (0.01578)190.80}{7} = 0.1798$$

These are shown graphically in Figure 11.

13. Determination of Nusselt numbers.

Completely mixed drops:

$$\frac{hD}{k} = -\frac{bC_{p_d}V\rho_d{}^{vD}}{A_d k \log_{10} e} = \frac{(0.0158)(0.999)(0.0750)(0.989)(13.8)(0.523)}{(0.434)(0.862)(0.0003330)}$$

$$= 68.6$$

Circulating drops:

$$\lambda_1 = \frac{b\,a^2\,v}{16\alpha_d \log_{10} e} = \frac{(0.0158)(0.262)^2(13.8)}{(16)(0.00157)(0.434)} = 1.370$$

From a graph similar to Figure 10 but using an expanded scale, gives $hD/k_d = 62.6$. Therefore

$$\frac{hD}{k} = \frac{(62.6)(0.00155)}{(0.000330)} = 294$$

Stagnant drops:

$$\psi_1 = \left(\frac{-b\, a^2\, v}{d \log_{10} e}\right)^{1/2} = \frac{(0.0158)(0.262)^2(13.8)}{(0.00157)(0.434)}^{1/2} = 4.68$$

Table XI shows that the maximum value of ψ_1 is 3.142, and therefore, stagnant drops can be eliminated as a possibility for this run. From Kramers correlation, $hD/k = 30$.

14. Dimensionless groups used in correlation:

$$Pr = \frac{\mu C_p}{k} = \frac{(0.0720)(0.500)}{(0.000330)} = 109.1$$

$$\frac{D\gamma\rho}{\mu^2} = \frac{(0.523)(47.5)(0.823)}{(0.0720)^2} = 3950$$

$$\frac{\mu + \mu_d}{2\mu + 3\mu_d} = \frac{7.20 + 0.57}{14.4 + 1.70} = 0.484$$

APPENDIX G. SOLUTION OF LAMINAR BOUNDARY LAYER EQUATION TO OBTAIN POINT OF SEPARATION

Starting with the equations of motion for a viscous incompressible fluid, Meksyn[43] derived the following relation for the laminar boundary layer on a solid sphere.

$$u''' + uu'' + \frac{\cos \varphi}{(\sin \frac{\varphi}{2})^2} [(u')^2 - 1] = 0 \qquad (G\text{-}1)$$

In this equation, φ is the angle measured from the rear stagnation point, and u is proportional to the velocity potential and is such that the tangential velocity is given by u' when the velocity at infinity is unity. One of the independent variables in (G-1) is proportional to the inviscid velocity potential for flow around a sphere. The other independent variable is proportional to the inviscid stream function and the indicated differentiation in (G-1) is with respect to this variable.

The boundary conditions associated with (G-1) are as follows:

1. on the surface of the sphere

$$u = 0$$

$$u' = v_s$$

2. at large distances from the sphere

$$u' \rightarrow 1$$

In conditions (1), v_s is the velocity on the surface of the sphere at the point where (G-1) is to be solved. For solid spheres, $v_s = 0$ and for liquid spheres, $v_s > 0$.

At the point where the boundary layer separates from the sphere, the shear on the surface becomes zero. Therefore, at this

point, an additional condition must be used in the solution of (G-1). This condition is as follows:

3. on the surface of the sphere

$$u'' = 0$$

From the solution of (G-1) with the three conditions given above, a value of the function involving the angle φ, at which separation takes place, can be determined.

The solution of (G-1) was accomplished with the aid of the electronic differential analyzer. A schematic diagram of the circuit used is presented in Figure 33. To obtain a solution on the computer for a particular value of v_s, the initial conditions (1) are set on the corresponding integrators, and a plot of u' versus time is observed for various settings on the potentiometer representing

$$\frac{\cos \varphi}{(\sin \frac{\varphi}{2})^2} \quad .$$

The correct setting on this potentiometer is taken as the one which produces the most rapid convergence of u' to unity. The change occurring in φ as v_s is increased is shown in Figure 16.

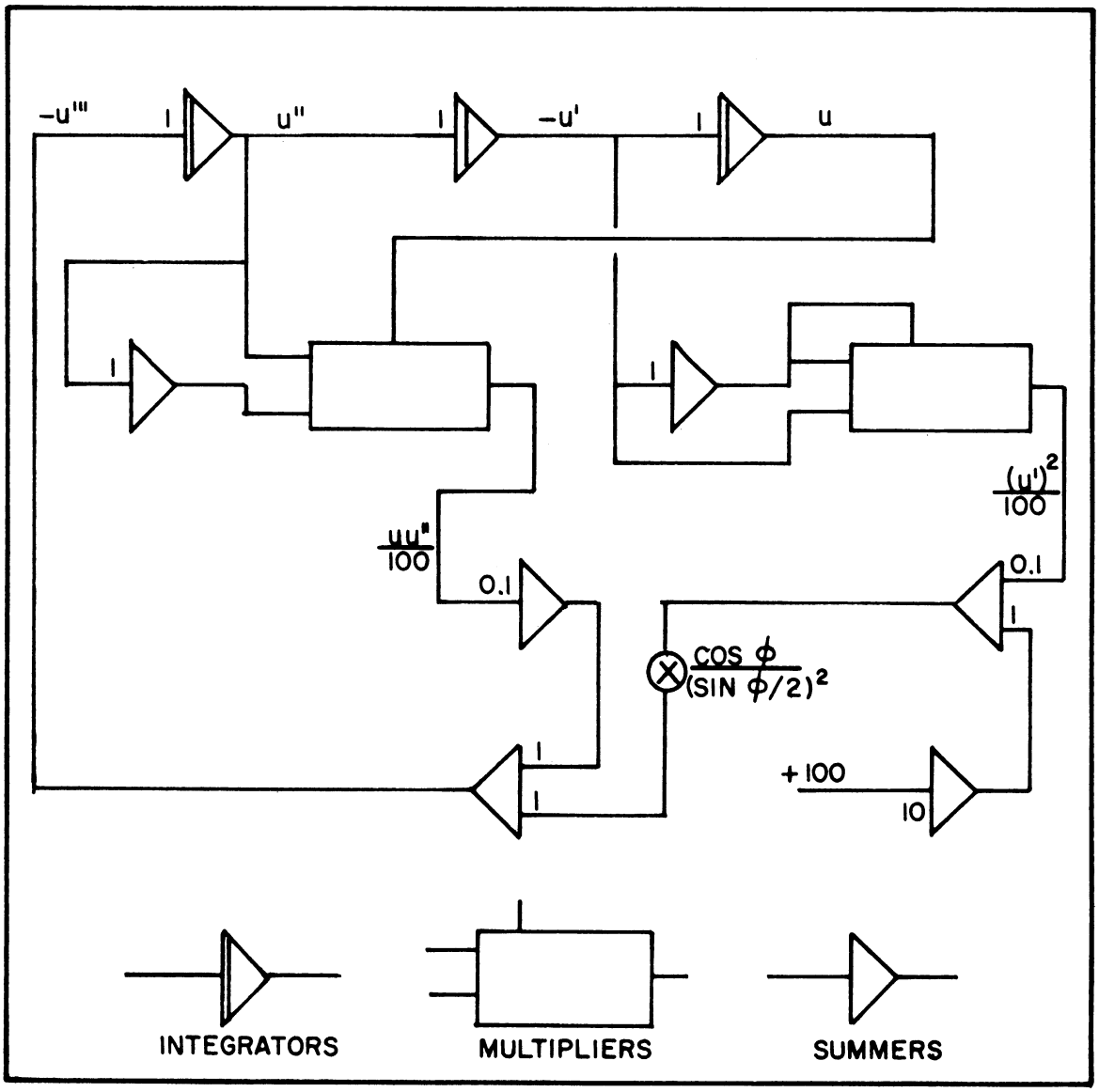

Figure 33. Electronic Differential Analyzer Circuit for Solving Boundary Layer Equation for Spheres

APPENDIX H. THE EFFECT OF MASS TRANSFER ON HEAT TRANSFER RATES

The solubility of dichlorobenzene in ethylene glycol is high compared to the other systems used in this research. Therefore, upon introducing ethylene glycol drops into Dowtherm A + E or Dowtherm E, some transfer of the continuous phase into the drop would occur. The exact rate of this transfer is not known, but for the maximum effect it can be assumed that at the time of collection, the drops are saturated with the continuous phase. If it is assumed that the temperature of the material being transferred is at the continuous phase temperature, then this will also maximize the effect.

Making a heat balance around the drop, in which the heat transferred due to the solution of the continuous phase in the drop material is included, gives the following relation.

$$\int_0^\theta h' A_d (t - \bar{T}) \, d\theta = \int_0^\theta h A_d (t - \bar{T}) \, d\theta + x \rho_d V C_p (t - \bar{T}_{av}) \qquad (H\text{-}1)$$

In this equation, h' is the apparent heat transfer coefficient, and h is the true heat transfer coefficient. The quantity x is the mass fraction of the continuous phase in the drop at the time of collection θ. For the purpose of calculation, the time average temperature was used for the average temperature $\bar{T}_{av}$.

Since it is known that $(t - \bar{T})$ is an exponential function of time, equation (H-1) can be integrated to give the increase in the Nusselt number due to mass transfer.

$$\Delta Nu = - \frac{x \rho_d D^2 C_p (t - \overline{T}_{av})}{6k (\overline{T} - T_i)} (\text{slope}) \qquad \text{(H-2)}$$

In equation (H-2), the term (slope) is the slope of the plot of the natural logarithm of $(t - \overline{T})$ versus time, and T_i is the initial drop temperature, calculated from the intercept of this plot at zero time. The value of x at 25°C as given in reference 10 is 0.045. For the purpose of these calculations a value of 0.1 was used, which is believed to be high for the temperature range under consideration. The values calculated by equation (H-2) for system C have been shown previously in Table VI.

APPENDIX I. MERCURY ARC AND POWER SUPPLY

A circuit diagram for the mercury arc power supply is shown in Figure 34, and the details of the mercury arc are shown in Figure 35. To operate, power is supplied to the heater on the mercury arc and the voltage adjusted to about twenty five volts. It takes this heater three or four minutes to completely vaporize the column of mercury in the glass capillary tube. During this period, the one half microfarad capacitor can be charged by supplying power to the filament transformer and to the high voltage transformer. The voltage to the high voltage transformer is adjusted to about sixty five volts, since the higher voltage exceeds the upper limit on the capacitor. Two or three minutes are allowed for the capacitor to reach full charge. The capacitor is discharged through the column of vaporized mercury by closing the relay.

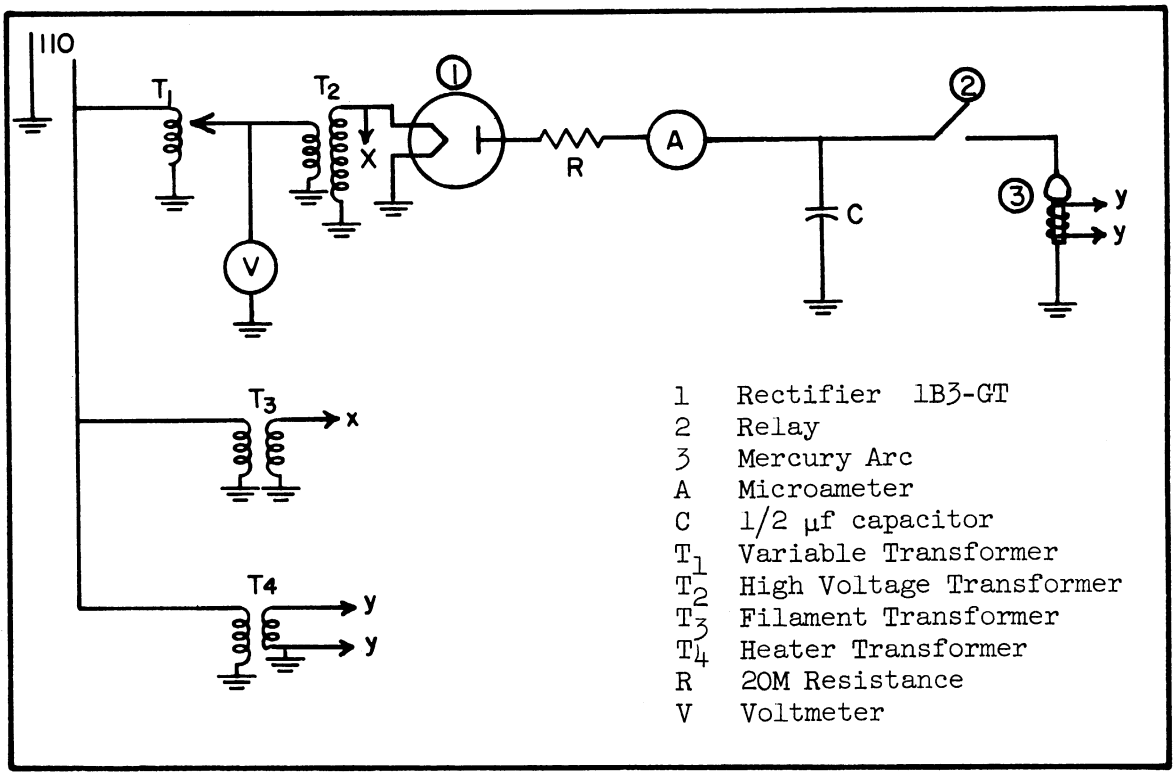

Figure 34. Circuit Diagram for Mercury Arc Power Supply

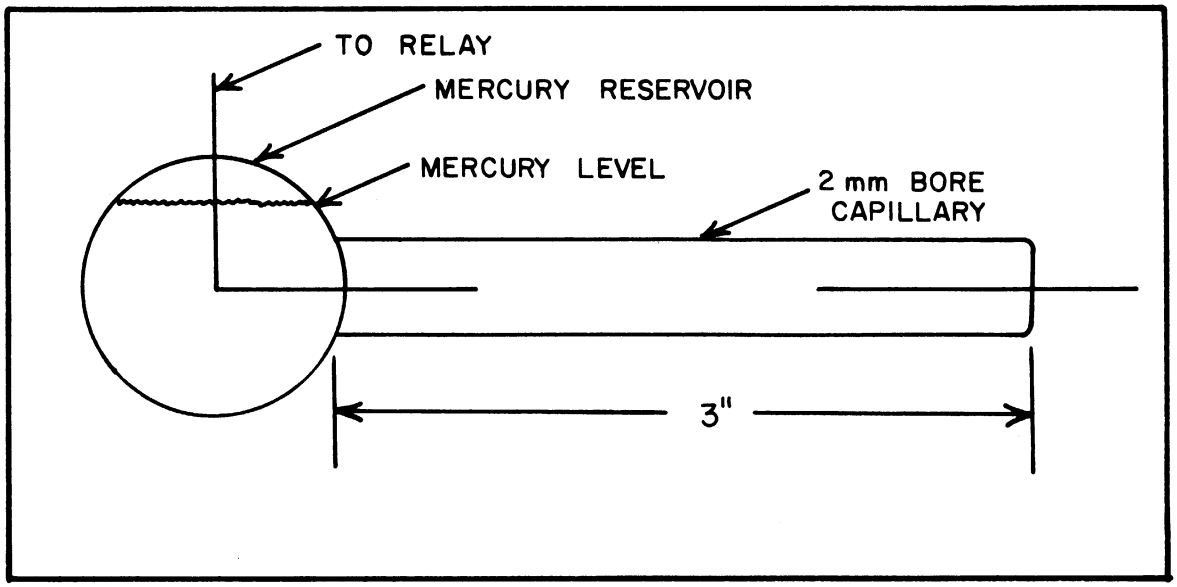

Figure 35. Details of Mercury Arc

TABLE OF NOMENCLATURE

A - area, $(cm)^2$

a - drop radius, cm

B_n - coefficients in equation (15), dimensionless

b - slope of $\log_{10}(t - T)$ versus z, $(cm)^{-1}$

C - a constant in equations (20) and (B-3), dimensionless

C_D - drag coefficient, $2V\Delta\rho g/Av^2$, dimensionless

C_n - coefficients in equation (16), dimensionless

C_p - specific heat, cal/gm °C

D - drop diameter, cm

D_o - diameter of dispersion nozzle, cm

d - used as a subscript to denote drop properties

F - correction factor in equation (1), dimensionless

f - frequency, $(sec)^{-1}$

$f(\varphi)$ - function relating boundary layer thickness on sphere to position

g - acceleration due to gravity, $cm/(sec)^2$

h - heat transfer coefficient, cal/sec $(cm)^2$ °C

h_c - heat transfer coefficient in drop collector, cal/sec $(cm)^2$ °C

i - intercept at zero time of $\log_{10}(t - T)$ versus time, dimensionless

K - mass transfer coefficient, cm/sec

k - thermal conductivity, cal/sec cm °C

L - flow rate of discontinuous phase, gm/sec

M - interfacial tension group, $D\gamma\rho/\mu^2$, dimensionless

m - a constant, dimensionless

n - used as an exponent, dimensionless

Nu - Nusselt number, hD/k, dimensionless

o - used as an exponent, dimensionless

P - physical properties group, $\rho^2\gamma^3/g\mu^4\Delta\rho$, dimensionless

p_i - pressure inside drop surface, dynes/$(cm)^2$

p_o - pressure outside drop surface, dynes/$(cm)^2$

Pr - Prandtl number, $\mu C_p/k$, dimensionless

$p(\xi)$ - functions used in the analysis for circulating drops, dimensionless

Q - quantity of heat, cal

q - used as an exponent, dimensionless

$q(\xi)$ - function used in the analysis for circulating drops, dimensionless

r - radial distance, cm

Re - Reynolds number, $Dv\rho/\mu$, dimensionless

S - distance, cm

T - drop temperature, °C

$\overline{T}$ - mean drop temperature over the volume of the drop, °C

t - continuous phase temperature, °C

$\overline{T}_{av}$ - time average of mean drop temperature, °C

T_i - initial drop temperature, °C

T_s - surface temperature of drop, °C

T_l - temperature of material at thermocouple No. 2 in collector, °C

u - velocity in x-direction, cm/sec, also used as velocity potential in equation (G-1)

V - drop volume, $(cm)^3$

v - drop velocity, cm/sec, velocity in y-direction for equations (8), (9), and (10)

v' - velocity, cm/sec, used in equation (6)

w - velocity in z-direction for equations (8), (9), and (10), cm/sec

We - Weber number, $v^2 D\rho/\gamma$, dimensionless

z - distance, cm

OTHER SYMBOLS

α - thermal diffusivity, $(cm)^2/sec$

β - azimuthal angle

γ - interfacial tension, dynes/cm, or orthogonal trajectories of ξ

Δ - difference

δ - boundary layer thickness, cm

Θ - time dependent part of solution for temperature inside circulating drop

θ - time, sec

θ_c - contact time, sec

λ_n - eigenvalues in equation (15), dimensionless

ρ - density, $gm/(cm)^3$

μ - viscosity, poises

$\underline{\underline{\Xi}}$ - eigenfunctions, used in analysis for circulating drops

ξ - isotherms for circulating drops

φ - polar angle for drops and spheres

ψ - stream function for flow inside circulating drops

ψ_n - eigenvalues in equation (16)

BIBLIOGRAPHY

1. Alexander, A. E., Johnson, P., Colloid Science, Oxford Press, 1949.

2. Bond, W. N., Phil. Mag. [7], 4, 889 (1927).

3. Bond. W. N., Newton, D. A., Phil. Mag. [7], 5, 795 (1928).

4. Carslaw, H. S., Jaeger, J. C., Conduction of Heat in Solids, pp. 202, 378, Oxford Press, 1949.

5. Cary, J. R., Trans. Am. Soc. Mech. Engrs., 75, 483 (1953).

6. Castleman, R. A., Nat. Advisory Comm. Aeronaut., Tech. Notes 231 (1926).

7. Cecil, O. B., Munch, R. H., Ind. Eng. Chem., 48, 437 (1956).

8. Coulson, J. M., Skinner, S. J., Chem. Eng. Sci., 1, 197 (1952).

9. Comings, E. W., Clapp, J. T., Taylor, J. F., Ind. Eng. Chem., 40, 1076 (1948).

10. Curme, G. O., Johnstone, F., Glycols, Reinhold Publishing Co., 1952.

11. Eckert, E. R. G., Introduction to the Transfer of Heat and Mass, 1st ed., pp. 88-98, McGraw-Hill Book Co., New York, 1950.

12. Garner, F. H., Hale, A. R., Chem. Eng. Sci., 2, 157 (1953).

13. Garner, F. H., Skelland, A. H. P., Ind. Eng. Chem., 48, 51 (1956).

14. Garner, F. H., Skelland, A. H. P., Chem. Eng. Sci., 4, 149 (1956).

15. Garwin, L., Smith, B. D., Chem. Eng. Prog., 49, 591 (1953).

16. Goldstein, S., Modern Developments in Fluid Dynamics, Oxford Press, 1938.

17. Gunn, R., J. Geophysical Res., 54, 383 (1949).

18. Haberman, W. L., Morton, R. K., David W. Taylor Model Basin, Report 8 (1953).

19. Handbuch der Experimental Physik, Vol. 4, part 2, 376 (1932).

20. Handbook of Chemistry and Physics, 30th ed., Chem. Rubber Publish. Co., 1947.

21. Harkins, W. O., Brown, F. E., J. Am. Chem. Soc., 41, 499 (1919).

22. Hayworth, C. B., Treybal, R. E., Ind. Eng. Chem., 42, 1174 (1950).

23. Higbie, R., Trans. Am. Inst. Chem. Engrs., 31, 365 (1935).

24. Hu, S., Kintner, R. C., Amer. Inst. Chem. Engrs. J., 1, 42 (1955).

25. Hughes, R. R., Gilliland, E. R., Chem. Eng. Prog., 48, 497 (1952).

26. Ingebo, R. D., Nat. Advisory Comm. Aeronautics, Tech. Notes 2368 (1951).

27. Ingebo, R. D., Nat. Advisory Comm. Aeronautics, Tech. Notes 3762 (1956).

28. International Critical Tables, McGraw-Hill, New York, 1929.

29. Jakob, M., Heat Transfer, Vol. 1, J. Wiley and Sons, Inc., 1949.

30. Johnstone, H. F., Pigford, R. L., Chapin, J. H., Trans. Am. Inst. Chem. Engrs., 37, 95 (1941).

31. Kinzer, G. D., Gunn, R., Jour. of Meteorology, 8, 71 (1951).

32. Kramers, H., Physica, 12, 61 (1946).

33. Kronig, R., Brink, J. C., App. Sci. Research, A2, 142 (1949-51).

34. Kronig, R., van der Veen, B., Ijzerman, P., App. Sci. Research, A3, 103 (1951-54).

35. Lamb, H., Hydrodynamics, 6th ed., Dover Publications, New York (1932).

36. Licht, W., Conway, J. B., Ind. Eng. Chem., 42, 1151 (1950).

37. Licht, W., Pansing, W. F., Ind. Eng. Chem., 45, 1885 (1953).

38. Lindland, K. P., Terjesen, S. G., Chem. Eng. Sci., 5, 1 (1956).

39. Lynn, S., Straatemeier, J. R., Kramers, H., Chem. Eng. Sci., 4, 49 (1955).

40. McAdams, W. H., Heat Transmission, 2nd ed., pp. 237, McGraw-Hill Book Co., New York, 1942.

41. McDonald, J. E., Journal of Meteorology, 11, 478 (1954).

42. McDowell, R. V., Myers, J. E., Amer. Inst. Chem. Engrs. J., 2, 384 (1956).

43. Meksyn, D., Proc. Roy. Soc., 194A, 218 (1948).

44. Millikan, C. B., Trans. ASME, 54, 29 (1932).

45. Möller, W., Phys. ZS., 39, 64 (1938).

46. Peebles, F. N., Garber, H. J., Chem. Eng. Prog., 49, 88 (1953).

47. Pierce, R. D., Heat Transfer and Fluid Dynamics in Mercury-Water Spray Columns, Ph.D. thesis in ChE, U. of Mich., 1954.

48. Smoluchowski, M. S., Proc. of 5th International Cong. of Math., Vol. II, 192 (1912).

49. Spells, K. E., Proc. Phys. Soc. (London), 65B, 541 (1952).

50. Stanton, T. E., Marshall, D., Aero. Res. Comm. Rep. and Mem., No. 1358 (1930).

51. Tomotika, S., British Aero. Res. Committee, Reports and Memoranda No. 1678, (1936).

52. Treybal, R. E., Liquid Extraction, McGraw-Hill Book Co., pp. 328-329, New York, 1951.

53. Turrell, F. M., Tables of Surfaces and Volumes of Spheres and of Prolate and Oblate Spheroids, and Spheroidal Coefficients, 1st ed., Univ. of Cal. Press, (1946).

54. West, F. B., Robinson, P. A., Morgenthaler, A. C., Ind. Eng. Chem., 43, 234 (1951).

55. Woolf, J. R., Sibbitt, W. L., Ind. Eng. Chem., 46, 1947 (1954).